INVESTIGATION OF MINIMUM RESPONSE FOR DAMAGE ASSESSMENT

by

JEFFREY PAUL KIRK

Presented to the Faculty of the Graduate School of

The University of Texas at Arlington in Partial Fulfillment

of the Requirements

for the Degree of

MASTER OF SCIENCE IN MECHANICAL ENGINEERING

THE UNIVERSITY OF TEXAS AT ARLINGTON

August 2005

ACKNOWLEDGEMENTS

First of all, I would like to express my gratitude for Dr. Bo P. Wang. It was Dr. Wang who piqued my interest in minimum response, and provided the inspiration for possible application to damage assessment. The instruction and guidance that he offered, in the coursework prior to start of this project, and during conduct of this research, were invaluable. I would also like to thank Dr. Kent Lawrence and Dr. Wen Chan, not just for their time and attention as committee members, but also for the effective instruction that they provided in the coursework leading up to this project.

I will be forever grateful for all of the support that my manager, Jim Hutchinson, has provided from the beginning of this degree program. His words of support, and his continual effort to help me balance work and school activities, are very much appreciated.

Finally, I wish to offer thanks to my family. My dear wife has quietly endured the stacks of papers and books that have cluttered the house throughout the many months over which this thesis work was performed. She has also had to endure my compulsive frets over every mid-term and final exam encountered in this program. I am also very grateful for the unconditional love and support that my parents have continually given me since the day I was born.

July 19, 2005

ABSTRACT

INVESTIGATION OF MINIMUM RESPONSE

FOR DAMAGE ASSESSMENT

Publication No. _____

Jeffrey Paul Kirk, M.S.M.E.

The University of Texas at Arlington, 2005

Supervising Professor: Dr. Bo P. Wang

Assessment of structural damage based on changes in vibratory response characteristics has been researched for many years, with much attention directed toward the use of modal parameters. Modal responses contribute to form points of local minima in the frequency response of a system. The frequency and amplitude values corresponding to these points of minimum response can be analytically determined, experimentally measured, and shown to exhibit sensitivity to damage. This work was performed to investigate the possible contribution that explicitly targeted minimum response information could provide in a damage detection process. A simple 6-DOF

discrete spring-mass system was used to conduct preliminary evaluation of various frequency-based techniques adapted for minimum response. The study was extended to the analysis of simulated transverse crack damage in a cantilever beam, followed by experimental evaluation. Relevant conclusions are given, and areas for future work are defined.

TABLE OF CONTENTS

ACKNOWLEDGEMENTS ii

ABSTRACT iii

LIST OF ILLUSTRATIONS ix

LIST OF TABLES xi

Chapter

1. INTRODUCTION 1

1.1 Background 1

1.2 Motivation for Use of Minimum Response 4

1.3 Description of Research Approach 6

2. MINIMUM RESPONSE 9

2.1 Definition of Minimum Response Point 9

2.2 Mathematical Examination of Minimum Response Point 11

2.3 Matrix Formulation for Minimum Response 14

3. PRELIMINARY EVALUATION WITH DISCRETE SPRING-MASS SYSTEM 18

3.1 6-DOF System Description 18

3.2 Cawley-Adams Criterion Method 20

3.2.1 Mathematical Approach for C-A Criterion 21

3.2.2 Adjustment of Approach for Minimum Response Frequency 22

3.2.3 Analysis and Results 22
3.3 Damage Location Assurance Criterion 26
3.3.1 Description of the DLAC Function 26
3.3.2 Analysis and Results 28
3.4 Eigenvalue Sensitivity Formulation 30
3.4.1 Mathematical Review – Resonant Frequency Sensitivity 32
3.4.2 Formulation for Response Minima 35
3.4.3 Analysis with Inverse Sensitivity Approach 37
3.5 Minimization of Residual Force 44
3.5.1 Formulation of Residual Force and Optimization Problem 45
3.5.2 Formulation of Residual Error for Response Minima 49
3.5.3 Optimization Based on Residual Error 53
4. IDENTIFICATION OF MINIMUM RESPONSE 58
4.1 Description of Response Functions 58
4.2 Approach for Identification from Measured Data 60
4.2.1 Problem Description 60
4.2.2 Description of Elected Approach 62
4.2.3 Comment on Noise Sensitivity 67
5. APPLICATION TO BEAM STRUCTURE 68
5.1 Detailed FEM for Simulation of Damage 69
5.2 FEM for Assessment of Damage 73
5.3 Modeling of Damage 75

5.4 Application of C-A Criterion for Beam Damage 76

5.5 Eigenvalue Sensitivity Approach 84

5.6 Continuous Beam Theory 88

5.6.1 Model of Transverse Crack in Continuous Beam 89

5.6.2 Optimization Problem Definition and Results 94

5.7 Cracked-Beam Finite Element Approach 97

5.7.1 Formulation of a Cracked-Beam Element 98

5.7.2 Optimization Based on Cracked-Beam Element 99

5.7.3 Damage Assessment Results 101

6. EXPERIMENTAL APPLICATION TO BEAM STRUCTURE 106

6.1 Test Procedure 107

6.2 Preliminary Analysis and Results from Experimental Data 110

6.2.1 An Evaluation of Measurement Noise 110

6.2.2 Damage Assessment Evaluation 113

6.3 Study of Minimum Response Amplitude 115

6.3.1 Damage Sensitivity of Minimum Response Point Amplitude 116

6.3.2 Transfer Function Parameter Change Method 118

6.3.3 Adapted Method for Minimum Response 121

6.3.4 Application to Simulated Test Data 123

6.3.5 Application to Experimental Data 126

7. CONCLUSIONS AND FUTURE WORK 132

7.1 Conclusions 132

7.2 Future Work 134

Appendix

A. CONTINUOUS BEAM THEORY EQUATIONS 137

B. CRACKED-BEAM ELEMENT FORMULATION 144

C. EXPERIMENTAL BEAM RESONANT FREQUENCY DATA 146

REFERENCES 150

BIOGRAPHICAL INFORMATION 153

LIST OF ILLUSTRATIONS

Figure Page

2.1 Illustration of Minimum Response Points 10

3.1 System Information for 6-DOF Discrete Model 19

4.1 Illustration of Curve-Fit Frequency Span 63

4.2 Expanded View of Curve-Fit Span 63

5.1 Detailed 2-D Beam Model for Damage Simulation 70

5.2 Course Beam Model for Damage Identification Process 74

5.3 Comparison of C-A Results for Damage Case #1 78

5.4 Comparison of C-A Results for Damage Case #2 78

5.5 Comparison of C-A Results for Damage Case #4 78

5.6 Comparison of C-A Results for Damage Case #5 79

5.7 Comparison of C-A Results for Damage Case #7 79

5.8 Comparison of C-A Results for Damage Case #8 79

5.9 Comparison of C-A Results for Damage Case #10 80

5.10 Comparison of C-A Results for Damage Case #11 80

5.11 Comparison of C-A Results for Damage Case #13 80

5.12 Comparison of C-A Results for Damage Case #14 81

5.13 Comparison of C-A Results for Damage Case #16 81

5.14 Comparison of C-A Results for Damage Case #17 81

5.15 Comparison of C-A Results for Damage Case #19 82

5.16 Comparison of C-A Results for Damage Case #20 82

5.17 Comparison of C-A Results for Damage Case #22 82

5.18 Comparison of C-A Results for Damage Case #23 83

5.19 Comparison of C-A Results for Damage Case #25 83

5.20 Comparison of C-A Results for Damage Case #26 83

5.21 Analytical Representation of Crack Damage: (a) Cantilever Beam with Crack (b) Model of Cracked Beam 90

5.22 Segmented Model of Cracked Cantilever Beam with Single-Point Force 91

5.23 Schematic of Beam Element: (a) Undamaged (b) Cracked 99

5.24 Mode Shapes for Undamaged Cantilever Beam 104

5.25 Mode Shapes for Damaged (80% Crack at 0.75") Beam 104

6.1 Photograph of Test Setup 108

6.2 Transverse Cut in Beam #4 109

6.3 Example Mobility FRF Measurements – Before and After Damage 111

6.4 Measured Frequency and Amplitude Changes for Beam #2 (Damage within Element 1) 130

6.5 Measured Frequency and Amplitude Changes for Beam #4 (Damage within Element 4) 131

LIST OF TABLES

Table Page

3.1 C-A Criterion Based on Resonant Frequency 24

3.2 C-A Criterion Based on Minimum Response Point Frequency 24

3.3 Effect of Measurement Error on Damage Localization through the C-A Criterion Method 25

3.4 DLAC Values Based on Resonant Frequency Change 29

3.5 DLAC Values Based on Minimum Response Point Frequency Change 29

3.6 Damage Factors (Δa) Determined for Damage Condition #1 Based on Resonant Frequency Sensitivity 39

3.7 Damage Factors (Δa) Determined for Damage Condition #1 Based on Minimum Response Frequency Sensitivity 40

3.8 Damage Factors (Δa) Determined for Damage Condition #2 Based on Resonant Frequency Sensitivity 42

3.9 Damage Factors (Δa) Determined for Damage Condition #2 Based on Minimum Response Frequency Sensitivity 43

3.10 Damage Identification by Minimization of Residual Force through Optimization with Resonant Frequency Input 55

3.11 Damage Identification by Minimization of Residual Error through Optimization with Minimum Response Frequency Input 57

4.1 Evaluation of Minimum Response Frequency Extraction Process 66

5.1 Simulated Damage Cases Produced from Detailed Beam Model 72

5.2 Calculated Damage Coefficients – Comparison Between Beam Case #1 and Proportionally Damaged Models 86

5.3 Calculated Damage Coefficients – Comparison Between 0.050-in Crack Beam Damage Cases 88

5.4 Evaluation of Continuous Cracked-Beam Model 94

5.5 Results of Damage Detection through Optimization with Continuous Cracked-Beam Formulation 96

5.6 Results of Damage Detection through Optimization with Cracked-Beam Finite Element Formulation 102

6.1 Minimum Response Frequency Statistical Results 112

6.2 Minimum Response Amplitude Statistical Results 112

6.3 Comparison Between Variance and Change from Damage 113

6.4 Experimental Results Based on Resonant Frequency Change 114

6.5 Damage Assessment of Analytical Damage Cases Based on Amplitude Changes at Local Response Minima 125

6.6 Damage Assessment of Experimental Cases Based on Amplitude Changes at Local Response Minima 127

CHAPTER 1

INTRODUCTION

This chapter is divided into three sections. In the first section (1.1), a brief overview of the some of the background pertaining to the subject of damage detection is presented, to bring to mind the broad level motivation behind this thesis research. The second section (1.2) describes the specific motivation behind the selection of minimum response information for use in a damage detection process. Finally, in the third section (1.3), a description of the approach used for this research, as well as the organization of the remaining chapters of this thesis, are provided.

1.1 Background

In general, the integrity of all structures tends to degrade over time as a result of exposure to operational and environmental conditions. Repeated loadings provide potential for the generation and propagation of cracks. When composite materials are involved, these loadings may produce debonds and delaminations within the material. In addition, fasteners tend to loosen over time. Corrosion also acts to reduce the integrity of structure. All of these conditions, among others, are considered to be forms of damage. Any change in the state of a structural system, that adversely affects the current or future performance of the system, can be considered as damage.

A properly designed structural component is expected to function within all expected operational and environmental conditions over some specified service life. However, the occurrence of extreme, or unexpected, loading conditions could significantly reduce the life of the component, possibly leading to a complete catastrophic failure of the system. In addition, it is not uncommon for a system to remain in service well beyond its intended service life. Consider that the B-52 Stratofortress aircraft has been in service by the U.S. Air Force for over 40 years and is expected to remain in service beyond the year 2040. Likewise, the Federal Aviation Agency has an ongoing research program that is focused on the study of age-related problems for aging aircraft in the commercial fleet [24].

Clearly, the human safety factor associated with the structural reliability of aircraft, bridges, buildings, and other major structure, is of utmost importance. However, there are also cost issues that drive the need for the development of tools for assessment of structural health. Production facilities incur significant costs upon the breakdown of manufacturing equipment. Even planned periods of downtime for routine maintenance of equipment impose losses in production and profits. An effective monitoring system provides a means to extend the operation of equipment between maintenance cycles, and reduce the occurrence of unnecessary and expensive maintenance tasks.

Several related technologies have emerged over the years, to provide means for evaluation/assessment of system health. Some of these include [11]: (1) Non-Destructive Evaluation (NDE); (2) Structural Monitoring; (3) Structural Health

Monitoring (SHM); (4) Condition Monitoring; and (5) Health and Usage Monitoring Systems (HUMS). Non-Destructive Evaluation (NDE) techniques, which have been around for a long time, are primarily used for off-line (i.e. while out of service) inspection of components. The SHM process, however, is geared toward on-line assessment of system health. Currently, this technology is still in a stage of infancy. For that reason, there few fielded monitoring systems. Condition monitoring, essentially SHM for rotating machinery, is probably the technology that has seen the most advancement and implementation. Similarly, HUMS has emerged to address the structural health concerns for rotor aircraft.

A variety of methods have been developed to provide a means for the assessment of damage in structure based on information obtained from various input and output measurements. Some of these are based on direct visual identification of damage, such as through use of x-ray diffraction, dye penetrants, paints, and ultrasonics. There are various types of methods based on stress wave measurements that utilize acoustic, ultrasonic, or lamb wave inputs. Measurement of acoustic emissions can be used to detect the presence of cracks, or delaminations in composites. However, most of these methods are more suited for performance of non-destructive evaluations.

For SHM applications, much research has been conducted toward the development of vibration-based methods. These methods are attractive for SHM applications because vibration response can be acquired in real-time through any one or combination of a wide array of available sensors. The use of vibration response for damage assessment is the interest of this research.

1.2 Motivation for Use of Minimum Response

A vast amount of research has been conducted toward development of vibration-based methods for structural damage assessment. All of these methods are based on the idea that the response of a structure will be altered in some way by the presence of damage. The vibratory response of a linear structure can be represented as a linear combination of all of the natural modes of vibration of that structure. Each mode is characterized by a natural frequency, a mode shape that defines the spatial variation of the deflection pattern that occurs at the natural frequency, and an associated damping factor. Dependent on the amount of damping present, response amplification occurs at excitation frequencies near the resonant frequency. Thus, modal responses are generally easily produced and observed. The mode shapes and natural frequencies are system properties, dependent on the material mass and stiffness distributions within the structure. So, any changes to mass or stiffness, as a result of damage, will produce some change in the modal characteristics. For all of these reasons, many methods have been developed to take observed changes in the modal properties of a damaged structure, and attempt to infer from these changes, a description of the damage that has occurred.

It is not necessary to view changes in the modal properties by direct means alone. There are other characteristics, in the frequency response of a structure, that are dependent on the natural modes and which have been studied by researchers for potential damage assessment applications. For example, while resonant frequencies exhibit response amplification, there are other frequencies, termed *anti-resonances*,

which exhibit zero response regardless of the force level. The special characteristics associated with anti-resonant frequencies have captured the interest of many researchers looking to develop tools for model updating and damage assessment applications [10]. Along with anti-resonant frequencies, there are also frequencies for which the response for a given excitation will exhibit minimal amplification. These responses, referred to herein as *local response minima* or *minimum response points* seem to have held not much more than theoretical interest with respect to modal analysis [15]. In an exhaustive literature search, no direct application of minimum response for damage assessment was found.

In an advanced structural dynamics course, a very interesting matrix formulation was presented for calculation of minimum response frequencies [27], given the finite matrix approximations of the mass and stiffness distributions. From this formulation, sensitivities of these points to changes in mass and stiffness can also be quantified. Immediately, this presents potential for a damage assessment process.

The specific application for a damage assessment process based on minimum response has not yet been identified. However, consider structural systems that are inherently subjected to discrete frequency inputs (e.g. rotating machinery, rotor aircraft, etc.). For these systems, it is a natural tendency for the design process to build separation between the resonant frequencies and the discrete forcing frequencies. Optimally, the forcing frequencies will exist in the relatively stable response regions near minimum response points. Thus, there is potential that these forced responses

observed in operating vibration data could be used, based on knowledge of minimum response, to detect structural changes caused by damage.

The goal here is not to define the application, but to determine whether or not the potential is real, and if so, draw others to examine.

1.3 Description of Research Approach

The primary purpose of this research is to provide an introductory evaluation of the potential use for minimum response point information in the context of damage assessment. There are many aspects of damage assessment that must be considered for a practical application, and it is not feasible to address all of these at one time. The intended scope of this research is discussed below.

Probably the most important step in the creation of a successful SHM system is the selection of good *features*. *Features* are those quantities that are extracted from measured data, and supplied as input into the damage detection process. The pertinent data will typically include some measure of dynamic response, but may also include measurements of environmental and operational conditions. For example, in studies performed with modal data collected from the Z-24 bridge in Switzerland, it was necessary to quantify changes in the modal parameters due to temperature differentials across the bridge, so that damage-induced modal parameter changes could be effectively identified [25]. However, for the purpose of this introductory study, the effects of such external conditions were not considered.

The SHM process can be sub-divided into four levels: (1) detection – "has damage occurred?"; (2) localization – "where is the damage?"; (3) assessment – "what type and how severe?"; and (4) prognosis – "how long can I continue to operate?". The object of the detection (level 1) process is to search for changes in dynamic response, then compensate for the effects of noise and changing environmental and operational conditions, so that a reliable report of damage is attained, and excessive false positive reports are avoided. This is inherently a statistical problem. There is much on-going research devoted to development of new statistical approaches (extreme value statistics [29], pattern recognition, genetic algorithms, machine learning algorithms, etc.). The interest in this work, however, was to study the physical connection between damage and minimum response, and evaluate the potential for the extraction of effective features.

Therefore, the focus here is placed on localization (level 2) and assessment (level 3) of damage. For all evaluations conducted throughout this work, it is assumed that damage is already known to exist, and the goal is to see if the process that uses minimum response information can correctly assess the damage. As much as possible, parallel applications of modal response, for the same system/damage conditions, were performed to provide performance comparisons to aid in the evaluation of the minimum response based damage assessment results.

In Chapter 2 a more detailed description of *minimum response* is presented. The planned approach for this research was to first begin investigations through use of a one-dimensional discrete spring-mass system (Chapter 3). A variety of fundamental

approaches, identified from the published literature, were explored. The purpose was to establish the theoretical effectiveness with an idealized system, gain insight, and use the results to tailor an extension to beam structure. Identification of minimum response information from frequency-domain response data is presented in Chapter 4. In anticipation of experimental evaluation, analytical evaluations were performed for transverse crack damage in a cantilever beam (Chapter 5). Additional insight was gathered, and experimental evaluations were performed (Chapter 6). The conclusions derived from all of this work are discussed in Chapter 7, and recommendations for future work are given.

CHAPTER 2

MINIMUM RESPONSE

2.1 Definition of Minimum Response Point

Consider a linear structure that is subjected to sinusoidal excitation forces. The structure will exhibit a steady-state response at the excitation frequency, and the point-to-point variations in the amplitudes and directions of the response will reflect an operating deflection pattern. The response level at any given location is dependent on the modal properties of the structure and the particular loading pattern. When the excitation frequency coincides with a resonant frequency, then the operating deflection pattern reflects the specific pattern of the mode shape for that resonance, and response amplifications occur. Likewise, excitation at frequencies away from resonant frequencies yields lower response amplitudes.

Thus, somewhere in the frequency span between two separated resonant frequencies, there must be a frequency for which the response amplitude at a given location will drop to some minimum value, or disappear altogether. Also, because the operating deflection pattern varies with excitation frequency, then a frequency that yields a minimal response at one location will likely not correspond to a minimal response at another location.

The Frequency Response Function (FRF) is a frequency domain function that describes the amplitude and phase relationship between a response (output) and force (input), as a function of excitation frequency. Graphical representation of this function allows for visualization of the steady-state response characteristics of the structure at a specific location. Resonant frequencies are easily recognized as peaks in the FRF. Similarly, those frequencies that exhibit minimal response level are easily recognized. An example FRF, with these special response points indicated, is given in Figure 2.1.

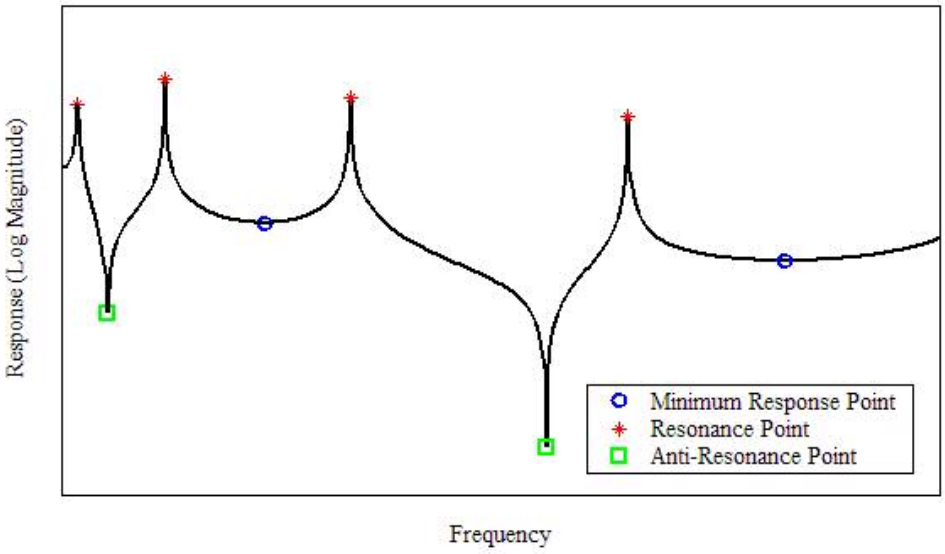

Figure 2.1 Illustration of Minimum Response Points

Among those frequencies that produce locally minimal response levels, there are some that theoretically yield no response at a given location. These points represent peaks in an inverse FRF relationship, and for that reason are labeled as *anti-resonant* frequencies. There is a clear distinction, however, between these anti-resonant

frequencies and those that are labeled herein as *local response minima*, or *minimum response points*, as indicated in Figure 2.1. One primary distinction is that, unlike anti-resonant response, in the vicinity of a local minimum response point, the response level is relatively stable to changes in frequency. It is this characteristic of minimum response points that provided motivation for this research.

One property that is shared between anti-resonant responses and local response minima is that the frequencies of both are non-global. That is, each and every response location will exhibit a unique set of local minima and anti-resonant frequencies. This is unlike the global nature of natural frequencies. Resonant frequencies are system characteristics, and as such, are evident in varying degrees in the responses at all locations. Measurement of response from one location may reveal all of the natural frequencies within the measured frequency range, but then other locations will contribute no new information. This uniqueness offered by anti-resonant frequency information has been shown to provide localization of damage in symmetrical structures [10] that was not possible with resonant frequency data alone. It is hoped that the same benefit can be derived from minimum response point frequencies.

2.2 Mathematical Examination of Minimum Response Point

In general, minimum response information can be derived from any frequency-domain response function. However, for purpose of clarity, this discussion is confined to the previously mentioned *Frequency Response Function* (FRF) for single-point excitation. There are many forms of the FRF. The form that is seems to be most

commonly used in analytical development is the *receptance*, or sometimes referred to as the *compliance*. The receptance defines the frequency response relationship between a *displacement* response and an applied force. It is this form that was used throughout this research effort, and from which minimum response points were defined. The mathematical representation, based on the principal of mode superposition, for the receptance (α_{ij}) between a response at coordinate *i*, and a force at coordinate *j*, of a linear undamped multiple-degree-of-freedom (MDOF) system is given by equation (2.1) below [18].

$$\alpha_{\mathbf{ij}}(\Omega) = \sum_{\mathbf{r}=1}^{\mathbf{m}} \frac{\phi_{\mathbf{ir}}\phi_{\mathbf{jr}}}{\omega_{\mathbf{r}}^2 - \Omega^2}, \qquad \text{for } m \text{ modes.} \tag{2.1}$$

where, $\phi_{kn} \equiv k^{\text{th}}$ coordinate of the n^{th} mass-normalized mode shape,

$\omega_n \equiv n^{\text{th}}$ resonant frequency.

Now, computing the derivative of the Receptance with respect to (Ω^2) yields,

$$\frac{d\,\alpha_{ij}}{d(\Omega^2)} = \sum_{\mathbf{r}=1}^{\mathbf{m}} \frac{\phi_{\mathbf{ir}}\phi_{\mathbf{jr}}}{(\omega_{\mathbf{r}}^2 - \Omega^2)^2}. \tag{2.2}$$

The frequencies (Ω_{m}) that correspond to local response minima are found where the slope of the receptance is zero in the frequency domain. That is, the minimum response frequencies correspond to the roots of the following equation,

$$\frac{\phi_{\mathbf{i}1}\phi_{\mathbf{j}1}}{(\omega_1^2 - \Omega_{\mathbf{m}}^2)^2} + \frac{\phi_{\mathbf{i}2}\phi_{\mathbf{j}2}}{(\omega_2^2 - \Omega_{\mathbf{m}}^2)^2} + \cdots + \frac{\phi_{\mathbf{i}m}\phi_{\mathbf{j}m}}{(\omega_m^2 - \Omega_{\mathbf{m}}^2)^2} = 0. \tag{2.3}$$

However, it is not possible to perform a direct solution, and even a numerical solution seems unrealistic if a large number of modes are included in the process.

An approximation for a minimum response frequency can be performed with the assumption that the response over the frequency span between two resonances is dominated by only those two modes. Assume for the moment that the first two modes completely dominate the response over the frequency range, $\omega_1 < \Omega < \omega_2$. Then, a minimum response point can be found at $\Omega = \Omega_{\mathbf{m}}$, if

$$\frac{\phi_{\mathbf{i}1}\phi_{\mathbf{j}1}}{(\omega_1^2 - \Omega_{\mathbf{m}}^2)^2} + \frac{\phi_{\mathbf{i}2}\phi_{\mathbf{j}2}}{(\omega_2^2 - \Omega_{\mathbf{m}}^2)^2} = 0 . \tag{2.4}$$

Since the denominator terms in equation (2.4) must be positive, then the equation can only be satisfied on the condition that $(\phi_{\mathbf{i}1}\phi_{\mathbf{j}1})(\phi_{\mathbf{i}2}\phi_{\mathbf{j}2}) < 0$. This could be used as a test condition in a search process. If the condition is satisfied, then a solution could be determined for the minimum response frequency located between the two modes. If the condition is not met, then the test condition could be applied to the next frequency span in the search process. This is still an undesirable approach because this formulation does not allow a direct means for determination of the sensitivity of minimum response frequencies to changes in the physical parameters of the system. An improved formulation for the determination of minimum response frequencies, that does provide an effective means for sensitivity analysis techniques, is presented in the following section.

Before concluding this section, an additional comment will be made regarding the condition, $(\phi_{\mathbf{i}1}\phi_{\mathbf{j}1})(\phi_{\mathbf{i}2}\phi_{\mathbf{j}2}) < 0$, for the existence of a local minimum between two

dominant modes. Suppose that the subject response location happens to be in very close proximity to a node line of the second mode, such that the first and third modes highly dominate the response for $\omega_1 < \Omega < \omega_3$. The implication is that the sensitivity of a minimum response point in this frequency range is likely to be very non-linearly sensitive to effects of damage. A damage induced shift of the node lines of the second mode could significantly change the degree of participation of the mode in the response, and cause a jump of the minimum response point to another frequency. This effect should be one of the considerations used in the selection of optimal response locations for a damage detection process.

2.3 Matrix Formulation for Minimum Response

A matrix formulation [27] for the direct computation of minimum response point frequencies from finite element mass and stiffness distribution matrices is summarized here. Given the finite element mass and stiffness matrices, **M** and **K**, respectively, an eigenvalue problem can be defined for a particular response location and input force pattern, such that the frequencies of minimum response for that location will be contained in the corresponding eigenvalue set.

The steady-state response amplitude at a point in a system due to a harmonic forcing function is denoted herein as $Resp(\Omega)$, where Ω denotes the excitation frequency. As described in the previous section, minimum and maximum response points occur at frequencies, Ω_m, where $d(Resp)/d\Omega = 0$.

The equation of motion for an undamped N-DOF discrete system under steady-state harmonic excitation is given by, $\mathbf{M\ddot{u}} + \mathbf{Ku} = \mathbf{F}e^{i\Omega t}$, where $\mathbf{F}$ is the input force amplitude vector [9]. For the steady-state response solution, $\mathbf{u} = \mathbf{U}e^{i\Omega t}$, where $\mathbf{U}$ is the response amplitude vector, the steady-state form of the equation of motion can be represented as,

$$(\mathbf{K} - \Omega^2\mathbf{M})\mathbf{U} = \mathbf{F}, \tag{2.5}$$

Differentiating both sides of equation (2.5) with respect to Ω^2 yields,

$$-\mathbf{MU} + (\mathbf{K} - \Omega^2\mathbf{M})\mathbf{U}' = \mathbf{F}' \tag{2.6}$$

where, $\mathbf{U}' = \dfrac{d\,\mathbf{U}}{d(\Omega^2)}$, and $\mathbf{F}' = \dfrac{d\,\mathbf{F}}{d(\Omega^2)}$.

For an input force vector of constant peak amplitude, $\mathbf{F}' = 0$, and equations (2.5) and (2.6) can be combined into a single matrix representation as,

$$\begin{bmatrix} \mathbf{K} - \Omega^2\mathbf{M} & 0 \\ -\mathbf{M} & \mathbf{K} - \Omega^2\mathbf{M} \end{bmatrix} \begin{Bmatrix} \mathbf{U} \\ \mathbf{U}' \end{Bmatrix} = \begin{Bmatrix} \mathbf{F} \\ 0 \end{Bmatrix} \tag{2.7}$$

and which can be rearranged as follows,

$$\left(\begin{bmatrix} \mathbf{K} & 0 \\ -\mathbf{M} & \mathbf{K} \end{bmatrix} - \Omega^2 \begin{bmatrix} \mathbf{M} & 0 \\ 0 & \mathbf{M} \end{bmatrix} \right) \begin{Bmatrix} \mathbf{U} \\ \mathbf{U}' \end{Bmatrix} = \begin{Bmatrix} \mathbf{F} \\ 0 \end{Bmatrix}. \tag{2.8}$$

It is desired to find the minimum response frequencies associated with the response at a particular location. For the response of the i^{th} DOF, $Resp = U_i$, or can be expressed as, $Resp = \mathbf{CU}$, where $\mathbf{C} = \begin{bmatrix} C_1 & \dots & C_{\mathbf{N}} \end{bmatrix}$, with $C_j = 1$ for $j = i$, and $C_j = 0$ for $j \neq i$. The goal is to find Ω_m such that $Resp' = \mathbf{CU}' = 0$. Thus, the following expression

can be written,

$$[\mathbf{0} \quad \mathbf{C}]\begin{Bmatrix}\mathbf{U}\\ \mathbf{U}'\end{Bmatrix} = 0\,. \tag{2.9}$$

If $\mathbf{G} \equiv$ null space of [0 **C**], then,

$$[0 \quad \mathbf{C}]\mathbf{G}\mathbf{q} = 0 \quad \Rightarrow \quad \begin{Bmatrix}\mathbf{U}\\ \mathbf{U}'\end{Bmatrix} = \mathbf{G}\mathbf{q}\,, \tag{2.10}$$

where **q** can be any arbitrary vector. Equation (2.10) can be substituted into equation (2.8) to yield the following,

$$\left(\begin{bmatrix}\mathbf{K} & 0\\ -\mathbf{M} & \mathbf{K}\end{bmatrix} - \Omega^2\begin{bmatrix}\mathbf{M} & 0\\ 0 & \mathbf{M}\end{bmatrix}\right)\mathbf{G}\mathbf{q} = \begin{Bmatrix}\mathbf{F}\\ 0\end{Bmatrix}. \tag{2.11}$$

Now, if equation (2.11) is pre-multiplied by a transformation matrix, $\mathbf{T}^T$, the right side becomes, $\mathbf{T}^T[\mathbf{F}^T \;\; 0]^T = ([\mathbf{F}^T \;\; 0]\mathbf{T})^T$. Note that if **T** is defined to be the null space of the matrix quantity $[\mathbf{F}^T \;\; 0]$, then equation (2.11) can be transformed into an eigenvalue problem with the final form given below,

$$(\mathbf{A} - \Omega^2\mathbf{B})\,\mathbf{q} = 0 \tag{2.12}$$

where, $\mathbf{A} = \mathbf{T}^T\begin{bmatrix}\mathbf{K} & 0\\ -\mathbf{M} & \mathbf{K}\end{bmatrix}\mathbf{G}$, and, $\mathbf{B} = \mathbf{T}^T\begin{bmatrix}\mathbf{M} & 0\\ 0 & \mathbf{M}\end{bmatrix}\mathbf{G}$

For mass and stiffness matrices of order *NxN*, there may be *(2N-1)* eigenvalues and *(2N-1)* eigenvectors, **q**, each of length *(2N-1)*. The transformation matrices **T** and **G**, are based on the response and force pattern for which the minimum response points are desired. The positive-real eigenvalues of equation (2.12) are the squared

frequencies (Ω^2_m) that correspond to points of minimum or maximum response for an undamped system. The second derivative of the response (equation 2.15) at each frequency (Ω_m) can be evaluated to determine whether or not the frequency corresponds to a point of minimum or maximum response. That is, if $Resp(\Omega_m) > 0$ and $Resp(\Omega_m)'' > 0$, or if $Resp(\Omega_m) < 0$ and $Resp(\Omega_m)'' < 0$, then Ω_m is a frequency at a point of minimum response amplitude.

Computing the derivative of equation (2.6) with respect to Ω^2 yields,

$$(\mathbf{K} - \Omega^2\mathbf{M})\mathbf{U}'' - 2\mathbf{M}\mathbf{U}' = \mathbf{F}'' \tag{2.13}$$

and since **F** is independent of frequency, then **U**′′ at $\Omega = \Omega_m$ can be found by,

$$\mathbf{U}'' = 2(\mathbf{K} - \Omega_m^2\mathbf{M})^{-1}\mathbf{M}\mathbf{U}'. \tag{2.14}$$

Consistent with the definition of *Resp*: $Resp'' = \mathbf{C}\mathbf{U}''$ (2.15)

CHAPTER 3

PRELIMINARY EVALUATION WITH DISCRETE SPRING-MASS SYSTEM

A simple one-dimensional discrete spring-mass system was used to conduct preliminary evaluations with several methods identified from published literature. With this dynamic system, damage could be represented unambiguously to allow for clear interpretation of performance results. The 6-DOF system used for this system is described in the following section (3.1).

3.1 6-DOF System Description

The 6-DOF undamped spring-mass system used for preliminary investigation of minimum response for damage detection is illustrated in Figure 3.1. Evenly distributed mass and stiffness elements were used to represent a uniform, homogeneous type system. With this model, the use of proportional damage for sensitivity analysis techniques, perturbation theory methods, etc, exactly corresponded to simulated damage conditions. Thus, the results obtained from all of the methods that were included in this analytical study were not confounded by misrepresentation of damage.

The matrix formulation for computation of minimum response parameters does not include damping effects. Consequently, damping was not included in this analysis. However, damping should be a consideration in future work.

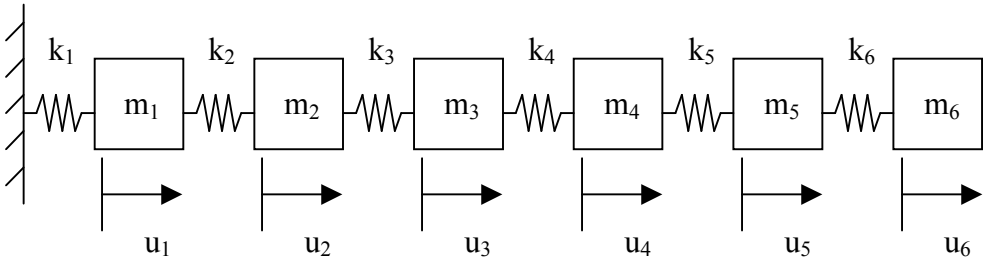

$m_1 = m_2 = m_3 = m_4 = m_5 = m_6 = 1$

$k_1 = k_2 = k_3 = k_4 = k_5 = k_6 = 100$

Modal Parameters

$\omega_1 = 2.41$ rad/s $\omega_2 = 7.09$ rad/s $\omega_3 = 11.36$ rad/s

$\omega_4 = 14.97$ rad/s $\omega_5 = 17.71$ rad/s $\omega_6 = 19.42$ rad/s

ϕ_1	ϕ_2	ϕ_3	ϕ_4	ϕ_5	ϕ_6
0.1327	0.3678	-0.5187	0.5507	0.4565	-0.2578
0.2578	0.5507	-0.3678	-0.1327	-0.5187	0.4565
0.3678	0.4565	0.2578	-0.5187	0.1327	-0.5507
0.4565	0.1327	0.5507	0.2578	0.3678	0.5187
0.5187	-0.2578	0.1327	0.4565	-0.5507	-0.3678
0.5507	-0.5187	-0.4565	-0.3678	0.2578	0.1327

Figure 3.1 System Information for 6-DOF Discrete Model

.

3.2 Cawley-Adams Criterion Method

One of the primary interests in this research concerned the question of whether or not minimum response point frequency changes caused by damage could be used to assess the location and severity of the damage. The Cawley-Adams Criterion method represented an ideal starting point since it was based on the use of frequency information only. The fundamental concept of the Cawley-Adams Criterion [5] is that the ratio of frequency change between two modes of vibration, as a result of damage, is only a function of the damage location. This method is intended to provide for localization of damage only, based on a comparison between theoretical and measured frequency changes.

The general approach is to determine the theoretical resonant frequency changes for a set of possible damage conditions, then compare the ratios of the frequency changes of selected mode pairs to corresponding measured ratios. In theory, at least two mode pairs are needed to identify the damage location uniquely or at least reduce the number of possible damage locations to the minimum number dictated by symmetry. However, due to inaccuracy in the theoretical simulation of damage, and presence of error in measured results, the inclusion of additional mode pairs is needed to provide for averaging of results. An error function was defined to provide comparison of theoretical to experimental frequency-change ratios. The mathematical approach is summarized in the following section.

3.2.1 Mathematical Approach for C-A Criterion

A matching error function, $e_s(p,q)$, is defined for computation of the error between the measured frequency-change ratios of modes p and q, to the theoretical ratios corresponding to damage at site *s*. The error function is defined as follows,

$$e_s(p,q) = \frac{\delta\Omega_p / \delta\Omega_q}{\delta\omega_p(s) / \delta\omega_q(s)} - 1, \qquad \text{if} \qquad \frac{\delta\omega_p(s)}{\delta\omega_q(s)} \le \frac{\delta\Omega_p}{\delta\Omega_q}$$

$$e_s(p,q) = \frac{\delta\omega_p(s) / \delta\omega_q(s)}{\delta\Omega_p / \delta\Omega_q} - 1, \qquad \text{if} \qquad \frac{\delta\omega_p(s)}{\delta\omega_q(s)} \ge \frac{\delta\Omega_p}{\delta\Omega_q} \tag{3.1}$$

where, $\delta\Omega \equiv$ measured frequency change,

$\delta\omega(s) \equiv$ theoretical frequency change due to damage at site *s*.

Then, a total matching error, $\bar{e}_s$, is obtained by summation of the error for all mode pairs,

$$\bar{e}_s = \sum_{p=1}^{m-1} \sum_{q=1}^{m-1} e_s(p,q) \quad \text{, for } m \text{ mode pairs} \tag{3.2}$$

The location that corresponds to the minimum error value is the indicated damage location. The interpretation can be improved by normalization of the total error such that the normalized error, E_s, assumes a value of 1 for the indicated damage location, as follows,

$$E_s = \frac{(e_s)_{min}}{e_s}. \tag{3.3}$$

3.2.2 Adjustment of Approach for Minimum Response Frequency

This approach was easily adapted to use minimum response frequency information. Rather than mode pairs, minimum response point frequency pairs were identified for each response location that was included in the damage localization process. Considering the non-global nature of response minima, there was no theoretical basis for pairing of minimum response frequencies from different response locations. Thus, sets of frequency pairs were identified, one set for each response location included in the analysis. Those response locations that exhibited less than two minimum response frequencies were left out of the damage identification process.

The matching error function, e_s , given by equation (3.1) was slightly redefined as, $(e_s)_r = e_s(p_r,q_r)$, where *p* and *q* refer to response minima points obtained from response location *r*. A total matching error, similar to equation (3.2), was redefined as,

$$\bar{e}_s = \sum_{r=1}^{N} \sum_{p_r=1}^{m_r} \sum_{q_r=1}^{m_r} e_s(p_r, q_r), \tag{3.4}$$

for *N* response locations, and m_r frequency pairs from location *r*.

3.2.3 Analysis and Results

The goal of this analysis was to obtain a base level evaluation of the effectiveness of minimum response information in a damage detection process, with comparison to similar results based on the original definition of the criterion (i.e. with resonant frequency). Numerous damage scenarios were created to include cases of both single-element and multiple-element damage conditions. The impact of truncated

frequency information was explored for some of these damage conditions. Finally, simulated measurement noise was introduced to evaluate the relative susceptibility of the process between the two subject frequency parameters.

Damage to the spring-mass system was simply represented as percentage reductions of stiffness in selected spring elements. Changes in resonant frequencies were calculated and treated as measured data. Minimum response point frequencies were also calculated for steady-state force arbitrarily applied at coordinate #1, and treated as measured data. The damage identification process was carried out as defined by equations (3.1) through (3.4), first with resonant frequencies only, then with minimum response frequencies only. A perturbation method was used to determine the theoretical sensitivity of these frequencies to damage at each element. The perturbations were arbitrarily defined as 10% stiffness reductions.

The numerical results provided in Tables 3.1 and 3.2 are encouraging in that the minimum response point frequency information was just as effective as resonant frequency for identification of damage locations. It is interesting to note that for the case of 20% stiffness reduction on elements #2 and #4, the use of only two resonant frequencies resulted in the misidentification of element #1 as the damaged element, while the corresponding use of only two minimum response point frequencies properly gave the strongest indications to elements #4 and #2, respectively. This result is consistent with the idea that each minimum response point contains information from all modes. Thus, even when only a few frequencies are used, in some degree all modes

are still included. On the contrary, the direct use of modal data will only provide the information of those modes explicitly included in the process.

Table 3.1 C-A Criterion Based on Resonant Frequency

Normalized Total Matching Error, E_s						
E_1	E_2	E_3	E_4	E_5	E_6	Damage Condition
.012	**1.000**	.011	.012	.009	.006	-20% on k_2 ; Use all 6 freqs
.002	**1.000**	.002	.001	0	0	-20% on k_2 ; Use first 2 freqs
.038	**1.000**	.039	**.057**	.034	.025	-20% on k_2 ; -5% on k_4 ; Use all 6 freqs
.077	**1.000**	.080	**.149**	.075	.058	-20% on k_2 ; -10% on k_4 ; Use all 6 freqs
.120	**1.000**	.122	**.284**	.119	.096	-20% on k_2 ; -15% on k_4 ; Use all 6 freqs
.166	**1.000**	.163	**.465**	.164	.139	-20% on k_2 ; -20% on k_4 ; Use all 6 freqs
.210	**1.000**	.210	**.734**	.212	.189	-15% on k_2 ; -20% on k_4 ; Use all 6 freqs
.204	**.711**	.201	**1.000**	.200	.195	-10% on k_2 ; -20% on k_4 ; Use all 6 freqs
.110	**.243**	.101	**1.000**	.093	.107	- 5% on k_2 ; -20% on k_4 ; Use all 6 freqs
1.000	**.105**	.027	**.183**	.039	.021	-20% on k_2 ; -20% on k_4 ; Use first 2 freq
.017	.003	.001	**1.000**	.006	.003	-20% on k_4 ; Use first 2 freq

Table 3.2 C-A Criterion Based on Minimum Response Point Frequency

Normalized Total Matching Error, E_s						
E_1	E_2	E_3	E_4	E_5	E_6	Damage Condition
.025	**1.000**	.075	.100	.074	.081	-20% on k_2 ; Use all 5 freqs (U_6)
.044	**1.000**	.006	.080	.053	.009	-20% on k_2 ; Use first 2 freqs (U_6)
.042	**1.000**	.158	**.236**	.147	.134	-20% on k_2 ; -5% on k_4 ; All 5 freqs (U_6)
.074	**1.000**	.315	**.536**	.286	.232	-20% on k_2 ; -10% on k_4 ; All 5 freqs (U_6)
.106	**1.000**	.477	**.960**	.439	.324	-20% on k_2 ; -15% on k_4 ; All 5 freqs (U_6)
.093	**.664**	.420	**1.000**	.391	.275	-20% on k_2 ; -20% on k_4 ; All 5 freqs (U_6)
.076	**.467**	.358	**1.000**	.324	.218	-15% on k_2 ; -20% on k_4 ; All 5 freqs (U_6)
.056	**.284**	.270	**1.000**	.241	.157	-10% on k_2 ; -20% on k_4 ; All 5 freqs (U_6)
.037	**.141**	.169	**1.000**	.148	.098	- 5% on k_2 ; -20% on k_4 ; All 5 freqs (U_6)
.329	**.535**	.032	**1.000**	.443	.048	-20% on k_2 ; -20% on k_4 ; Use 2 freqs(U_6)
.013	.009	.001	**1.000**	.022	.001	-20% on k_4 ; Use 2 freqs(U_6)

Another study was performed to compare the effect of frequency measurement error on damage localization with the Cawley-Adams criterion approach. A Monte-Carlo approach was used for which a Gaussian random error of constant variance was added to the frequency values prior to their input into the C-A equations. The normalized matching error was computed for a large number of samples. Results were obtained for two different single-element damage conditions. Three different levels of frequency error were applied. As expected, increased error in the *measured* frequency values resulted in higher incidence of misidentified damage locations. The percentages of samples for which the damage was correctly located are given in Table 3.3.

Table 3.3 Effect of Measurement Error on Damage Localization through the C-A Criterion Method

	Percentage of Measurements for which Damage was Correctly Identified			
	Damage Case: -20% on k_4		Damage Case: -20% on k_2	
Frequency Error	Use Resonant Frequencies	Use MRP Frequencies	Use Resonant Frequencies	Use MRP Frequencies
$\sigma = 0.02$	94 %	98 %	89 %	100%
$\sigma = 0.05$	58 %	77 %	57 %	73 %
$\sigma = 0.10$	23 %	43 %	29 %	32 %

The results in Table 3.3 are also encouraging as there is indication that this method tolerates more measurement error on minimum response frequency information than with resonant frequency data. Of course, this benefit can only be realized if minimum response frequencies can be measured with similar accuracy as resonant

frequencies. It is expected that the error associated with the measurement of minimum response frequencies will exceed that for resonant frequencies, as resonant frequencies exhibit higher response levels and are more sharply identifiable in the response spectrum. The identification of minimum response point frequencies from measured response data is addressed in Chapter 4.

3.3 Damage Location Assurance Criterion

In another method found in the published literature, is defined an indicator function labeled as the Damage Location Assurance Criterion (DLAC) [28]. Since this indicator function is also based strictly on the use of frequency-change, then it was of interest here for evaluation of minimum response point frequency.

3.3.1 Description of the DLAC Function

The DLAC function is a coherence function similar in form to the Modal Assurance Criterion. Measured resonant frequency values are collected into a parameter vector, from which a frequency-change vector is determined between the healthy and damaged states. The essential idea is to find the frequency-change vector predicted from finite element analysis for a known damage condition that is most correlated with the measured vector. Provided that the theoretical frequency-change vectors associated with damages not existent in the actual structure are sufficiently uncorrelated with the measured vector, then localization is possible.

The DLAC function is expressed as,

$$\mathrm{DLAC(s)} = \frac{\left| \{\Delta \mathbf{f}\}^{\mathrm{T}} \{\delta \mathbf{f}_{\mathrm{s}}\} \right|^2}{\{\Delta \mathbf{f}\}^{\mathrm{T}} \{\Delta \mathbf{f}\} \cdot \{\delta \mathbf{f}_{\mathbf{s}}\}^{\mathrm{T}} \{\delta \mathbf{f}_{\mathbf{s}}\}} , \tag{3.5}$$

where, $\{\Delta \mathbf{f}\} \equiv$ measured frequency-change vector,

$\{\delta \mathbf{f}_{\mathrm{s}}\} \equiv$ theoretical frequency-change vector for damage at site *s*.

A value of zero for this function indicates no correlation of the measured frequency-change to that predicted for the analytical damage pattern, and a value of 1 indicates exact correlation to that of the corresponding damage pattern. The frequency-change vectors can be defined as absolute changes, or as percentage changes. The use of absolute frequency change will inherently place additional weighting to the higher frequencies over the lower frequencies, as the higher frequencies are generally more sensitive to local damage. Conversely, use of percentage change shifts the weighting to the lower frequencies. Intuitively, it would seem that the use of absolute change would provide better performance. However, it has been shown that in the presence of noise the recommended approach [28] is to use percentage frequency-change rather than absolute frequency-change. Thus, percentage frequency change was used in the application of the DLAC function in this study.

Minimum response point frequencies can also be collected into parameter vectors, and input into the DLAC function. Several response locations, and perhaps responses from multiple force patterns, can be used to provide contributions into a single parameter vector. Note that it may also be beneficial to compute a DLAC result

from frequencies obtained from each measurement location separately. Conceivably, it may be possible to use this approach to identify optimal response locations. That is, identify those locations that are most likely to provide reliable localization of damage. At the present time, computation of a separate DLAC function for each response location has not been studied, and is left for future work. For this analysis, the minimum response frequencies from multiple locations were combined into a single parameter vector for localization of damage through the DLAC function.

3.3.2 Analysis and Results

An approach very similar to that used in study with the Cawley-Adams Criterion method was used here. Numerous single-element and multiple-element damage conditions were created through stiffness reductions of selected spring elements, and the corresponding resonant frequencies and minimum response point frequencies were computed, and treated as simulated test data. Stiffness reduction (10%) perturbations were performed for each element to produce a corresponding theoretical frequency-change vector for damage to that element. Results were obtained for the various damage cases, with DLAC values computed from resonant frequencies, and then from minimum response point frequencies.

Single-location damage conditions were clearly identified in all cases with use of resonant frequency vectors, and with use of minimum response frequency vectors. The results obtained for multiple-element damage cases are provided in Tables 3.4 and 3.5.

Table 3.4 DLAC Values Based on Resonant Frequency Change

DLAC(j) Values						
j = 1	**j = 2**	**j = 3**	**j = 4**	**j = 5**	**j = 6**	**Damage Condition**
.492	.994	.411	.464	.372	.428	-20% on k_2 ; Use all 6 freqs
.537	.970	.462	.620	.429	.475	-20% on k_2 ; -5% on k_4 ; Use all 6 freqs
.562	.920	.484	.731	.460	.500	-20% on k_2 ; -10% on k_4 ; Use all 6 freqs
.578	.866	.490	.806	.477	.513	-20% on k_2 ; -15% on k_4 ; Use all 6 freqs
.590	.816	.487	.856	.485	.520	-20% on k_2 ; -20% on k_4 ; Use all 6 freqs
.582	.762	.486	.890	.488	.520	-15% on k_2 ; -20% on k_4 ; Use all 6 freqs
.571	.688	.474	.944	.480	.516	-10% on k_2 ; -20% on k_4 ; Use all 6 freqs
.555	.593	.446	.980	.458	.508	- 5% on k_2 ; -20% on k_4 ; Use all 6 freqs
.684	1.000	.382	.522	.189	.051	-20% on k_2 ; Use first 3 freqs
.913	.852	.385	.870	.554	.209	-20% on k_2 ; -20% on k_4 ; Use first 3 freq

Table 3.5 DLAC Values Based on Minimum Response Point Frequency Change

DLAC(j) Values						
j = 1	**j = 2**	**j = 3**	**j = 4**	**j = 5**	**j = 6**	**Damage Condition**
.510	.995	.740	.785	.774	.812	-20% on k_2 ; Use all 5 freqs (U_6)
.740	.788	.891	.996	.880	.822	-20% on k_4 ; Use all 5 freqs (U_6)
.649	.919	.884	.963	.891	.836	-20% on k_2 ; -20% on k_4 ; All 5 freqs(U_6)
.513	.996	.813	.844	.659	.774	-20% on k_2 ; Use 8 freqs (U_6 and U_4)
.780	.821	.897	.996	.684	.784	-20% on k_4 ; Use 8 freqs (U_6 and U_4)
.676	.929	.919	.977	.741	.799	-20% on k_2 and k_4 ; 8 freqs (U_6 and U_4)

These frequency-change vectors do not possess properties of orthogonality, so there will be some cross-correlation between vectors even when the imposed damage is exactly identical to one of the model stiffness perturbations. The frequency-change vectors defined from minimum response point frequencies exhibit higher cross-correlation than those vectors formed from resonant frequencies. Thus, the differentiation of damaged elements from undamaged elements is not very strong. It was hoped that the ability to add additional local minima frequencies from another response location would help to reduce the degree of cross-correlation, but as shown in Table 3.5, that did not happen. It is expected that a more complicated structural system, particularly for which the model of damage will be less representative, will present much more difficulty with localization of damage from DLAC results obtained through use of minimum response frequencies.

3.4 Eigenvalue Sensitivity Formulation

The eigenvalue sensitivity formulation [12] provides an efficient means for the estimation of resonant frequency changes that result from changes in physical or geometrical parameters represented in a finite element model. This is a commonly used formulation, with numerous applications.

Typically, finite element analysis predictions of natural frequencies and mode shapes are not in complete agreement with measured data obtained from the actual structure. It is generally assumed that the measured data are correct, and that there must be error in the finite element model stiffness and/or mass representations. Given that

assumption, the engineer must adjust material and geometrical properties of the model, to improve the modal predictions, until results are in acceptable agreement with the measured data. This is the *model update* problem. The solution is non-unique, but knowledge of the sensitivities of the resonant frequencies to changes in model parameters helps guide the engineer to determine an optimal solution. The eigenvalue sensitivity formulation provides a means to estimate these sensitivities directly from the elemental mass and stiffness matrices of the finite element model. Once these sensitivities are known, the engineer can perform parametric studies without the need to resolve the eigenequation for every model parameter under consideration.

The model update problem is mentioned here because it is very similar to the damage detection problem. When a finite element model is available, a model update approach can be used to identify damage-induced changes in model parameters, which can then be related to a specific damage condition. It is shown in Chapter 2 that minimum response point frequencies can be determined from the solution of an eigenequation. Thus, the eigenvalue sensitivity formulation can also be extended to minimum response point frequencies, so that the frequency-sensitivities of these local minima points can be utilized in a damage detection process just as resonant frequency sensitivities have been used [1].

A brief mathematical review of the eigenvalue sensitivity formulation, for resonant frequency sensitivity, is provided in the following section. Then in section 3.4.2, a slightly modified formulation for determination of minimum response point frequency sensitivity is presented.

3.4.1 Mathematical Review – Resonant Frequency Sensitivity

The equation of motion of an undamped N-DOF discrete system under a free vibration condition is given by, $\mathbf{M}\ddot{\mathbf{u}} + \mathbf{K}\mathbf{u} = 0$, where **M** and **K** represent the finite element mass and stiffness distributions, and **u** is the N-DOF time-domain response vector in the physical coordinates of the system. Substitution of the homogeneous solution, $\mathbf{u} = \mathbf{U}e^{i\omega t}$, back into the equation of motion, results in the following relationship: $\mathbf{K}\mathbf{U} = \omega^2\mathbf{M}\mathbf{U}$. The values of ω and **U** that satisfy this equation are the natural frequencies and mode shapes of the system. The eigenvalue form of this equation is,

$$\mathbf{K}\{\phi\}_r = \lambda_r \mathbf{M}\{\phi\}_r \,, \tag{3.6}$$

where, λ_r ≡ eigenvalue of the r^{th} mode,

$\{\phi\}_r$ ≡ eigenvector, or mode shape, of the r^{th} mode.

The partial derivative of equation (3.6) with respect to some damage parameter, denoted as *a*, yields the following expression after some rearrangement,

$$\frac{\partial \lambda_r}{\partial a} = \frac{\{\phi\}_r^T \left(\frac{\partial \mathbf{K}}{\partial a} - \lambda_r \frac{\partial \mathbf{M}}{\partial a} \right) \{\phi\}_r}{\{\phi\}_r^T \mathbf{M} \{\phi\}_r} \,. \tag{3.7}$$

If it can be assumed that the damage condition does not affect the mass matrix, such that $\partial\mathbf{M}/\partial a = 0$, and if the mode shapes are mass-normalized (i.e. $\{\phi\}^T \mathbf{M}\{\phi\} = 1$), then equation (3.7) can be simplified [12] to,

$$\frac{\partial \lambda_r}{\partial a} = \{\phi\}_r^T \frac{\partial \mathbf{K}}{\partial a} \{\phi\}_r \,. \tag{3.8}$$

Equation (3.8) gives the rate of change of the r^{th} eigenvalue with respect to some selected damage parameter. Similarly, the rate of change can be determined with respect to each of many parameters. The total change of the r^{th} eigenvalue as a result of changes in multiple parameters can be represented by the first order Taylor series approximation given as,

$$\Delta\lambda_{\mathbf{r}} = \frac{\partial\lambda_{\mathbf{r}}}{\partial a_1}\Delta a_1 + \frac{\partial\lambda_{\mathbf{r}}}{\partial a_2}\Delta a_2 + \cdots + \frac{\partial\lambda_{\mathbf{r}}}{\partial a_{\mathbf{n}}}\Delta a_{\mathbf{n}} \quad , \qquad \text{for } n \text{ parameters.} \tag{3.9}$$

The eigenvalue changes for m modes and n parameters can be combined into a single matrix expression given as,

$$\{\Delta\lambda\} = \mathbf{D}\{\Delta a\} \quad , \tag{3.10}$$

$$\text{where, } \mathbf{D} = \begin{bmatrix} \phi_1^{\mathbf{T}} \dfrac{\partial \mathbf{K}}{\partial a_1}\phi_1 & \cdots & \phi_1^{\mathbf{T}} \dfrac{\partial \mathbf{K}}{\partial a_n}\phi_1 \\ \vdots & & \vdots \\ \phi_{\mathbf{m}}^{\mathbf{T}} \dfrac{\partial \mathbf{K}}{\partial a_1}\phi_{\mathbf{m}} & \cdots & \phi_{\mathbf{m}}^{\mathbf{T}} \dfrac{\partial \mathbf{K}}{\partial a_n}\phi_{\mathbf{m}} \end{bmatrix}. \tag{3.11}$$

The sensitivity matrix (**D**) can be calculated from the finite element model. Then, for some measured frequency change caused by damage, the desire is to determine the corresponding change in the damage parameters that can be then used to identify the actual damage. If the sensitivity matrix happens to be a square matrix and of full rank, then the corresponding inverse relationship is simply given by,

$$\{\Delta a\} = \mathbf{D}^{-1}\{\Delta\lambda\}. \tag{3.12}$$

Unfortunately, this is generally not the situation. There is a limited amount of resonant frequency information that is available to be measured. A typical finite

element model will have many elements, which means that many parameters are needed to differentiate the possible damage conditions. Thus, it is generally the case that $m < n$. In this case, **D** does not have a true inverse, and there is not a unique solution for $\{\Delta a\}$. It may be possible to limit the number of damage parameters under evaluation based on advanced knowledge that damage is more likely to occur in specific locations. In the situation that $m > n$, then there is more frequency information available than the number of damage parameters under evaluation, and the pseudo-inverse of **D** can be used to determine a least-squares solution for $\{\Delta a\}$.

Of course, damage that is not represented by the parameters included in the analysis will produce erroneous results. Also, the first order approximations that are used to formulate the sensitivity matrix may be sufficient for small damage, but introduce significant error for larger damages. While the use of minimum response point eigenvalue sensitivities would still be subject to the same first order approximation errors, etc, it was thought that perhaps the minimum response point frequency information could provide a means to reduce the rank deficiency problems described above. Thus, a sensitivity formulation for the eigenvalues of local response minima was examined. The mathematical approach is provided in the following sub-section.

3.4.2 Formulation for Response Minima

Recall the eigenvalue equation (2.12) that was derived in Chapter 2 for local minimum response points, and rearranged in similar form to equation (3.6) as,

$$\mathbf{A}\{\mathrm{q}\}_{\mathrm{m}} = \lambda_{\mathbf{m}}\mathbf{B}\{\mathrm{q}\}_{\mathrm{m}} \text{ , for the } m^{\text{th}} \text{ minimum response point.} \tag{3.13}$$

The partial derivative of equation (3.13) with respect to some damage parameter, denoted as *a*, after some rearrangement yields the following expression,

$$(\mathbf{A}-\lambda_{\mathbf{m}}\mathbf{B})\frac{\partial \mathbf{q}_{\mathbf{m}}}{\partial a}-\frac{\partial \lambda_{\mathbf{m}}}{\partial a}\mathbf{B}\,\mathbf{q}_{\mathbf{m}} = -\left(\frac{\partial \mathbf{A}}{\partial a}-\lambda_{\mathbf{m}}\frac{\partial \mathbf{B}}{\partial a}\right)\mathbf{q}_{\mathbf{m}}. \tag{3.14}$$

Consider also, the corresponding adjoint eigenvalue equation for the non-symmetric matrices **A** and **B**, which is expressed as,

$$(\mathbf{A}^{\mathrm{T}} - \lambda_{\mathrm{m}}\mathbf{B}^{\mathbf{T}})\mathbf{p}_{\mathrm{m}} = 0 \ , \tag{3.15}$$

where, $\mathbf{p}_{\mathrm{m}} \equiv m^{\text{th}}$ eigenvector of the adjoint problem.

If equation (3.14) is transposed, and post-multiplied by $\mathbf{p}_{\mathrm{m}}$, then the following result is obtained,

$$\frac{\partial \mathbf{q}_{\mathbf{m}}^{\mathbf{T}}}{\partial a}(\mathbf{A}^{\mathbf{T}}-\lambda_{\mathbf{m}}\mathbf{B}^{\mathbf{T}})\mathbf{p}_{\mathbf{m}}-\frac{\partial \lambda_{\mathbf{m}}}{\partial a}\mathbf{q}_{\mathbf{m}}^{\mathbf{T}}\mathbf{B}^{\mathbf{T}}\mathbf{p}_{\mathbf{m}} = -\mathbf{q}_{\mathbf{m}}^{\mathbf{T}}\left(\frac{\partial \mathbf{A}^{\mathbf{T}}}{\partial a}-\lambda_{\mathbf{m}}\frac{\partial \mathbf{B}^{\mathbf{T}}}{\partial a}\right)\mathbf{p}_{\mathbf{m}}. \tag{3.16}$$

From equation (3.15), the first term of equation (3.16) is eliminated, and after rearrangement, the eigenvalue sensitivity can be expressed as,

$$\frac{\partial \lambda_{\mathbf{m}}}{\partial a} = \frac{\mathbf{q}_{\mathbf{m}}^{\mathbf{T}}\left(\frac{\partial \mathbf{A}^{\mathbf{T}}}{\partial a}-\lambda_{\mathbf{m}}\frac{\partial \mathbf{B}^{\mathbf{T}}}{\partial a}\right)\mathbf{p}_{\mathbf{m}}}{\mathbf{q}_{\mathbf{m}}^{\mathbf{T}}\mathbf{B}^{\mathbf{T}}\mathbf{p}_{\mathbf{m}}}. \tag{3.17}$$

If it can be assumed that the damage condition does not affect the mass matrix, such that $\partial \mathbf{M} / \partial a = 0 \;\Rightarrow\; \partial \mathbf{B} / \partial a = 0$, and if the mode shapes are normalized such that $\mathbf{q}_\mathbf{m}^\mathbf{T} \mathbf{B}^\mathbf{T} \mathbf{p}_\mathbf{m} = 1$, then equation (3.17) can be simplified to,

$$\frac{\partial \lambda_\mathbf{m}}{\partial a} = \mathbf{q}_\mathbf{m}^\mathbf{T} \frac{\partial \mathbf{A}^\mathbf{T}}{\partial a} \mathbf{p}_\mathbf{m} \;\Rightarrow\; \frac{\partial \lambda_\mathbf{m}}{\partial a} = \mathbf{q}_\mathbf{m}^\mathbf{T} \mathbf{G}^\mathbf{T} \begin{bmatrix} \partial \mathbf{K} / \partial a & 0 \\ 0 & \partial \mathbf{K} / \partial a \end{bmatrix} \mathbf{T}\, \mathbf{p}_\mathbf{m} . \tag{3.18}$$

Generalized forms of the eigenvectors $\mathbf{q}_\mathrm{m}$ and $\mathbf{p}_\mathrm{m}$ can be defined by $\boldsymbol{\psi}$ and $\boldsymbol{\beta}$ as follows,

$$\boldsymbol{\psi} = \mathbf{G}\, \mathbf{q}_\mathrm{m} \text{ , and } \boldsymbol{\beta} = \mathbf{T}\, \mathbf{p}_\mathrm{m} . \tag{3.19}$$

The generalized eigenvectors are then partitioned to facilitate expansion of equation (3.18) into a form that closely resembles the resonant frequency eigenvalue sensitivity expression given by equation (3.8). The minimum response eigenvalue sensitivity can be represented as,

$$\frac{\partial \lambda_\mathbf{m}}{\partial a} = \{\psi_\mathrm{u}\}^\mathrm{T} \frac{\partial \mathbf{K}}{\partial a} \{\beta_\mathrm{u}\} + \{\psi_\ell\}^\mathrm{T} \frac{\partial \mathbf{K}}{\partial a} \{\beta_\ell\} , \tag{3.20}$$

where, $\boldsymbol{\psi} = \begin{Bmatrix} \boldsymbol{\psi}_\mathbf{u} \\ \boldsymbol{\psi}_\ell \end{Bmatrix}$, and $\boldsymbol{\beta} = \begin{Bmatrix} \boldsymbol{\beta}_\mathbf{u} \\ \boldsymbol{\beta}_\ell \end{Bmatrix}$.

Equation (3.20) gives the rate of change of the m^{th} eigenvalue with respect to some selected damage parameter. Similarly, the rate of change can be determined with respect to each of many parameters. The total change of the m^{th} eigenvalue as a result of changes in multiple parameters can be represented by the first order approximation given as,

$$\Delta \lambda_\mathbf{m} = \frac{\partial \lambda_\mathbf{m}}{\partial a_1} \Delta a_1 + \frac{\partial \lambda_\mathbf{m}}{\partial a_2} \Delta a_2 + \cdots + \frac{\partial \lambda_\mathbf{m}}{\partial a_\mathbf{n}} \Delta a_\mathbf{n} , \quad \text{for } n \text{ parameters.} \tag{3.21}$$

The eigenvalue changes for k local response minima points and n parameters can be combined into a single matrix expression given as, $\{\Delta\lambda\} = \mathbf{D}\{\Delta a\}$, from equation (3.10), except that now **D** is defined as,

$$\mathbf{D} = [\mathrm{D_{ij}}] = \{\psi_{\mathrm{u}}\}_{\mathrm{i}}^{\mathrm{T}} \frac{\partial \mathbf{K}}{\partial a_{\mathrm{j}}} \{\beta_{\mathrm{u}}\}_{\mathrm{i}} + \{\psi_{\ell}\}_{\mathrm{i}}^{\mathrm{T}} \frac{\partial \mathbf{K}}{\partial a_{\mathrm{j}}} \{\beta_{\ell}\}_{\mathrm{i}} \ , \tag{3.22}$$

for local minima point $i = 1 \ldots k$, and n parameters $j = 1 \ldots n$.

3.4.3 Analysis with Inverse Sensitivity Approach

The global stiffness matrix of a complete system is a summation of all elemental stiffness contributions. Thus, a simple, though unsophisticated, method to obtain a parameterized form for the stiffness of the damaged system is as follows,

$$\mathbf{K}_{\mathbf{damaged}} = \sum_{\mathbf{j}=1}^{\mathbf{n}} \mathrm{a}_{\mathrm{j}} \mathbf{K}_{\mathbf{j}} \ , \text{ for } n \text{ elements,} \tag{3.23}$$

where, $\mathrm{a_j} \equiv$ damage parameter for element j ($0 < \mathrm{a_j} < 1$), and

$\mathbf{K_j} \equiv$ Element stiffness matrix in the global coordinates.

Here the damage is represented as a proportional stiffness reduction in all directions within the element. This representation is referred to herein as *proportional damage*. This representation is exact for the one-dimensional spring-mass system described in Section 3.1. For finite element models of physical structures, this representation is far from exact and will introduce difficulties when used in a damage detection process.

At this point, it was desired to use the 6-DOF spring-mass system to determine the effectiveness of minimum response point information in a damage detection process

based on the sensitivity relations presented in the preceding sections. A comparative analysis was also performed through use of the resonant frequency sensitivity relations.

Since the system is comprised of six spring elements, then in theory, a total of six frequencies must be used to obtain a determinant set of equations. There are only six resonant frequencies. However, there are as many as fifteen (15) minimum response frequencies available if all possible response locations and local minima points are included. The approach was to first verify the ability to use resonant frequency information to identify location and magnitude of damage, and then demonstrate the capabilities that frequencies from response minima could provide, with the thought in mind that with actual structure only the lower frequencies will generally be predicted and measured accurately.

The results obtained for two different damage conditions are presented here. The frequencies of the damaged system were determined, and then treated as *measured* data. For each imposed damage condition, various combinations of the available frequency components were utilized in the damage detection scheme. A minimal norm solution for equation (3.12) was sought to obtain $\{\Delta a\}$ for each applied frequency set. At this time, the analysis did not include effects of measurement noise.

The first damage condition is defined as a 20% stiffness reduction of k_2, and a 10% stiffness reduction of k_4 (i.e. $a_2 = -0.20$, and $a_4 = -0.10$). The computed values of $\{\Delta a\}$, based on resonant frequency sensitivity, for this damage condition are presented in Table 3.6. Similarly, the corresponding results based on minimum response

frequency, for various frequency sets assembled from one or more response locations, are presented in Table 3.7.

When all six resonant frequencies are included in the analysis, a very good identification of the damage is obtained. The computed damage factors do not exactly match the actual applied factors because the sensitivity formulation uses only a first order approximation of the non-linear relationship between frequency and damage parameter. As expected, as the quantity of frequency data is reduced, the predicted damage coefficients begin to deviate further from the exact values. When fewer that four frequencies were used, significant differences were observed.

Table 3.6 Damage Factors (Δa) Determined for Damage Condition #1
Based on Resonant Frequency Sensitivity

Tabulation of Predicted a_i (Actual Damage: $a_2 = -0.20$ and $a_4 = -0.10$)						
a_1	a_2	a_3	a_4	a_5	a_6	Resonant Frequencies Included:
-.04	-.21	.02	-.11	.03	-.01	All 6 frequencies
-.04	-.21	.03	-.10	.03	-.02	First 5 frequencies
-.06	-.18	.03	-.12	.05	-.01	First 4 frequencies
-.10	-.14	-.01	-.06	-.00	.07	First 3 frequencies
-.09	-.10	-.08	-.03	.00	.01	First 2 frequencies

Table 3.7 Damage Factors (Δa) Determined for Damage Condition #1
Based on Minimum Response Frequency Sensitivity

Tabulation of Predicted a_i (Actual Damage: $a_2 = -0.20$ and $a_4 = -0.10$)						
a_1	a_2	a_3	a_4	a_5	a_6	Local Minima Points Included:
-.00	-.17	.05	-.12	-.01	-.05	U_6: All 5 frequencies
-.01	-.17	.06	-.12	-.01	-.05	U_6: First 4 frequencies
-.02	-.15	.06	-.14	.01	-.05	U_6: First 3 frequencies
-.07	-.05	.03	-.06	-.07	.01	U_6: First 2 frequencies
-.02	-.12	.01	-.04	-.08	-.08	U_5: All 4 frequencies
-.01	-.12	.01	-.05	-.09	-.07	U_5: First 3 frequencies
-.06	-.03	-.05	-.05	-.05	-.02	U_5: First 2 frequencies
.00	-.13	-.06	-.10	.03	-.06	U_4: All 3 frequencies
.00	-.13	-.06	-.10	.03	-.06	U_4: First 2 frequencies
-.00	-.16	-.04	-.02	.03	-.02	U_3: All 2 frequencies
-.11	-.08	.06	-.07	-.01	-.02	U_3 ... U_6: 5 frequencies ($< \omega_3$)
-.02	-.20	.01	-.10	-.00	-.02	U_3 ... U_6: 8 frequencies ($< \omega_4$)
-.10	-.07	.06	-.09	-.01	-.02	U_4 ... U_6: 4 frequencies ($< \omega_3$)
-.12	-.35	.04	.09	.02	-.03	U_4 ... U_6: 7 frequencies ($< \omega_4$)
-.03	-.17	.01	-.15	.03	-.01	U_5 and U_6: 5 frequencies ($< \omega_4$)
.01	-.18	.00	-.15	.00	-.01	U_5 and U_6: 7 frequencies ($< \omega_5$)
-.02	-.16	.05	-.14	.01	-.04	U_4 and U_6: 5 frequencies ($< \omega_4$)
-.06	-.20	.05	-.08	.03	-.04	U_4 and U_6: 6 frequencies ($< \omega_5$)

In the results presented in Table 3.7, there is indication that minimum response information can provide benefit to a damage detection process. As expected, when the frequency information from a particular response location is truncated, then the ability to properly identify the damage is diminished. The results given in the lower half of

Table 3.7, though, indicate that the combination of truncated frequency data from multiple locations can boost the accuracy in the damage prediction. One qualification, however, is that a truncated frequency set from some locations will not provide a positive contribution to the identification process. This is evident in Table 3.7 by those entries that include data from the DOF #5 response (U_5). At least for the particular damage condition tested, there is a strong trend indicated in the results that the frequency data from DOF #5 is actually detrimental to the detection process. The frequency data from this response point, when used alone, fails to provide a proper identification of the damage, and in general, seems to introduce inefficiency when combined with frequencies from other responses.

A second damage condition was generated for additional supporting results. This condition (Damage Condition #2) is defined as a 20% stiffness reduction of k_1, and a 10% stiffness reduction of k_4 (i.e. $a_1 = -0.20$, and $a_4 = -0.10$). As was done for the previous condition, results were first obtained by application of resonant frequency data. Then, the detection process was performed for various combinations of minimum response frequency data. For reference, the results are provided in Tables 3.8 and 3.9, respectively. Similar observations are gathered from these results.

Table 3.8 Damage Factors (Δa) Determined for Damage Condition #2
Based on Resonant Frequency Sensitivity

Tabulation of Predicted a_i (Actual Damage: $a_1 = -0.20$ and $a_4 = -0.10$)						
a_1	a_2	a_3	a_4	a_5	a_6	Resonant Frequencies Included:
-.24	-.00	.01	-.11	.00	.02	All 6 frequencies
-.20	.00	-.02	-.15	-.01	.04	First 5 frequencies
-.13	-.09	-.02	-.08	-.09	.01	First 4 frequencies
-.13	-.09	-.01	-.09	-.08	.00	First 3 frequencies
-.12	-.07	-.05	-.07	-.08	-.03	First 2 frequencies

Table 3.9 Damage Factors (Δa) Determined for Damage Condition #2
Based on Minimum Response Frequency Sensitivity

Tabulation of Predicted a_i (Actual Damage: a_1 = -0.20 and a_4 = -0.10)						
a_1	a_2	a_3	a_4	a_5	a_6	Local Minima Points Included:
-.20	.03	.05	-.13	-.03	-.02	U_6: All 5 frequencies
-.19	.04	.03	-.15	-.04	-.01	U_6: First 4 frequencies
-.12	-.05	.01	-.08	-.12	-.00	U_6: First 3 frequencies
-.11	-.06	.02	-.09	-.11	-.01	U_6: First 2 frequencies
-.22	.01	-.02	-.04	-.06	.00	U_5: All 4 frequencies
-.14	.02	-.06	-.08	-.09	.04	U_5: First 3 frequencies
-.11	-.04	-.02	-.08	-.11	.01	U_5: First 2 frequencies
-.24	.05	-.03	-.07	-.01	-.05	U_4: All 3 frequencies
-.20	.03	-.06	-.06	-.09	-.04	U_4: First 2 frequencies
-.09	.01	-.08	-.00	-.05	-.03	U_3: All 2 frequencies
-.20	-.10	.00	-.13	.03	.00	U_3 ... U_6: 5 frequencies ($< \omega_3$)
-.24	.05	.02	-.12	.01	-.01	U_3 ... U_6: 8 frequencies ($< \omega_4$)
-.18	-.08	.01	-.15	.03	-.00	U_4 ... U_6: 4 frequencies ($< \omega_3$)
-.41	-.20	.07	.19	.05	-.02	U_4 ... U_6: 7 frequencies ($< \omega_4$)
-.20	-.14	.02	.03	-.07	-.00	U_5 and U_6: 5 frequencies ($< \omega_4$)
-.24	-.00	.02	-.10	.01	.00	U_5 and U_6: 7 frequencies ($< \omega_5$)
-.27	.05	.07	-.12	.03	-.03	U_4 and U_6: 5 frequencies ($< \omega_4$)
-.34	-.05	.08	.01	.05	-.04	U_4 and U_6: 6 frequencies ($< \omega_5$)

3.5 Minimization of Residual Force

There are a number of approaches found in the literature that are based directly on the force balance relationship expressed in the generalized eigenvalue equation [2][13]. The eigenvalue equation, $\mathbf{K}\phi = \lambda\mathbf{M}\phi$, represents a force balance between the elastic deformation forces on the left side, and the inertial forces expressed on the right side. A similar equation exists for the damaged structure. The mass and stiffness matrices are analytically derived. The natural frequencies and mode shapes that satisfy the above equation may be measured or analytically derived quantities. In either case, a stiffness change caused by damage will create an imbalance that must be countered by a corresponding change in the frequencies and mode shapes, to return balance to the system of equations. The imbalance, or difference between the left and right sides of this generalized motion equation, is defined herein as the residual force. Additionally, any measurement errors or analytical approximations of the modal parameters will result in residual force errors that must be considered.

Damage is indicated by observed changes in the frequencies and mode shapes. An optimization problem can be defined to determine the necessary changes in the analytical stiffness and mass matrices that are necessary to minimize the residual force components. There are a variety of ways that the optimization problem can be formulated. The problem is inherently indeterminant as there are fewer equations than unknowns present. However, additional constraints can be applied in the iterative process to achieve some optimal solution.

Since similar eigenequation exists from which eigenvalues and eigenvectors can be analytically determined for points of local response minima, then a residual error approach may also be extended to minimum response. That is the interest here. A mathematical description of the residual force based on the generalized equations of motion, and the formulation of the optimization problem that was utilized in this study are presented in the following section. Then, in the subsequent section, the mathematical approach used for the extension of this approach to minimum response is given. The final section will provide a summary of analysis results and observations.

3.5.1 Formulation of Residual Force and Optimization Problem

The eigenvalue equations for the healthy and damaged states of the structure are given below as,

$$\mathbf{K}\phi = \lambda \mathbf{M}\phi \qquad \text{, for healthy structure} \tag{3.24}$$

$$\overline{\mathbf{K}}\,\overline{\phi} = \overline{\lambda}\,\overline{\mathbf{M}}\,\overline{\phi} \qquad \text{, for damaged structure} \tag{3.25}$$

$$\Rightarrow (\mathbf{K} + \Delta\mathbf{K})\overline{\phi} = \overline{\lambda}(\mathbf{M} + \Delta\mathbf{M})\overline{\phi}\,. \tag{3.26}$$

It is reasonable to assume that for most general situations, the damage condition produces no appreciable changes in the mass properties of the system, and it is assumed here that $\Delta\mathbf{M} = 0$.

K and **M** are *known* quantities derived from a finite element model of the system. The frequency changes that result from damage are relatively easy to measure. On the contrary, mode shapes are more difficult to measure with sufficient accuracy, considering that local damage produces only small changes. In addition, an expansion

process is needed to transform the measured mode shapes into the full coordinate space of the finite element model. The analytical mode shape of the healthy system can be used as an approximation for the corresponding mode shape of the damaged system. This results in an additional residual force term. With an approximation for the mode shape of the damage system, the total residual force, R_i, can be defined from equation (3.26) as,

$$\mathbf{R}_i \equiv (\mathbf{K} - \bar{\lambda}\mathbf{M})\tilde{\phi}_i + (\Delta\mathbf{K})\tilde{\phi}_i \quad , \text{ for the } i^{\text{th}} \text{ mode,} \tag{3.27}$$

where, $\tilde{\phi}_i \equiv$ approximation for the i^{th} damaged mode shape, and

$\bar{\lambda}_i \equiv$ from i^{th} measured frequency of damaged system.

The goal of this approach is to find the stiffness change, $\Delta\mathbf{K}$, such that the residual force is minimized. Since the damaged mode shapes are approximated, then some residual force will remain. For this analysis, it is assumed that the analytical mode shapes of the healthy system are reasonable approximations for the damaged shapes. The optimization process is further enhanced through update of the mode shape approximations based on intermediate values of $\Delta\mathbf{K}$.

For the 6-DOF system of this study, it is proper to represent $\Delta\mathbf{K}$ as a summation of all of the element stiffness contributions with an associated damage coefficient, α, applied for each element such that,

$$\Delta\mathbf{K} = \sum_{\mathbf{j}=1}^{\mathbf{p}} \alpha_{\mathbf{j}}\mathbf{K}_{\mathbf{j}} \quad , \text{ for } j = 1 \ldots p \text{ elements, and} \tag{3.28}$$

$\mathbf{K}_j \equiv$ Stiffness contribution of Element j.

A residual force vector can be computed for each of the measured resonant frequencies. The total force, summed over all coordinates of the model, can be represented by the square-magnitude of the residual force vector for the i^{th} mode as follows,

$$\left|\mathbf{R_i}\right|^2 = \mathbf{R_i^T R_i} = \left((\mathbf{K} - \bar{\lambda}_\mathbf{i}\mathbf{M})\tilde{\phi}_\mathbf{i} + \Delta\mathbf{K}\tilde{\phi}_\mathbf{i} \right)^\mathbf{T} \left((\mathbf{K} - \bar{\lambda}_\mathbf{i}\mathbf{M})\tilde{\phi}_\mathbf{i} + \Delta\mathbf{K}\tilde{\phi}_\mathbf{i} \right). \tag{3.29}$$

Performing the matrix transposes and multiplications, yields the following,

$$\begin{aligned}\left|\mathbf{R_i}\right|^2 = {} & \tilde{\phi}_\mathbf{i}^\mathbf{T}(\mathbf{K} - \bar{\lambda}_\mathbf{i}\mathbf{M})(\mathbf{K} - \bar{\lambda}_\mathbf{i}\mathbf{M})\tilde{\phi}_\mathbf{i} + \tilde{\phi}_\mathbf{i}^\mathbf{T}(\mathbf{K} - \bar{\lambda}_\mathbf{i}\mathbf{M})\Delta\mathbf{K}\tilde{\phi}_\mathbf{i} + \\ & + \tilde{\phi}_\mathbf{i}^\mathbf{T}\Delta\mathbf{K}(\mathbf{K} - \bar{\lambda}_\mathbf{i}\mathbf{M})\tilde{\phi}_\mathbf{i} + \tilde{\phi}_\mathbf{i}^\mathbf{T}(\Delta\mathbf{K})(\Delta\mathbf{K})\tilde{\phi}_\mathbf{i}\end{aligned} \tag{3.30}$$

$$R^2 = \sum_{\mathbf{i}=1}^{\mathbf{m}} \left|\mathbf{R_i}\right|^2 \equiv \text{square-magnitude of total residual force over } m \text{ modes.} \tag{3.31}$$

An optimization problem can be then defined, with the intention of finding an optimal stiffness change necessary to minimize the total residual force magnitude [2]. With the stiffness change represented as a function of a set of damage coefficients, the goal of the optimization procedure is to find the set of coefficients, $\{\alpha\}$, that minimize the residual force magnitude, or minimize R^2.

Analytical representations of the gradients of R^2 with respect to the damage coefficients provide more accurate determinations of step size in the solution process. The partial derivative of equation (3.30) with respect to α_j is given by,

$$\begin{aligned}\frac{\partial\left|\mathbf{R_i}\right|^2}{\partial\alpha_\mathbf{j}} = {} & \tilde{\phi}_\mathbf{i}^\mathbf{T}(\mathbf{K} - \bar{\lambda}_\mathbf{i}\mathbf{M})\mathbf{K_j}\tilde{\phi}_\mathbf{i} + \tilde{\phi}_\mathbf{i}^\mathbf{T}\mathbf{K_j}(\mathbf{K} - \bar{\lambda}_\mathbf{i}\mathbf{M})\tilde{\phi}_\mathbf{i} + \\ & + \tilde{\phi}_\mathbf{i}^\mathbf{T}\left(\mathbf{K_j}\sum_{\mathbf{p}=1}^{\mathbf{n}} \alpha_\mathbf{p}\mathbf{K_p} + \sum_{\mathbf{p}=1}^{\mathbf{n}} \alpha_\mathbf{p}\mathbf{K_p}\mathbf{K_j} \right)\tilde{\phi}_\mathbf{i}\end{aligned} \tag{3.32}$$

for mode *i*, and damage coefficient of element *j* of *n* elements.

Equation (3.32) can be further reduced to the following form,

$$\frac{\partial \left|\mathbf{R_i}\right|^2}{\partial \alpha_\mathbf{j}} = \mathrm{b_{ij}} + \mathrm{a_{ij1}}\alpha_1 + \mathrm{a_{ij2}}\alpha_2 + \cdots + \mathrm{a_{ijn}}\alpha_\mathbf{n} \tag{3.33}$$

where, $\mathrm{b_{ij}} = \widetilde{\phi}_\mathbf{i}^{\mathbf{T}}(\mathbf{K} - \overline{\lambda}_\mathbf{i}\mathbf{M})\mathbf{K_j}\widetilde{\phi}_\mathbf{i} + \widetilde{\phi}_\mathbf{i}^{\mathbf{T}}\mathbf{K_j}(\mathbf{K} - \overline{\lambda}_\mathbf{i}\mathbf{M})\widetilde{\phi}_\mathbf{i}$

$$\mathrm{a_{ijk}} = \widetilde{\phi}_\mathbf{i}^{\mathbf{T}}(\mathbf{K_j}\mathbf{K_k} + \mathbf{K_k}\mathbf{K_j})\widetilde{\phi}_\mathbf{i}$$

Based on equation (3.31), the gradients for the objective function are given by,

$$\frac{\partial R^2}{\partial \alpha_\mathbf{j}} = \sum_{\mathbf{i}=1}^{\mathbf{m}} \frac{\partial \left|\mathbf{R_i}\right|^2}{\partial \alpha_\mathbf{j}}, \text{ for } m \text{ modes.} \tag{3.34}$$

Thus, $$\frac{\partial R^2}{\partial \alpha_\mathbf{j}} = \sum_{\mathbf{i}=1}^{\mathbf{m}} \mathrm{b_{ij}} + \sum_{\mathbf{i}=1}^{\mathbf{m}} \mathrm{a_{ij1}}\alpha_1 + \sum_{\mathbf{i}=1}^{\mathbf{m}} \mathrm{a_{ij2}}\alpha_2 + \cdots + \sum_{\mathbf{i}=1}^{\mathbf{m}} \mathrm{a_{ijn}}\alpha_\mathbf{n} \ . \tag{3.35}$$

$$\Rightarrow \qquad \frac{\partial R^2}{\partial \alpha_\mathrm{j}} = \hat{\mathrm{b}}_\mathrm{j} + [\,\hat{\mathrm{a}}_{\mathrm{j1}}\ \ \hat{\mathrm{a}}_{\mathrm{j2}}\ \cdots\ \hat{\mathrm{a}}_{\mathrm{jn}}\,]\{\alpha\}\ , \tag{3.36}$$

$$\text{where, } \hat{\mathrm{b}}_\mathrm{j} = \sum_{\mathrm{i}=1}^{\mathrm{m}} \mathrm{b_{ij}} \quad \text{, and , } \hat{\mathrm{a}}_\mathrm{jk} = \sum_{\mathrm{i}=1}^{\mathbf{m}} \mathrm{a_{ijk}}\ .$$

The final optimization problem statement can be formulated as follows,

$$\text{Find } \alpha_\mathrm{j} \text{ to minimize } R^2 = \sum_{\mathbf{i}=1}^{\mathbf{m}} \left|\mathbf{R_i}\right|^2 \text{, for } m \text{ modes,} \tag{3.37}$$

For, $\left|\mathbf{R_i}\right|^2$ $\equiv$ by Equation (3.30) ,

$\dfrac{\partial R^2}{\partial \alpha_\mathrm{j}}$ $\equiv$ by Equation (3.36),

$\Delta\mathbf{K}$ $\equiv$ by Equation (3.28),

$\tilde{\phi}$ $\equiv$ by the following: $(\mathbf{K}+\Delta\mathbf{K})\tilde{\phi} = \bar{\lambda}\mathbf{M}\tilde{\phi}$.

Subject to the constraints: 1) $\alpha_j \le 0$,

2) $\left|\Delta\lambda_{\text{measured}} - \Delta\lambda_{\text{analysis}}\right| < \varepsilon$, where $\varepsilon \equiv$ tolerance

3.5.2 Formulation of Residual Error for Response Minima

A *residual error* relationship was established from the response minima eigenvalue equation, just as was done in the previous section for residual force in the modal eigenvalue equation. Once established, it was then possible to conduct comparative analyses on various generated damage conditions for evaluation of the performance of minimum response information in this type of damage detection process.

Recall the response minima eiqenvalue equation that was presented in Chapter 2: $(\mathbf{A}-\lambda\mathbf{B})\mathbf{q} = 0$, where the eigenvalues (λ) represent the squared frequency values at the points of local response minima. For a damaged system, the eigenvalue equation can be expanded as follows,

$$\left(\mathbf{A}+\Delta\mathbf{A}-\bar{\lambda}(\mathbf{B}+\Delta\mathbf{B})\right)\bar{\mathbf{q}} = 0,$$

$$\Rightarrow\ (\mathbf{A}-\bar{\lambda}\mathbf{B})\,\bar{\mathbf{q}} + (\Delta\mathbf{A}-\bar{\lambda}\Delta\mathbf{B})\,\bar{\mathbf{q}} = 0. \qquad (3.38)$$

where, $\bar{\lambda}$ and $\bar{\mathbf{q}}$ are the eigenvalues and eigenvectors of the damage system.

The matrix quantities $\Delta\mathbf{A}$ and $\Delta\mathbf{B}$ can be written in terms of the mass and stiffness matrices (see Chapter 2), as follows,

$$\Delta\mathbf{A} = \mathbf{T}^{\mathrm{T}}\begin{bmatrix} \Delta\mathbf{K} & 0 \\ -\Delta\mathbf{M} & \Delta\mathbf{K} \end{bmatrix}\mathbf{G}\,, \text{ and, } \Delta\mathbf{B} = \mathbf{T}^{\mathrm{T}}\begin{bmatrix} \Delta\mathbf{M} & 0 \\ 0 & \Delta\mathbf{M} \end{bmatrix}\mathbf{G}\,. \tag{3.39}$$

The assumption that local structural damage will not produce any appreciable changes to the mass properties of the system will be applied here just as was done in the previous section. Thus, it is assumed that $\Delta\mathbf{M} = 0$. It is not practical to obtain measurements of the eigenvectors from the damaged structure. The approach taken here is to use approximations for the eigenvectors of the damaged system. These approximated eigenvectors are denoted as $\tilde{\mathbf{q}}$. These assumptions are combined with equations (3.38) and (3.39) to obtain an expression for the residual error given by,

$$\mathbf{R}_{\mathbf{i}} = (\mathbf{A} - \bar{\lambda}_{\mathbf{i}}\mathbf{B})\,\tilde{\mathbf{q}}_{\mathbf{i}} + \mathbf{T}^{\mathrm{T}}\begin{bmatrix} \Delta\mathbf{K} & 0 \\ 0 & \Delta\mathbf{K} \end{bmatrix}\mathbf{G}\tilde{\mathbf{q}}_{\mathbf{i}}\,, \tag{3.40}$$

for the i^{th} minimum response point.

Equation (3.40) is very similar to the residual force definition given by equation (3.27). The *system matrices*, **A** and **B**, are determined from the analytical model. Measurements of the minimum response frequencies from the damaged structure provide knowledge of the eigenvalues, $\bar{\lambda}$. The eigenvectors of the healthy system will be used as the initial approximation for the damaged system eigenvectors.

The proportional damage model, represented by equation (3.28), was used here to define the stiffness change, $\Delta\mathbf{K}$, in terms of the elemental stiffness contributions and associated scaling factors, $\{\alpha\}$. A residual error vector is computed for each minimum response point included in the analysis, which may include points from multiple measurement locations. The magnitude of the error vector represents a summation of

the error over all coordinates of the model. At the risk of being too repetitive, the residual error for each mode is defined as follows,

$$\left|\mathbf{R_i}\right|^2 = \mathbf{R_i^T R_i}\text{, for the } i^{\text{th}} \text{ point of minimum response} \tag{3.41}$$

$$\begin{aligned}\Rightarrow \quad \left|\mathbf{R_i}\right|^2 = \; & \tilde{\mathbf{q}}_\mathbf{i}^\mathbf{T}(\mathbf{A}^\mathbf{T} - \bar{\lambda}_\mathbf{i}\mathbf{B}^\mathbf{T})(\mathbf{A} - \bar{\lambda}\mathbf{B})\,\tilde{\mathbf{q}} + \\ & + \tilde{\mathbf{q}}_\mathbf{i}^\mathbf{T}(\mathbf{A}^\mathbf{T} - \bar{\lambda}_\mathbf{i}\mathbf{B}^\mathbf{T})\mathbf{T}^\mathbf{T}\begin{bmatrix}\Delta\mathbf{K} & 0\\ 0 & \Delta\mathbf{K}\end{bmatrix}\mathbf{G}\,\tilde{\mathbf{q}} + \\ & + \tilde{\mathbf{q}}_\mathbf{i}^\mathbf{T}\mathbf{G}^\mathbf{T}\begin{bmatrix}\Delta\mathbf{K} & 0\\ 0 & \Delta\mathbf{K}\end{bmatrix}\mathbf{T}(\mathbf{A} - \bar{\lambda}\mathbf{B})\tilde{\mathbf{q}} + \\ & + \tilde{\mathbf{q}}_\mathbf{i}^\mathbf{T}\mathbf{G}^\mathbf{T}\begin{bmatrix}\Delta\mathbf{K} & 0\\ 0 & \Delta\mathbf{K}\end{bmatrix}\mathbf{T}\mathbf{T}^\mathbf{T}\begin{bmatrix}\Delta\mathbf{K} & 0\\ 0 & \Delta\mathbf{K}\end{bmatrix}\mathbf{G}\,\tilde{\mathbf{q}}\;.\end{aligned} \tag{3.42}$$

Some simplification of equation (3.42) can be made through the following definitions,

$$\mathbf{U_i} = (\mathbf{A} - \bar{\lambda}\mathbf{B})\,\tilde{\mathbf{q}}_\mathbf{i}\;,\quad \mathbf{V_i} = \mathbf{T}(\mathbf{A} - \bar{\lambda}\mathbf{B})\,\tilde{\mathbf{q}}_\mathbf{i}\;,\quad \mathbf{P_i} = \mathbf{G}\,\tilde{\mathbf{q}}_\mathbf{i}\;,\text{ and } \mathbf{T}\mathbf{T}^\mathbf{T} = \mathbf{I}\,. \tag{3.43}$$

$$\begin{aligned}\Rightarrow \left|\mathbf{R_i}\right|^2 = \; & \mathbf{U_i^T U_i} + \mathbf{V_i^T}\begin{bmatrix}\Delta\mathbf{K} & 0\\ 0 & \Delta\mathbf{K}\end{bmatrix}\mathbf{P_i} + \mathbf{P_i^T}\begin{bmatrix}\Delta\mathbf{K} & 0\\ 0 & \Delta\mathbf{K}\end{bmatrix}\mathbf{V_i} + \\ & + \mathbf{P_i^T}\begin{bmatrix}\Delta\mathbf{K} & 0\\ 0 & \Delta\mathbf{K}\end{bmatrix}\begin{bmatrix}\Delta\mathbf{K} & 0\\ 0 & \Delta\mathbf{K}\end{bmatrix}\mathbf{P_i}\end{aligned} \tag{3.44}$$

The vectors $\mathbf{V}_\mathrm{i}$ and $\mathbf{P}_\mathrm{i}$ for an *N*-DOF system are of length 2*N*, and may be partitioned into upper and lower components with each of length *N*. Equation (3.44) can then be expressed with these partitioned vector quantities as follows,

$$\left|\mathbf{R_i}\right|^2 = \mathbf{U_i^T U_i} + \{V_u\}_i^T \Delta\mathbf{K} \{P_u\}_i + \{V_\ell\}_i^T \Delta\mathbf{K} \{P_\ell\}_i + \{P_u\}_i^T \Delta\mathbf{K} \{V_u\}_i + \\ + \{P_\ell\}_i^T \Delta\mathbf{K} \{V_\ell\}_i + \{P_u\}_i^T \Delta\mathbf{K}\,\Delta\mathbf{K} \{P_u\}_i + \{P_\ell\}_i^T \Delta\mathbf{K}\,\Delta\mathbf{K} \{P_\ell\}_i \tag{3.45}$$

where, $\mathbf{V} = \begin{Bmatrix} \mathbf{V_u} \\ \mathbf{V_\ell} \end{Bmatrix}$, and $\mathbf{P} = \begin{Bmatrix} \mathbf{P_u} \\ \mathbf{P_\ell} \end{Bmatrix}$.

Also, the gradients of the square-magnitude residual error vectors with respect to the damage coefficients defined by equation (3.28) are computed as follows,

$$\frac{\partial\left|\mathbf{R_i}\right|^2}{\partial\alpha_\mathbf{j}} = c_{ij} + \sum_{\mathbf{p}=1}^{\mathbf{n}} \alpha_\mathbf{p} \{P_u\}_i^T \mathbf{K_j K_p} \{P_u\}_i + \sum \alpha_\mathbf{p} \{P_u\}_i^T \mathbf{K_p K_j} \{P_u\}_i + \\ + \sum_{p=1}^{\mathbf{n}} \alpha_p \{P_\ell\}_i^T \mathbf{K_j K_p} \{P_\ell\}_i + \sum_{\mathbf{p}=1}^{\mathbf{n}} \alpha_\mathbf{p} \{P_\ell\}_i^T \mathbf{K_p K_j} \{P_\ell\}_i \tag{3.46}$$

for *n* elements, and where,

$$c_{ij} = \{V_u\}_i^T \mathbf{K_j} \{P_u\}_i + \{V_\ell\}_i^T \mathbf{K_j} \{P_\ell\}_i + \{P_u\}_i^T \mathbf{K_j} \{V_u\}_i + \{P_\ell\}_i^T \mathbf{K_j} \{V_\ell\}_i \tag{3.47}$$

Equation (3.46) can be further simplified into a matrix form, given by,

$$\frac{\partial\left|\mathbf{R_i}\right|^2}{\partial\alpha_\mathbf{j}} = c_{ij} + [d_{ij1}\ \ d_{ij2}\ \cdots\ d_{ijn}]\{\alpha\}\ , \tag{3.48}$$

where, $d_{ijk} = \{P_u\}_i^T (\mathbf{K_j K_k} + \mathbf{K_k K_j}) \{P_u\}_i + \{P_\ell\}_i^T (\mathbf{K_j K_k} + \mathbf{K_k K_j}) \{P_\ell\}_i$

for the i^{th} response point, the j^{th} damage coefficient, over $k = 1 \ldots n$ elements.

Summing the contributions of residual error over all minimum response point frequencies yields a total squared-magnitude error that is given by,

$R^2 = \sum_{\mathbf{i}=1}^{\mathbf{m}} \left| \mathbf{R_i} \right|^2$, for *m* points of local minimum response.

$$\Rightarrow \frac{\partial R^2}{\partial \alpha_j} = \hat{c}_j + [\hat{d}_{j1} \;\; \hat{d}_{j2} \;\; \cdots \;\; \hat{d}_{jn}]\{\alpha\} \;, \tag{3.49}$$

where, $\hat{c}_j = \sum_{\mathbf{i}=1}^{\mathbf{m}} c_{ij}$, and $\hat{d}_{jk} = \sum_{\mathbf{i}=1}^{\mathbf{m}} d_{ijk}$.

The final optimization problem statement can be formulated in precisely the same manner as that given in the previous section based on residual force in the modal eigenvalue equation, and is given by,

Find α_j to minimize $R^2 = \sum_{\mathbf{i}=1}^{\mathbf{m}} \left| \mathbf{R_i} \right|^2$, for *m* local minima points, (3.50)

for, $\left| \mathbf{R_i} \right|^2$ ≡ by Equation (3.45) ,

$\frac{\partial R^2}{\partial \alpha_j}$ ≡ by Equation (3.49),

$\Delta \mathbf{K}$ ≡ by Equation (3.28),

$\tilde{\mathbf{q}}$ ≡ by the following: $(\mathbf{A} + \Delta\mathbf{A})\,\tilde{\mathbf{q}} = \bar{\lambda}\mathbf{B}\,\tilde{\mathbf{q}}$.

Subject to the constraints: 1) $\alpha_j \le 0$,

2) $\left| \Delta\lambda_{\mathbf{measured}} - \Delta\lambda_{\mathbf{analysis}} \right| < \varepsilon$, where $\varepsilon \equiv$ tolerance.

3.5.3 Optimization Based on Residual Error

Numerous damage conditions were generated for the 6-DOF spring-mass system and optimization solutions were obtained through use of modal parameter data, then through use of minimum response point data. The corresponding optimization

problems are defined by equations (3.37) and (3.50), respectively. One of the necessary conditions for the stated optimization problems is the update of the eigenvector approximations in the iterative solution process. This update was conducted by resolving the associated eigenvalue problem with an updated stiffness matrix. For a general formulation, this is not a desirable approach, and that is acknowledged here. This would result in a computationally expensive process for large models. However, the goal of this research is to first determine whether or not minimum response data could provide useful information to a damage detection process. Thus, a brute force approach was used.

The algorithm *fmincon* provided in the MATLAB Optimization Toolbox was utilized to perform the iterative solution steps. This algorithm uses a Sequential Quadratic Programming method to provide for the constrained minimization of the supplied objective function. The first-order gradients of the objective function were also supplied to the algorithm to improve convergence of the solutions.

Solutions were obtained for all six possible cases of single-element damage, and two cases of multiple-element damage. For each damage condition, multiple solutions were obtained to evaluate the damage detection process with varied degrees of data set truncation. The frequency changes induced by the test damage condition were computed directly, and were treated as measured data. No simulation of measurement noise was included for this part of the study.

The results corresponding to the use of *measured* resonant frequency data are provided in Table 3.10. For these tabulated results, the predicted damage coefficients

are shown in comparison to those that were used to produce the actual damage condition. In the column on the far right side it is indicated which *measured* data components were included for the damage prediction. The damage predictions that failed to meet acceptable agreement with the known actual condition are indicated in the shaded sections of Table 3.10.

Table 3.10 Damage Identification by Minimization of Residual Force through Optimization with Resonant Frequency Input

Predicted Damage						**Actual Damage**	**Frequency Data Sets Tested**
α_1	**α_2**	**α_3**	**α_4**	**α_5**	**α_6**		
-.20	0	0	0	0	0	$\alpha_1 = -0.2$	1) All 6 Freqs
0	-.20	0	0	0	0	$\alpha_2 = -0.2$	2) First 5 Freqs
0	0	-.20	0	0	0	$\alpha_3 = -0.2$	
0	0	0	-.20	0	0	$\alpha_4 = -0.2$	3) First 4 Freqs
0	0	0	0	-.20	0	$\alpha_5 = -0.2$	
0	0	0	0	0	-.20	$\alpha_6 = -0.2$	
-.10	**-.08**	**-.03**	**-.06**	**-.05**	**0**	**$\alpha_1 = -0.2$**	First 3 Freqs
0	-.20	0	0	0	0	$\alpha_2 = -0.2$	
0	0	-.20	0	0	0	$\alpha_3 = -0.2$	
0	0	0	-.20	0	0	$\alpha_4 = -0.2$	
0	0	0	0	-.20	0	$\alpha_5 = -0.2$	
0	0	0	0	0	-.20	$\alpha_6 = -0.2$	
-.10	**-.07**	**-.05**	**-.05**	**-.05**	**-.02**	**$\alpha_1 = -0.2$**	First 2 Freqs
-.02	**-.12**	**-.11**	**0**	**0**	**0**	**$\alpha_2 = -0.2$**	
0	0	-.20	0	0	0	$\alpha_3 = -0.2$	
-.06	**-.01**	**-.00**	**-.05**	**-.07**	**-.03**	**$\alpha_4 = -0.2$**	
0	**0**	**0**	**-.01**	**-.17**	**-.09**	**$\alpha_5 = -0.2$**	
0	0	0	0	0	-.20	$\alpha_6 = -0.2$	
0	-.20	0	-.20	0	0	$\alpha_2 = -0.2$, and $\alpha_4 = -0.2$	All 6 Freqs
0	-.20	0	-.20	0	0	$\alpha_2 = -0.2$, and $\alpha_4 = -0.2$	First 5 Freqs
0	-.20	0	-.20	0	0	$\alpha_2 = -0.2$, and $\alpha_4 = -0.2$	First 4 Freqs
0	-.20	0	-.20	0	0	$\alpha_2 = -0.2$, and $\alpha_4 = -0.2$	First 3 Freqs
-.12	**-.10**	**-.08**	**-.06**	**-.04**	**-.01**	**$\alpha_2 = -0.2$, and $\alpha_4 = -0.2$**	First 2 Freqs
0	0	-.20	0	0	-.20	$\alpha_3 = -0.2$, and $\alpha_6 = -0.2$	First 3 Freqs
-.07	**-.06**	**-.05**	**-.03**	**-.02**	**-.01**	**$\alpha_3 = -0.2$, and $\alpha_6 = -0.2$**	First 2 Freqs

Note: Cases of incorrect damage assessment are indicated by shaded rows.

It was found that when three or more resonant frequency components were included, then the damage condition was precisely determined for all cases, with the exception of one single-element damage condition. When only two frequency components were included, the solution process failed to properly identify the damage in all but one of the conditions tested.

A similar set of results was obtained through the residual error formulation with minimum response point frequency. These results are given in Table 3.11. Frequency data from various response points were combined. However, only one force input location, DOF #6, was considered.

There are some very interesting observations from this set of results. It can be seen that with the exception of one multiple-element damage condition, that the inclusion of four or more frequency points yielded a precise prediction of the damage. This compares with the approximate success rate achieved with the inclusion of three resonant frequencies, in Table 3.10. Note also, that there were some single-element damage conditions that were successfully identified with only two minimum response point frequencies included in the process. This compares to only a single successful damage prediction when only two resonant frequencies were included. Most importantly, note that for data sets that included only the first one or two frequencies from multiple locations, the damage prediction success rate was very good. This is encouraging because in a practical application, only the modes in a limited baseband frequency range can be analytically predicted, and measured, with sufficient accuracy.

Table 3.11 Damage Identification by Minimization of Residual Error through Optimization with Minimum Response Frequency Input

Predicted Damage						Applied Damage	Frequency Data Sets Tested
α_1	α_2	α_3	α_4	α_5	α_6		
-.20	0	0	0	0	0	$\alpha_1 = -0.2$	U_1 Response 1) All 5 MR Freqs 2) First 4 MR Freqs U_2 and U_4 : 1) 2 MR Freqs each
0	-.20	0	0	0	0	$\alpha_2 = -0.2$	
0	0	-.20	0	0	0	$\alpha_3 = -0.2$	
0	0	0	-.20	0	0	$\alpha_4 = -0.2$	
0	0	0	0	-.20	0	$\alpha_5 = -0.2$	
0	0	0	0	0	-.20	$\alpha_6 = -0.2$	
-.06	**0**	**0**	**-.04**	**-.14**	**0**	**$\alpha_1 = -0.2$**	U_1 Response 3) First 3 MR Freqs
0	-.20	0	0	0	0	$\alpha_2 = -0.2$	
0	0	-.20	0	0	0	$\alpha_3 = -0.2$	
-.00	**-.17**	**-.01**	**-.02**	**-.06**	**0**	**$\alpha_4 = -0.2$**	
0	0	0	0	-.20	0	$\alpha_5 = -0.2$	
0	0	0	0	0	-.20	$\alpha_6 = -0.2$	
0	**0**	**-.01**	**0**	**-.20**	**0**	**$\alpha_1 = -0.2$**	U_1 Response 4) First 2 Freqs
0	-.20	0	0	0	0	$\alpha_2 = -0.2$	
0	0	-.20	0	0	0	$\alpha_3 = -0.2$	
-.01	**-.11**	**0**	**-.06**	**-.07**	**0**	**$\alpha_4 = -0.2$**	
0	0	0	0	-.20	0	$\alpha_5 = -0.2$	
0	**0**	**-.21**	**-.06**	**0**	**0**	**$\alpha_6 = -0.2$**	
-.20	0	0	0	0	0	$\alpha_1 = -0.2$	U_3 Response 1) All 3 Freqs
0	-.20	0	0	0	0	$\alpha_2 = -0.2$	
0	0	-.20	0	0	0	$\alpha_3 = -0.2$	
-.13	**-.19**	**-.01**	**-.03**	**0**	**0**	**$\alpha_4 = -0.2$**	
0	0	0	0	-.20	0	$\alpha_5 = -0.2$	
-.05	**0**	**-.10**	**0**	**0**	**-.16**	**$\alpha_6 = -0.2$**	
0	-.20	0	-.20	0	0	$\alpha_2 = -0.2$, and $\alpha_4 = -0.2$	U_1, All 5 Freqs
0	-.20	0	-.20	0	0	$\alpha_2 = -0.2$, and $\alpha_4 = -0.2$	U_1, First 4 Freqs
-.00	**-.31**	**-.00**	**-.02**	**-.08**	**0**	**$\alpha_2 = -0.2$, and $\alpha_4 = -0.2$**	**U_1, First 3 Freqs**
0	-.20	0	-.20	0	0	$\alpha_2 = -0.2$, and $\alpha_4 = -0.2$	U_2 and U_4 : First 2 Freqs each
0	-.20	0	-.20	0	0	$\alpha_2 = -0.2$, and $\alpha_4 = -0.2$	U1, U2, U3, and U4 : Lowest Freq each
0	0	-.20	0	0	-.20	$\alpha_3 = -0.2$, and $\alpha_6 = -0.2$	U_2 and U_4 : First 2 Freqs each
-.01	**-.00**	**-.21**	**-.01**	**-.12**	**0**	**$\alpha_3 = -0.2$, and $\alpha_6 = -0.2$**	U1, U2, U3, and U4 : Lowest Freq each

Note: Cases of incorrect damage assessment are indicated by shaded rows.

CHAPTER 4

IDENTIFICATION OF MINIMUM RESPONSE

The previous work was centered on a purely analytical spring-mass system, for which the minimum response point frequencies were calculated directly from the assembled mass and stiffness matrices. These calculated results were then treated as measured data for input into a damage identification process. In practical application, minimum response point information must be obtained from measured response data. Thus, it was necessary to establish some procedure for identification of minimum response points directly from measured data.

4.1 Description of Response Functions

The minimum response point is, by its definition herein, a characteristic point associated with some chosen frequency-domain response function. There are many types of frequency-domain functions that may be considered, such as Frequency Response Functions (FRF), Power Spectral Density (PSD) functions, swept-sine amplitude spectrums, etc. The FRF is the most commonly used measurement for system identification purposes (experimental modal analysis), and was chosen as the basis function for this study because it is most conveniently relatable to the matrix formulation for minimum response.

There are various forms of the FRF. The *Receptance* FRF, frequently denoted as $\alpha_{ij}(\Omega)$, defines the harmonic relationship, in terms of amplitude and phase, between the displacement response of the i^{th} DOF, to the input force applied to the j^{th} DOF, as a function of excitation frequency (Ω). Similarly, the *Mobility* FRF represents the corresponding relationship between velocity response and force, and the *Accelerance* (sometimes called *Inertance*) FRF expresses the response in terms of acceleration. Note that different functions will reflect different minimum response points, so it is important to be sure that comparisons between analytical and experimental results are based on consistent functions. The displacement response function (receptance) was consistently used throughout this study.

The analytical derivation of the receptance for an N-DOF system is based on the condition of forced harmonic motion. However, with the advent of digital computing and the Fast Fourier Transform (FFT), other forms of excitation such as continuous random, burst random, or impulse, may be used as well to excite the structure in test. It is not the intent here to enter into a discussion of signal processing methods, but a brief mention of the measurement process is warranted to support a more complete description of the processed result.

Typically, the output signals from the various sensors are digitized at some fixed sample rate, sufficient to capture the frequencies of interest, over some sample period (T). The sampled time-domain values are then transformed into equivalent frequency-domain representations through application of the FFT. The result of the FFT is a complex-valued function evaluated at discrete equally spaced frequencies

($\Delta f = 1/T$ Hz). The output/input relationships are established from these results. Electrical noise will be present on the sensor output signals, and there are noise/error sources associated with the signal processing operations. Thus, an ensemble of data sample periods is collected, to provide for averaging of the frequency-domain functions. Averaged FRF spectra generally converge very rapidly to the mean values. Nevertheless, there will always be some effect of noise in the FRF measurement, and it must be kept in mind that because of assumptions involved with application of the FFT calculation, the measured FRF is only an estimate of the *true* FRF of the system.

4.2 Approach for Identification from Measured Data

Identification of minimum response points is somewhat analogous to the parameter estimation task used in modal analysis for identification of resonant frequency, damping, and modal residues. Both require identification of parameters through some curve fit procedure. However, the similarities end there.

4.2.1 Problem Description

Modal parameters are system properties, and in themselves, define the frequency response characteristics of the system. Thus, they are directly represented in the strict mathematical formulations that are fit to the measured data in the estimation process. The formulations are derived from the equations of motion, and therefore must be consistent with the physical units of the data set.

Minimum response points, on the other hand, are consequences of the system parameters, and as such, are local to each particular response location. Likewise, there is no direct formulation for the FRF in terms of minimum response point parameters. Therefore, any curve-fit formulation used to identify a minimum response point would still implicitly depend on the modal parameters.

Consider an analytically derived response function, which is free of noise. The obvious method to locate the local minima is to first determine the derivative of the function through a finite difference method. Then a search for zero-crossings would reveal the minimum and maximum response points. A similarly determined second derivative function would provide the necessary test condition to differentiate the minimum response points from maximum response points. Interpolation between frequency lines would be applied to obtain the best estimate for the frequency and amplitude values corresponding to the zero-crossing point of the derivative function. In essence, the absence of noise allows use of a linear curve-fit across a single-increment frequency span.

With the presence of noise, it is necessary to widen the span over which the curve-fit is applied, and in doing so, a linear curve-fit becomes inadequate. In addition, the level of noise in a finite difference result can be considerably amplified over that contained in the original function. As a result, the locations of zero-crossings in the derivative of a noisy function can be difficult to identify.

4.2.2 Description of Elected Approach

The immediate need for an identification process was for the planned application to beam response data. The bending modes for a uniform beam of rectangular cross-section are well separated. Upon inspection of the magnitude of a typical FRF for a beam vibration response, it is observed that the behavior of the FRF curve in the vicinity of the minimum response point is very smooth and appears quadratic in form. Thus, a rather unsophisticated approach was adopted as a first cut at this process.

Based on the observed form of the FRF curve, a crude polynomial curve fit was implemented to obtain an analytical approximation of the FRF in the vicinity of the minimum response point. Application of a curve-fit requires definition of the location and width of the frequency span to be included. Since the damage assessment process was intended to make use of a validated finite element model, then it was assumed that good estimates of the minimum response frequencies and resonant frequencies were available from the model. These estimates were employed to guide the curve-fit process. For a given analytical minimum response point (Ω_m), the resonant frequencies on either side of the point ($\omega_r < \Omega_m$ and $\omega_{r+1} > \Omega_m$), were considered in the definition of the frequency span. Arbitrarily, a starting span-width was defined as follows,

$$\textit{Frequency Span} \equiv f_l : f_u \ ,$$

where, $\qquad f_l \equiv \Omega_m - |\Omega_m - \omega_r|/2 \ , \qquad f_u \equiv \Omega_m + |\Omega_m - \omega_{r+1}|/2.$

As an example, this span is illustrated in Figure 4.1, and an expanded view is given in Figure 4.2. The resonant frequencies are clearly indicated and the minimum response point is marked.

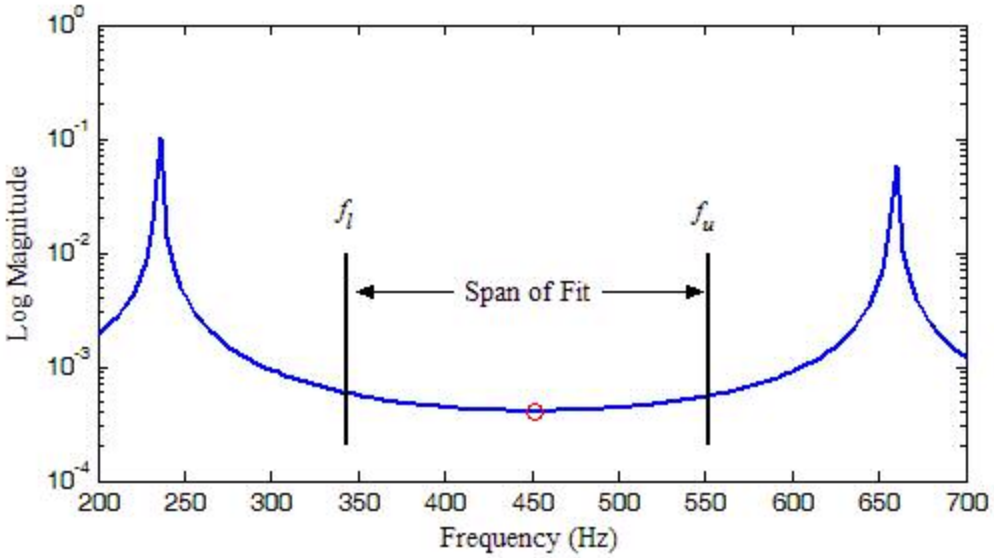

Figure 4.1 Illustration of Curve-Fit Frequency Span

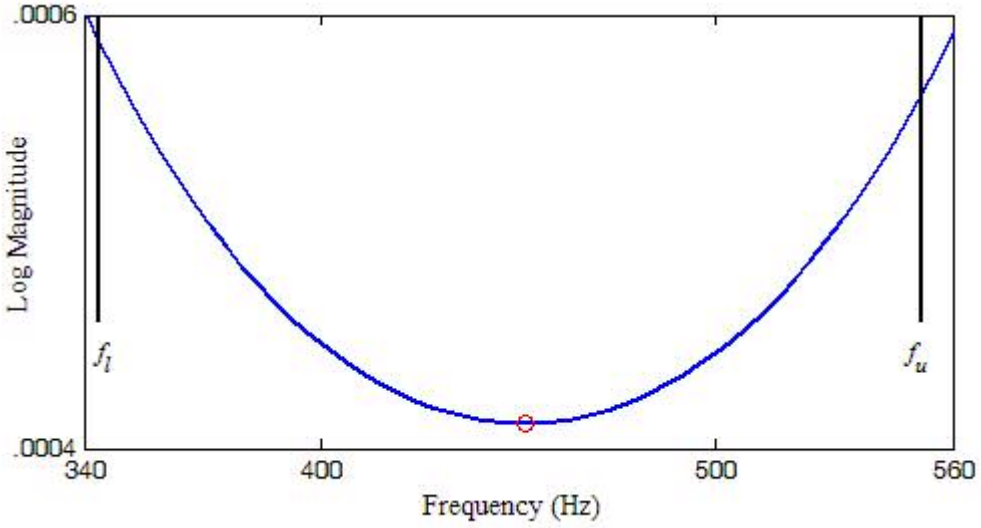

Figure 4.2 Expanded View of Curve-Fit Span

If it is assumed that damage induces only small changes to the resonant frequencies and minimum response points, and the modes are well separated, then it is assumed that the analytical frequency values for the undamaged structure will provide an equally valid definition of the frequency span for a curve-fit applied to the response from a damaged structure. Tests of this approach on simulated data from the undamaged system, and for a damaged system, were conducted for verification.

Several forms of the curve-fit function were explored. The details of this exploration are not given here, but ultimately, a fourth-order polynomial was selected to model the logarithmic magnitude of the response in terms of squared-frequencies. That is, the following form was adopted for the i^{th} point in the span,

$$y_i = log(|\alpha_i|) = c_1 + c_2 \Omega_{\mathbf{i}}^2 + c_3 \Omega_{\mathbf{i}}^4 + c_4 \Omega_{\mathbf{i}}^6 + c_5 \Omega_{\mathbf{i}}^8 . \quad (4.1)$$

The least-squares method was used to find the coefficients c. An additional modification to the procedure was incorporated to further reduce the variance error between the curve-fit and the measured values. For this modification, the frequency span was gradually squeezed toward the anticipated minimum response point, and the variance error was determined for each iteration. The iterations were continued until either reduction in the error was no longer realized, or until a minimum span width was reached. Given that the polynomial form provides accurate representation of the data, then the derivative of y with respect to frequency is easily computed, and a root solver is then used to find the frequency value that corresponds to zero slope.

A finite element beam model was used to produce simulated FRF data, for which *exact* minimum response points were known through application of the matrix

formulation described in Chapter 2. The details of this model are presented in the following chapter (Section 5.2). The procedure was applied to the simulated FRF data, and all extracted minimum response point frequency values were within three decimal points of accuracy in comparison to the exact values.

Next, a proportional damage condition (30% stiffness reduction of the root element) was created, and the corresponding frequency responses were computed for each translational coordinate. The procedure was applied to this simulated data set, with use of the undamaged frequency values to guide the extraction process. The extracted results were in excellent agreement with the exact values, as indicated in Table 4.1.

It is granted that the procedure is unsophisticated, and is not rigorously developed from fundamental equations. Nevertheless, it performs well with noise free data. A more rigorous approach could have been to extract the resonant frequencies and mode shapes from the measured data set, through one of many available modal analysis techniques, then use this modal model to synthesize FRF functions for desired locations. If the modal model were perfect, then the synthesized FRF functions would be free of noise and would provide near-exact differentiable representations of the measured functions. The minimum response points would be easily identified from these. This approach is not considered to be acceptable here, because small errors in the estimated modal parameters produce relatively larger errors in the synthesized functions away from the resonances. The contribution of out-of-band modes can only be estimated. In

addition, the modal analysis procedure typically requires much user interaction, which is inhibitory for an active health monitoring process.

Table 4.1 Evaluation of Minimum Response Frequency Extraction Process

	Minimum Response Frequency Values (Beam Model defined in Section 5.2; Input at Location 2)		
	Undamaged System	**Damaged System**	
Response Location	***Exact* Frequency**	***Exact* Frequency**	**Extracted Frequency**
13	134.5	130.29	130.26
	451.4	439.79	439.79
	988.4	968.65	968.65
	1739.4	1712.17	1712.17
12	141.8	137.15	137.12
	470.2	457.67	457.67
	1041.8	1019.56	1019.56
11	156.7	150.82	150.82
	918.4	895.84	895.80
	1714.4	1686.46	1686.46
10	383.6	367.86	367.72
	976.6	955.70	955.70
	1781.0	1751.00	1751.00
9	431.6	418.95	418.95
	1033.0	1009.21	1009.21

4.2.3 Comment on Noise Sensitivity

The question remains as to how sensitive this approach is to measurement noise. Various methods of injecting noise into the simulated data were explored, but all presented difficulty with interpretation. Typically, there will be a broadband background noise component that is relatively flat in comparison to the dynamic range exhibited in the response data, and there will be discrete frequency noise components. Examples of discrete noise include 60 Hz, and harmonics thereof, that are generated from standard electrical power used to operate test equipment. With respect to the broadband noise, displacement measurements are more susceptible at higher frequencies, and acceleration response measurements are generally more susceptible at lower frequencies.

Certainly, the addition of noise will increase the potential variance in the minimum response point frequency and amplitude values obtained in the identification process. How much noise can be tolerated also depends on the damage sensitivity of these values. The intentions were to present some results from an analytical noise sensitivity study. However, in Chapter 6, results from experimental application of the procedure are presented, and one experiment was performed to assess variance in the extracted minimum response point values due to measurement noise, and also provide a basis to judge the significance of the variance. Thus, there is no further discussion here.

CHAPTER 5

APPLICATION TO BEAM STRUCTURE

The beam structure was chosen for the next phase of this study. This provided a means for continued analytical investigation with the opportunity for experimental validation, yet not introduce undue complexity at this stage of research. It was hoped that the information gained at this stage would encourage further study on more complex structure.

First it was necessary to perform some analytical development prior to any experimental application. A finite element modeling technique was used to generate a detailed model of a cantilevered beam structure, for the simulation of damage conditions. Forced response data for numerous damage conditions were generated, and were used as simulated test data. A description of this beam model is provided in the following section.

For conduct of a damage detection process, a much more coarsely defined beam model was utilized. The relationship between the fidelity of the detailed model and that of the course model was intended to be representative of the corresponding relationship that would typically exist between an actual structure and the analytical model of that structure. A description of the course model is provided in Section 5.2. The remaining

sections of this chapter detail the various damage detection approaches that were included in this study.

5.1 Detailed FEM for Simulation of Damage

One likely form of structural damage associated with beam structure is transverse crack damage. A detailed finite element model was developed strictly for the purpose of modeling transverse crack damage, to provide a means for the generation of simulated test data. The model was assembled in a particular manner to allow simulation of transverse cracks of varied depths and locations along the length of the beam.

Ansys 5.3 (Student Edition) was used to construct the finite element model of an aluminum beam structure with a length of 13-inches, width of 1-inch, and thickness of 0.200-inch. The model was constructed of 4-node quadrilateral 2-D (ANSYS PLANE42) solid elements. Smaller sized elements were placed at locations where simulation of damage was desired. Damage was produced by direct removal of one or more of these finer scaled elements. It is acknowledged that the complete removal of the element also resulted in a very small loss of mass. However, the loss of mass was relatively tiny in comparison to the associated loss of stiffness. Also, it was anticipated that experimental validation would not be conducted on beams with true crack damage, but rather on beams damaged by narrow saw cuts. Therefore, this modeling approach maintained the most consistency with the planned experimental application. A crude illustration of the model is given in Figure 5.1.

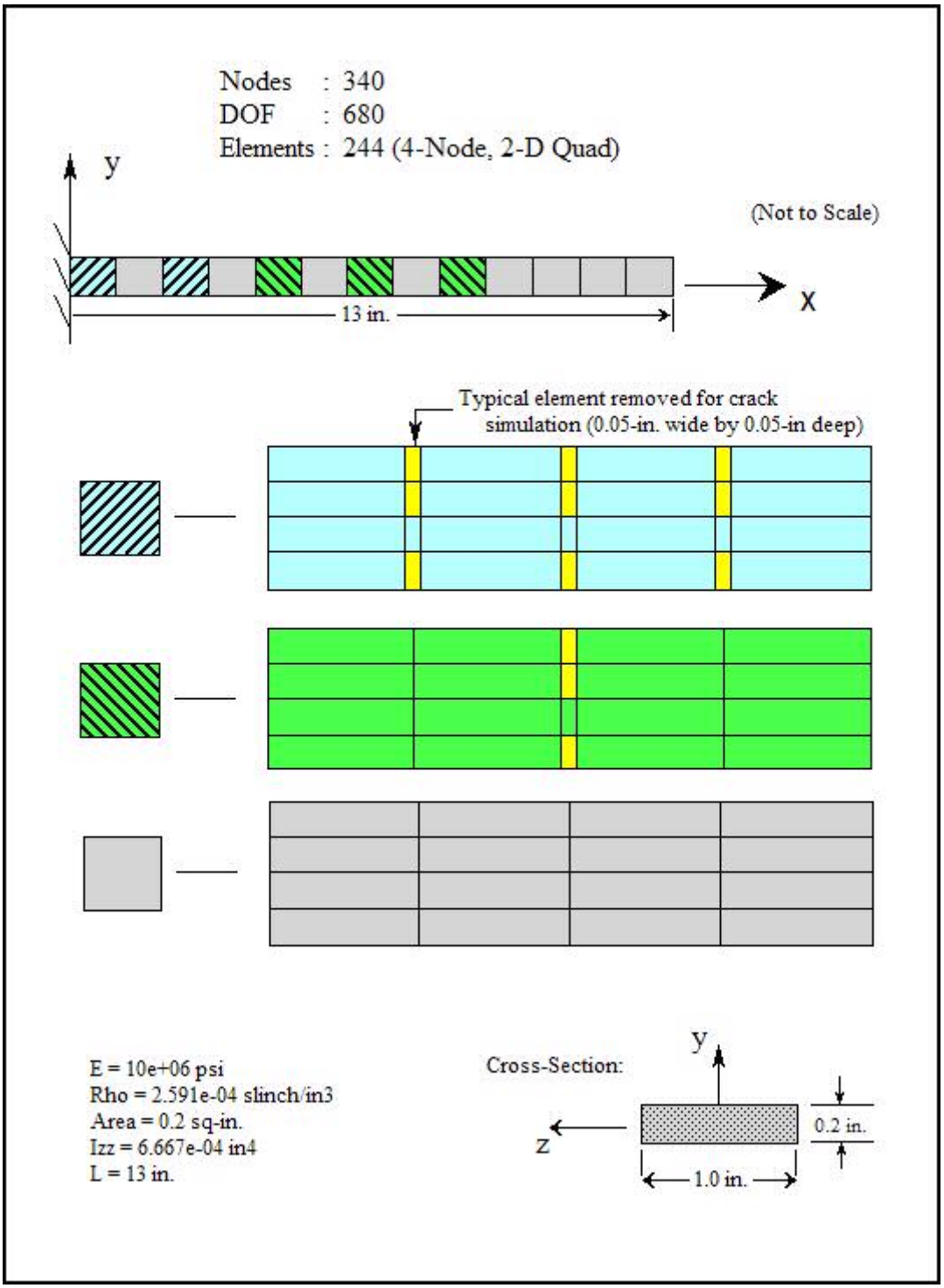

Figure 5.1 Detailed 2-D Beam Model for Damage Simulation

A total of 27 individual damage conditions were generated. These conditions are listed in Table 5.1. Elements were removed to create 0.050-inch wide slots to serve as simulations of transverse cracks. Slot depth variations were limited to 25% and 50% of the beam thickness. The slots were positioned at several distances from the root of the beam: 0.25, 0.50, 0.75, 2.25, 2.50, 2.75, 4.5, 6.5, and 8.5 inches. All of these damage cases are characterized as single-crack damages. It was intended to also create multiple-crack damage conditions, however, due to time constraints it was necessary to leave that for future work.

The fixed-free cantilever boundary conditions were used for all analysis and experimental efforts in this study. For the original baseline model, and for each damage case model, the frequencies and mode shapes of the first 10 modes were determined through an iterative modal analysis solution method (Lanczos). These modes were subsequently used to support steady-state harmonic analyses for computation of the frequency response at several node points along the length of the beam. The input loading was applied at a single location for all damage cases. Arbitrarily, a unit-amplitude oscillatory force loading was applied at a node located 2-inches from the beam root. Translational responses were computed for a subset of nodes positioned at 1-inch intervals along the top surface of the beam. These node points were intended to map to the node points of the course beam model that would be used to perform the damage identification processes.

Table 5.1 Simulated Damage Cases Produced from Detailed Beam Model

Case	Location from Root, (inch)	Crack Depth and Type	Damaged Element in Course Model
1	0.25	0.050” Top Cut	1
2	0.25	0.100” Top Cut	
3	0.25	0.050” Top/Bottom Cut	
4	0.50	0.050” Top Cut	
5	0.50	0.100” Top Cut	
6	0.50	0.050” Top/Bottom Cut	
7	0.75	0.050” Top Cut	
8	0.75	0.100” Top Cut	
9	0.75	0.050” Top/Bottom Cut	
10	2.25	0.050” Top Cut	3
11	2.25	0.100” Top Cut	
12	2.25	0.050” Top/Bottom Cut	
13	2.50	0.050” Top Cut	
14	2.50	0.100” Top Cut	
15	2.50	0.050” Top/Bottom Cut	
16	2.75	0.050” Top Cut	
17	2.75	0.100” Top Cut	
18	2.75	0.050” Top/Bottom Cut	
19	4.50	0.050” Top Cut	5
20	4.50	0.100” Top Cut	
21	4.50	0.050” Top/Bottom Cut	
22	6.50	0.050” Top Cut	7
23	6.50	0.100” Top Cut	
24	6.50	0.050” Top/Bottom Cut	
25	8.50	0.050” Top Cut	9
26	8.50	0.100” Top Cut	
27	8.50	0.050” Top/Bottom Cut	

Note: Width of All Simulated Cuts = 0.05-inch

The output frequency response data were used as simulated test data for input into a subsequent damage assessment process. It is from this data that the minimum response point values were extracted. The resonant frequencies obtained from the ANSYS modal solutions were used as direct input to the applicable assessment processes. Again, the sole purpose of this model was for the generation of simulated test data. All references to *measured* data in this chapter are in reference to the response output obtained from this detailed model.

5.2 FEM for Assessment of Damage

MATLAB was used to perform the matrix operations for generation of mass and stiffness matrices for a model constructed of 4-DOF, two-dimensional beam elements based on Bernoulli-Euler beam theory. The beam element formulation includes one translational degree-of-freedom and one rotational degree-of-freedom at each end point. A total of thirteen elements were used to model the 13-inch beam, for a total of 26 degrees-of-freedom with the fixed-end constraint applied. An illustration of the beam model is given in Figure 5.2

For reference, the general formulation of an element stiffness matrix [8], $\mathbf{K}^{\mathbf{e}}$, is given by the following integral,

$$\mathbf{K}^{\mathbf{e}} = \int \mathbf{B}^{\mathbf{T}}\mathbf{E}\mathbf{B}\, dV \tag{5.1}$$

where, **B** is the strain-displacement matrix, and **E** is the material property matrix. The strain-displacement matrix defines the relationship between displacements of the body, and the associated strains that develop as a result of those displacements. The material

property matrix contains the stiffness parameters that relate the strain distribution in the body to the corresponding stresses.

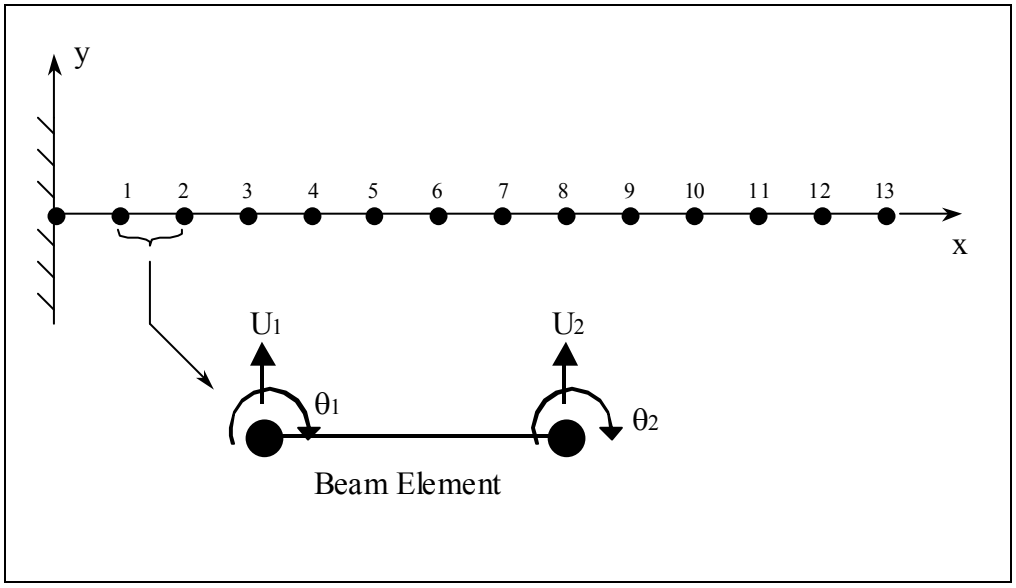

Figure 5.2 Course Beam Model for Damage Identification Process

For the special case of transverse vibration of a two-dimensional Bernoulli-Euler beam, the strain energy depends strictly on the curvature, d^2y/dx^2, of the beam. Shape functions, **N**, define the interpolation of displacements throughout the element, based solely on the nodal displacements. Therefore, from two-dimensional elastic beam theory, $\mathbf{B} = (d^2/dx^2)\mathbf{N}$, and **E** = EI, where E is the modulus of elasticity, and I is the cross-sectional area moment of inertia about the axis of bending.

The resulting element stiffness matrix for a beam element of length *L* is given by the following [8],

$$\mathbf{K}^{e} = EI\begin{bmatrix} 12/L^3 & 6/L^2 & -12/L^3 & 6/L^2 \\ 6/L^2 & 4/L & -6/L^2 & 2/L \\ -12/L^3 & -6/L^2 & 12/L^3 & -6/L^2 \\ 6/L^2 & 2/L & -6/L^2 & 4/L \end{bmatrix} \tag{5.2}$$

for the nodal degree-of-freedom displacement vector, $\mathbf{d} = [\ U_1\ \ \theta_1\ \ U_2\ \ \theta_2\ ]^T$. The nodal coordinates listed in the displacement vector, **d,** are shown in Figure 5.2. The general formula for generation of a *consistent* mass matrix, consistent because it is based on the same shape functions that form the stiffness matrix, is given by $\mathbf{M}^{e} = \int \mathbf{N}^{T}\mathbf{N}\rho\, dV$, where ρ is the mass density of the material. For the beam element with cross-sectional area, A, the mass matrix [8] is given as,

$$\mathbf{M}^{e} = \frac{\rho AL}{420}\begin{bmatrix} 156 & 22L & 54 & -13L \\ 22L & 4L^2 & 13L & -3L^2 \\ 54 & 13L & 156 & -22L \\ -13L & -3L^2 & -22L & 4L^2 \end{bmatrix} \tag{5.3}$$

5.3 Modeling of Damage

All of the damage assessment methods discussed in Chapter 3 rely on analytical representations of structural damage, so that damage assessment can be performed in a supervised fashion. Either through use of sensitivity analysis, or model perturbation, frequency changes corresponding to a set of simulated damage conditions are determined, and are then subsequently compared to measured frequency changes obtained from the damaged structure. How well a set of theoretical frequency-changes will correlate to a measured set is dependent on how representative the simulated

damage condition is to the actual damage present in the structure. Likewise, if the actual damage is not at all represented by the damage-model, then the damage identification process will likely yield a poor assessment, with considerable ambiguities.

For the theoretical one-dimensional spring-mass system used in the initial phase of this research, the application of scaling factors for proportional element damage provided exact representation. Meaningful simulation of damage in a physical structure presents considerable more challenge. The finite element modeling technique provides a discrete representation of a continuous system, for which the physical damage is likely to be highly local within one or more of the discrete element sections. The physical characteristics of the damage are not easily related to the parameters used in the formulation of the element.

As a starting point, proportional damage was assumed, and two of the damage identification techniques previously studied were applied for comparative evaluation of resonant frequency and minimum response frequency information for damage detection applications. Subsequently, an alternative model of damage was examined to provide additional comparative results, and is discussed later in this chapter.

5.4 Application of C-A Criterion for Beam Damage

The Cawley-Adams criterion method and the adaptation of the method for minimum response point frequency were presented in Section 3.2. The use of minimum response frequencies in this method provided very clear localization of all possible conditions of single-element damage in the analytical 6-DOF system. Of course, the

model of damage for perturbation of the analytical model was consistent with the *actual* damage. The interest was now to apply this same primitive approach in a more practical situation, where the actual damage cannot be accurately represented with a proportional damage model, and the minimum response point values must be extracted from measured response data.

The damage localization process was performed on each of the 27 damage cases produced from the detailed finite element model. Other than for the source of the input data, the method was applied in precisely the same manner as that described in Chapter 3 for the 6-DOF discrete system. Similarly, localization results based on resonant frequency and minimum response frequency changes were determined independently to provide for performance comparisons.

The analysis frequency range was limited to frequencies below 2000 Hz. Thus, only the first five resonant frequencies were included in the study. Likewise, the available frequency response data was truncated at 2000 Hz. Within this frequency range, a total of twenty-two minimum response points were visually detected among the thirteen measured frequency response functions. For a fair comparison of performance between resonant frequency input and minimum response frequency input, only the response measurement from the beam tip was carried forward for application of the Cawley-Adams approach. From the beam tip response measurement, all five mode responses, and four minimum response points are available.

Comparison results for the eighteen single-side crack cases are graphically presented in Figures 5.3 through 5.20.

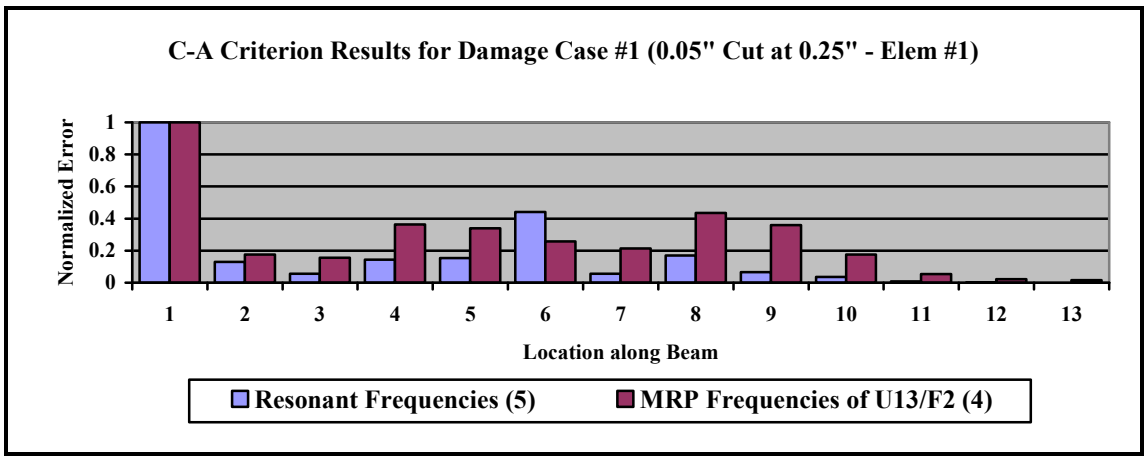

Figure 5.3 Comparison of C-A Results for Damage Case #1

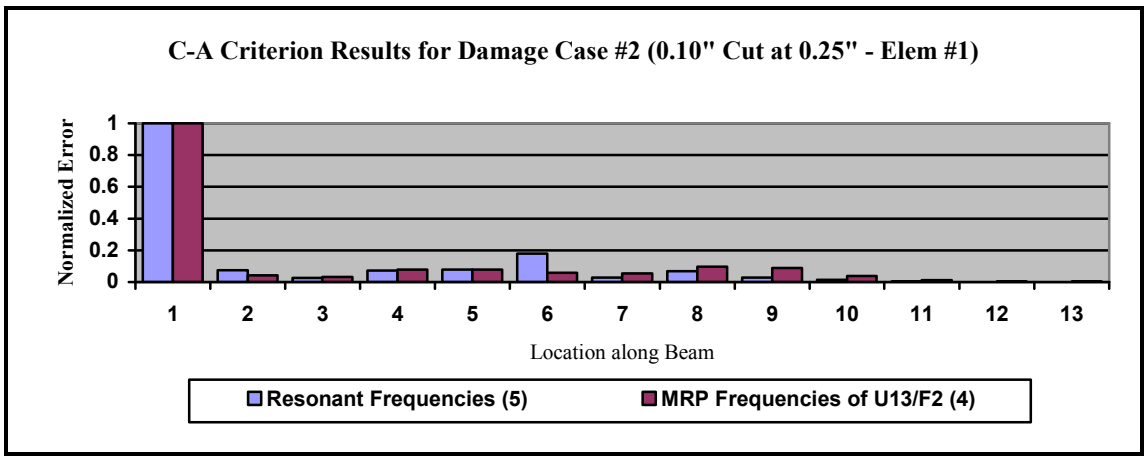

Figure 5.4 Comparison of C-A Results for Damage Case #2

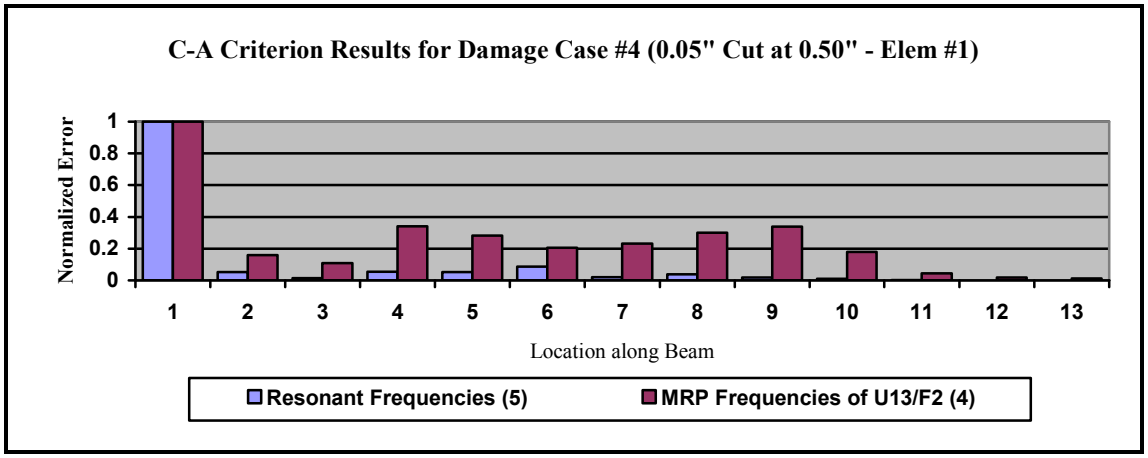

Figure 5.5 Comparison of C-A Results for Damage Case #4

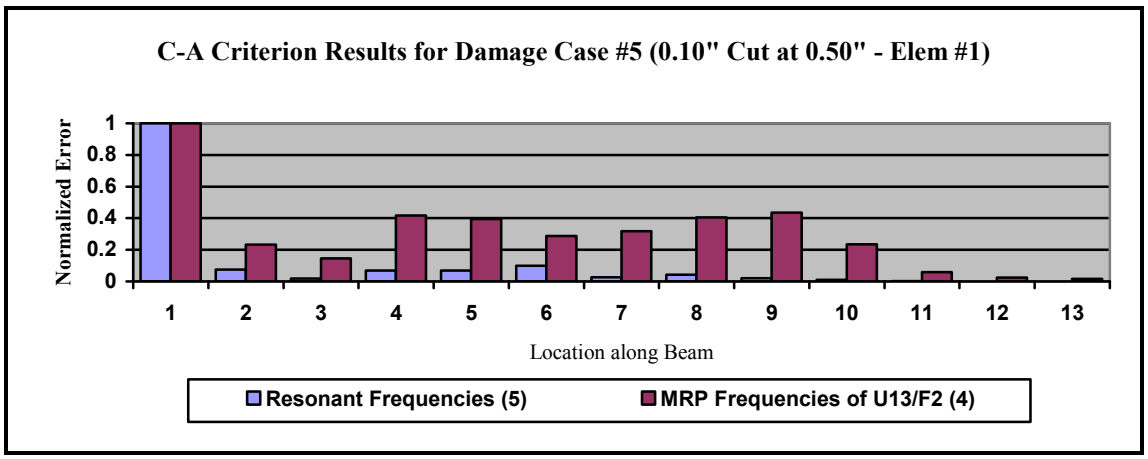

Figure 5.6 Comparison of C-A Results for Damage Case #5

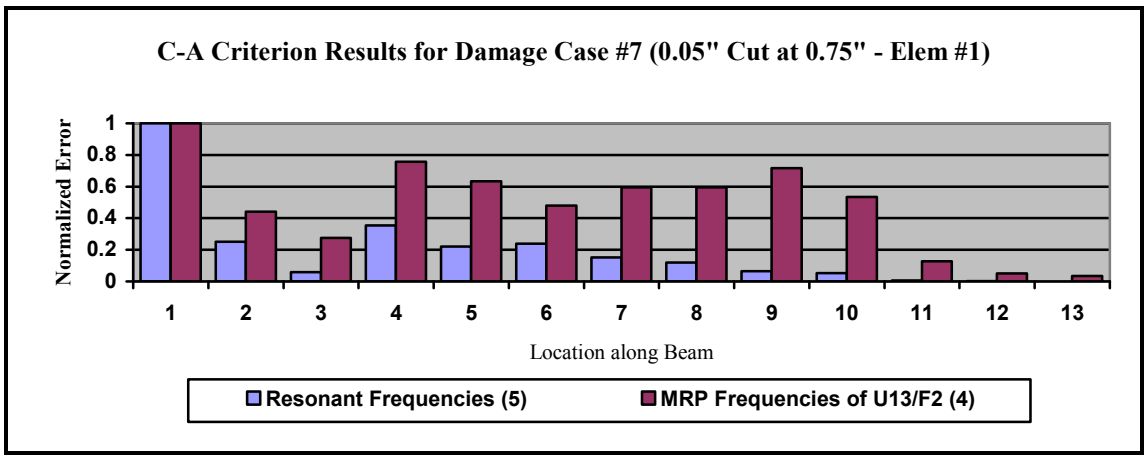

Figure 5.7 Comparison of C-A Results for Damage Case #7

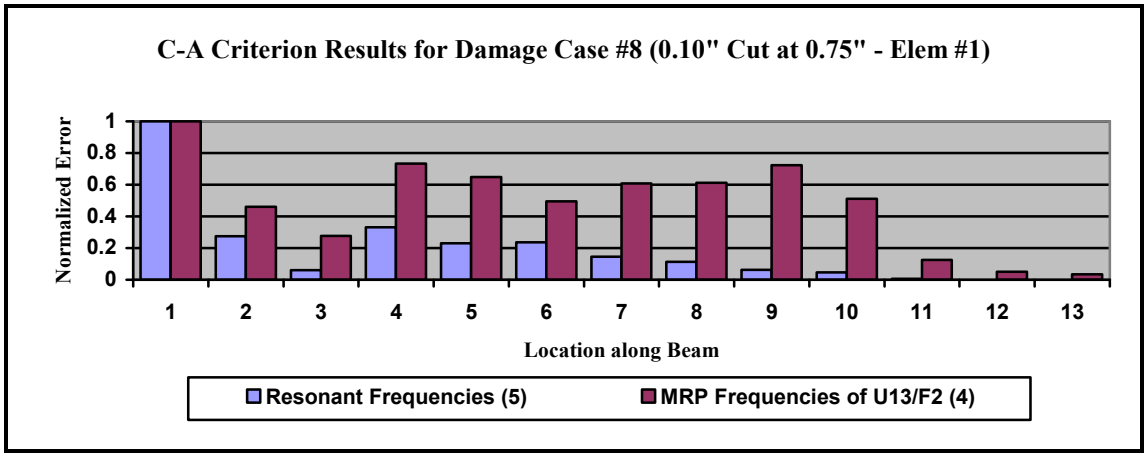

Figure 5.8 Comparison of C-A Results for Damage Case #8

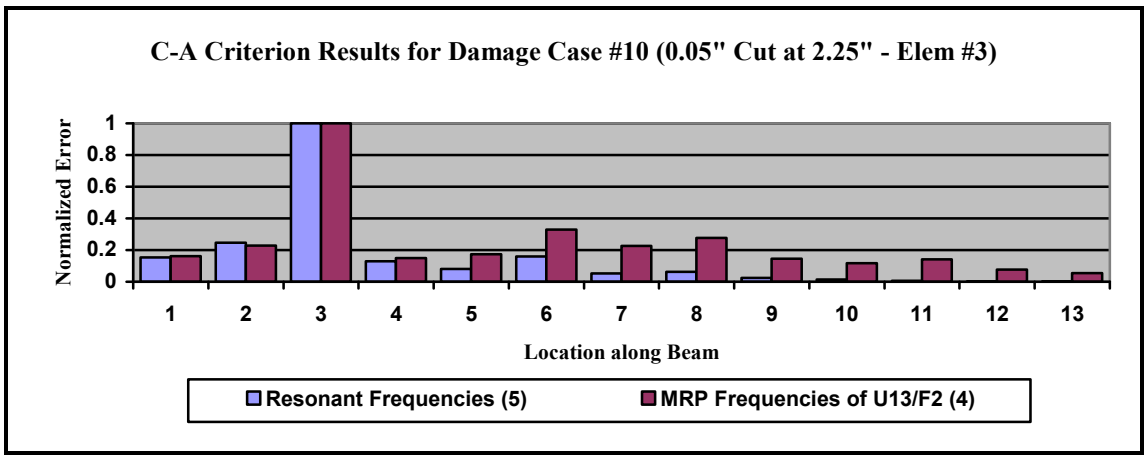

Figure 5.9 Comparison of C-A Results for Damage Case #10

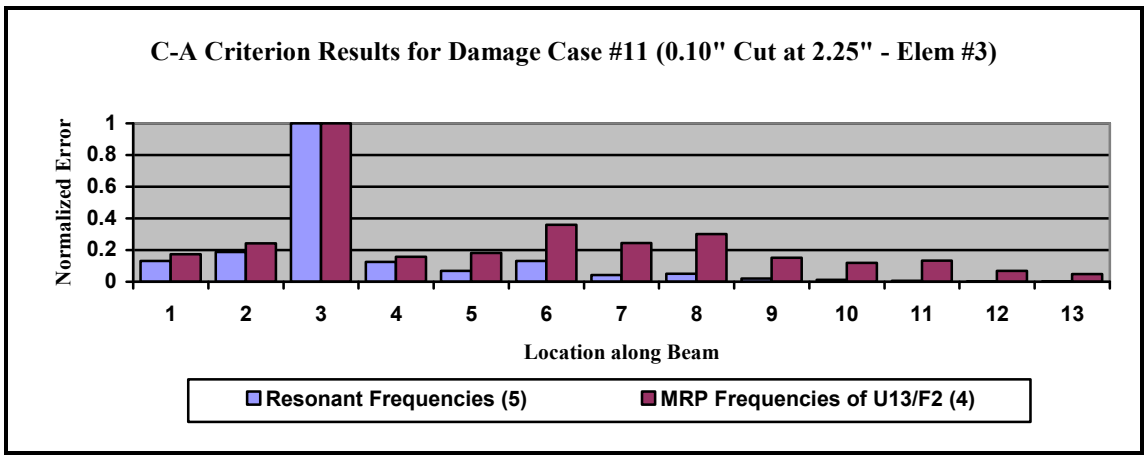

Figure 5.10 Comparison of C-A Results for Damage Case #11

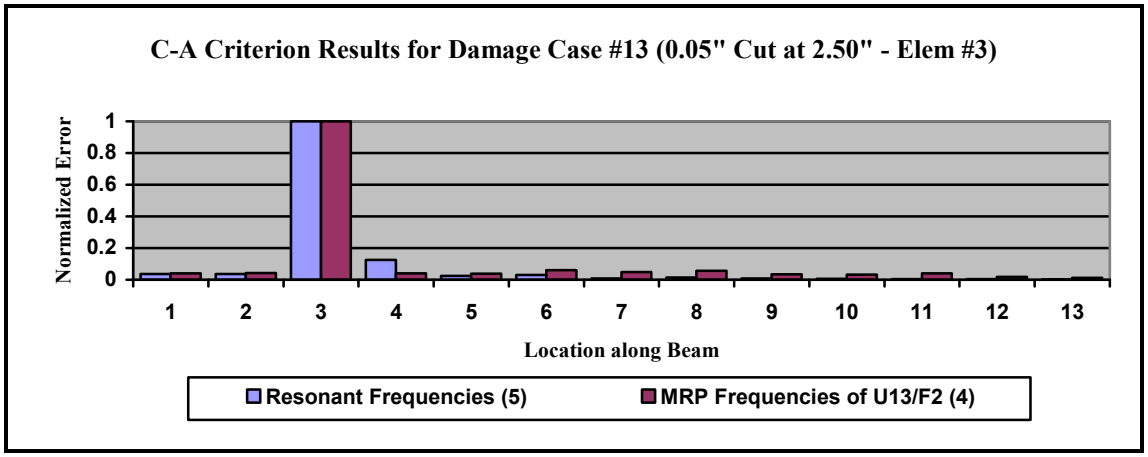

Figure 5.11 Comparison of C-A Results for Damage Case #13

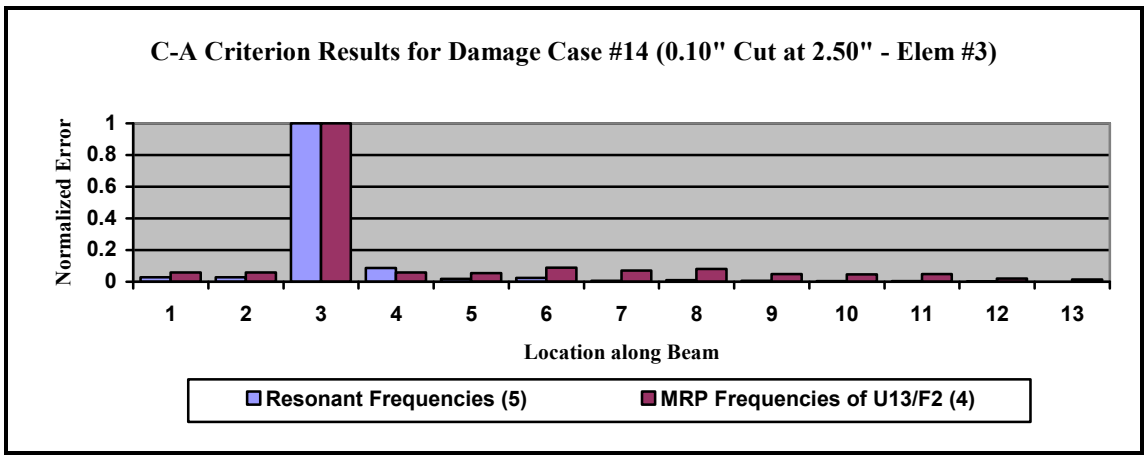

Figure 5.12 Comparison of C-A Results for Damage Case #14

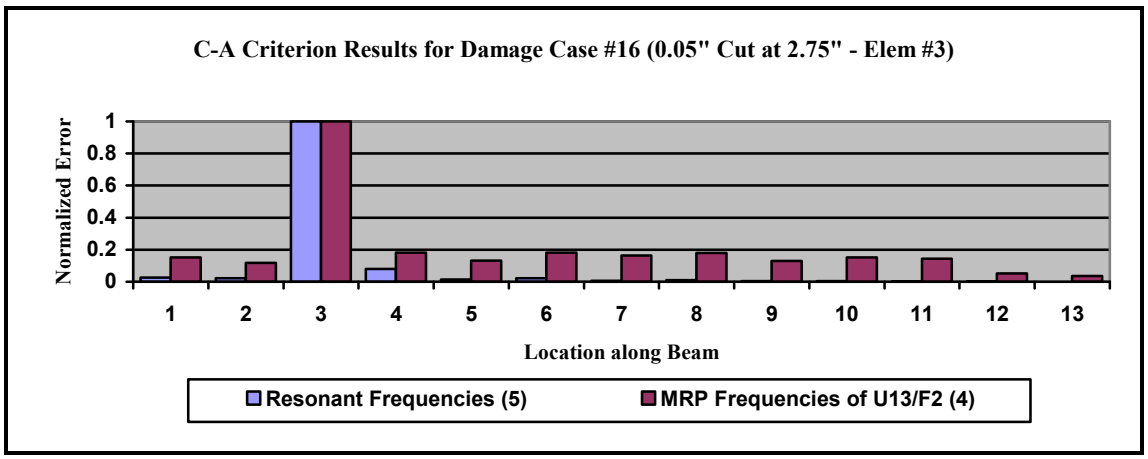

Figure 5.13 Comparison of C-A Results for Damage Case #16

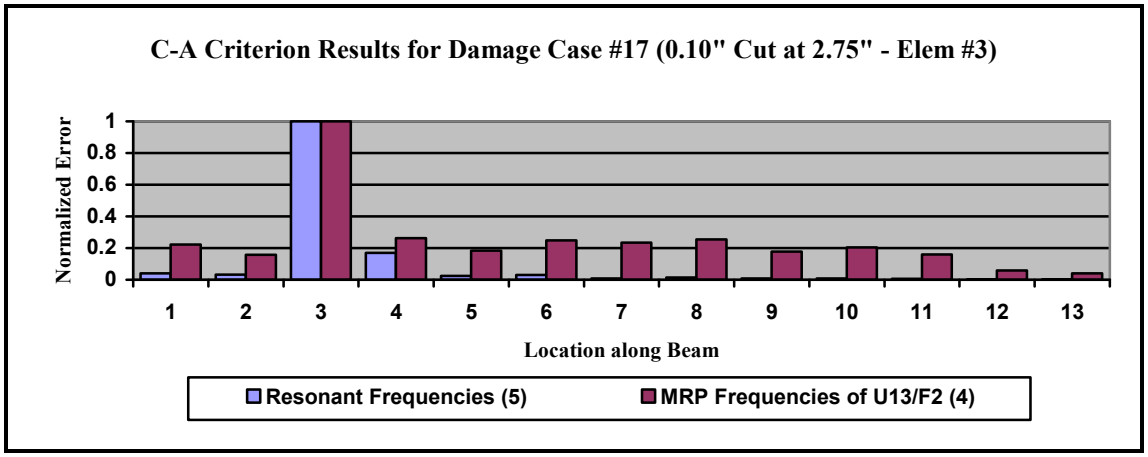

Figure 5.14 Comparison of C-A Results for Damage Case #17

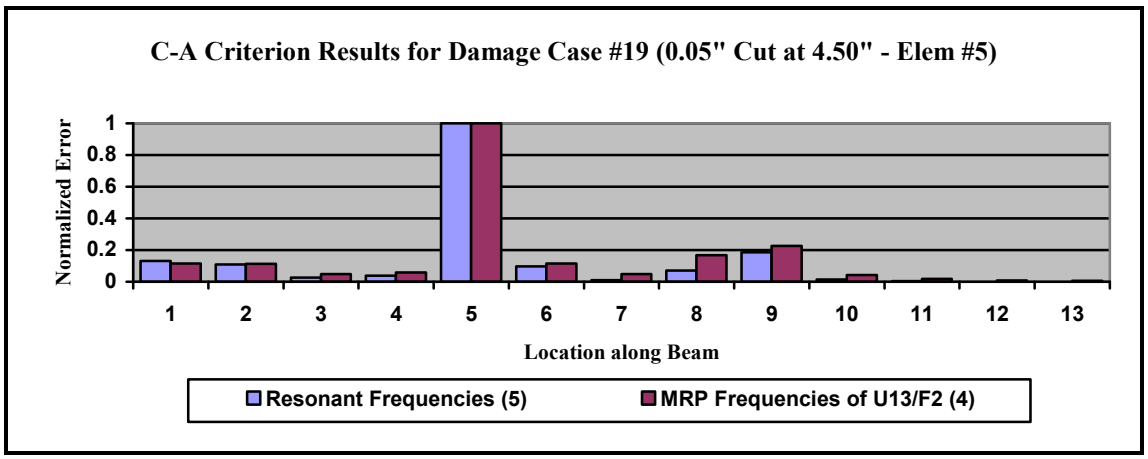

Figure 5.15 Comparison of C-A Results for Damage Case #19

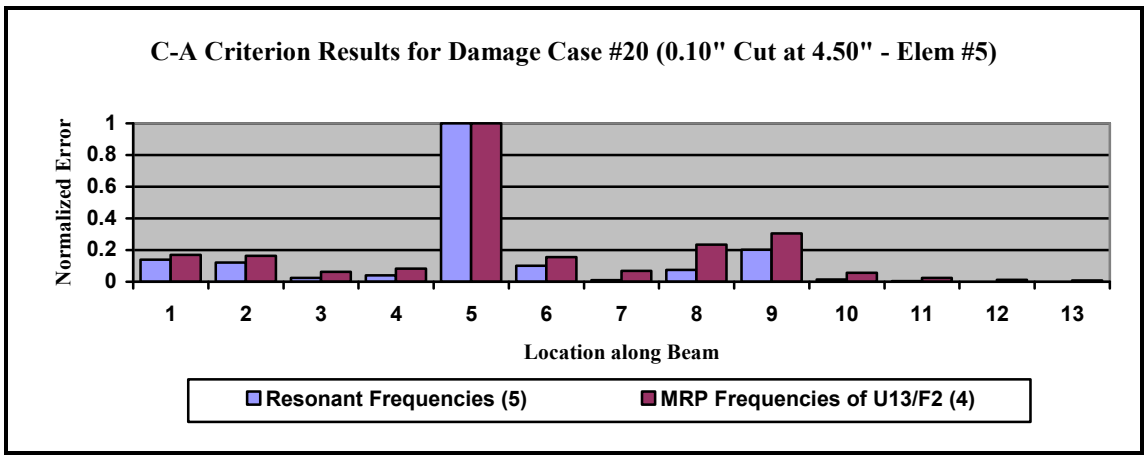

Figure 5.16 Comparison of C-A Results for Damage Case #20

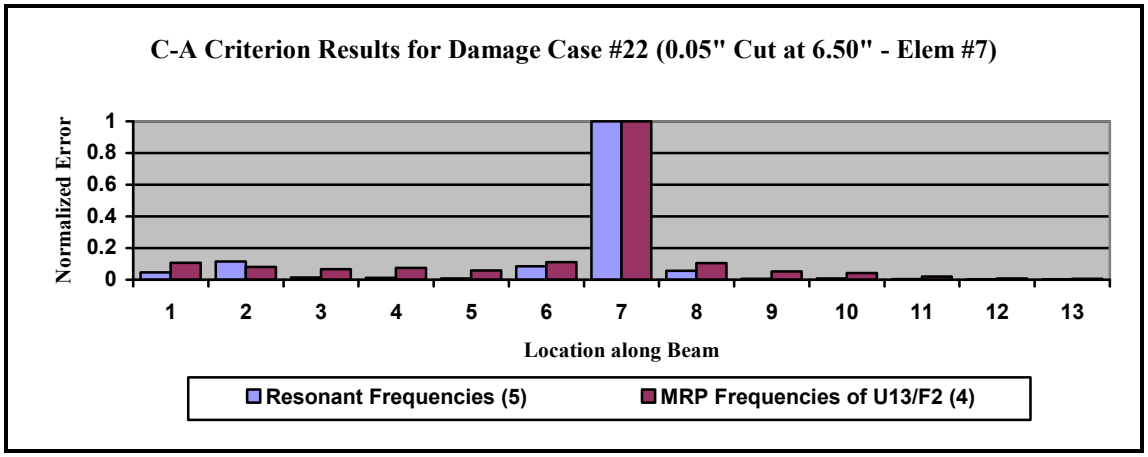

Figure 5.17 Comparison of C-A Results for Damage Case #22

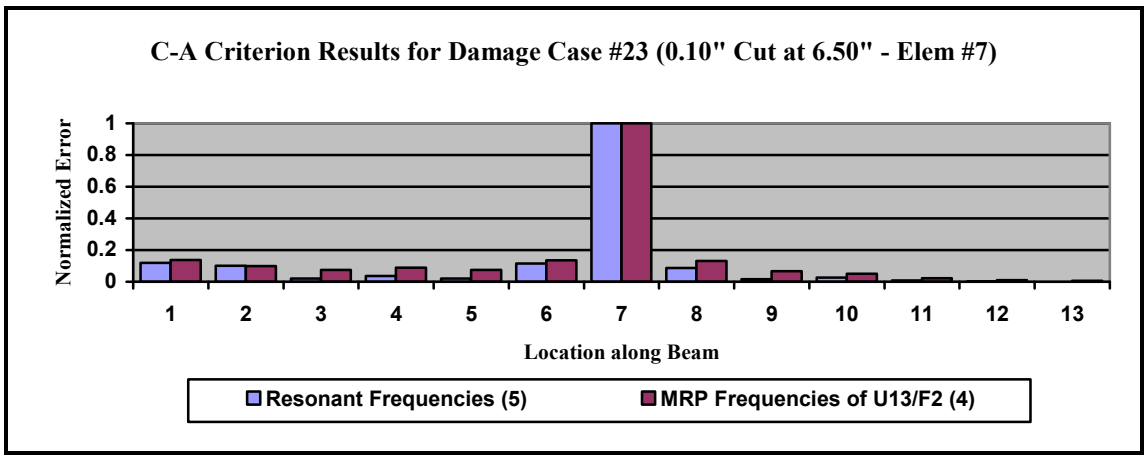

Figure 5.18 Comparison of C-A Results for Damage Case #23

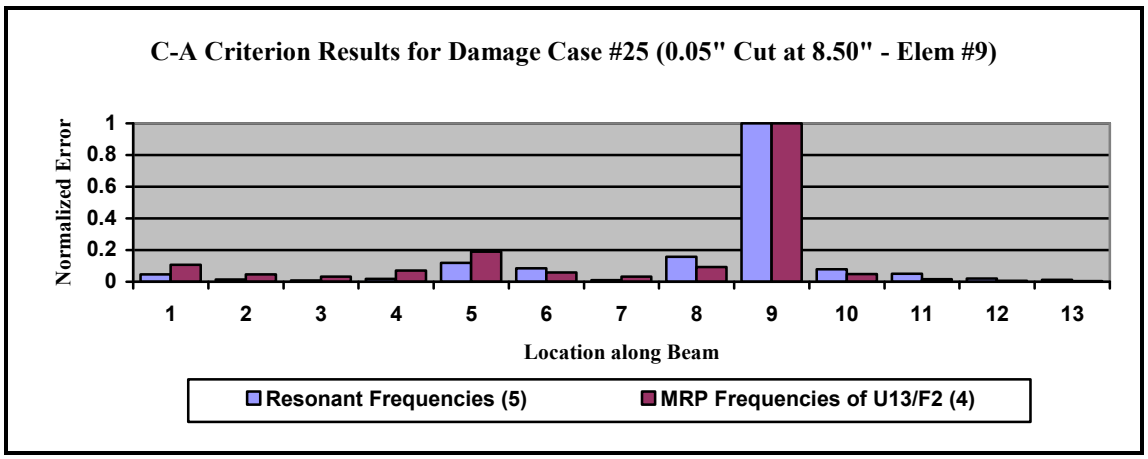

Figure 5.19 Comparison of C-A Results for Damage Case #25

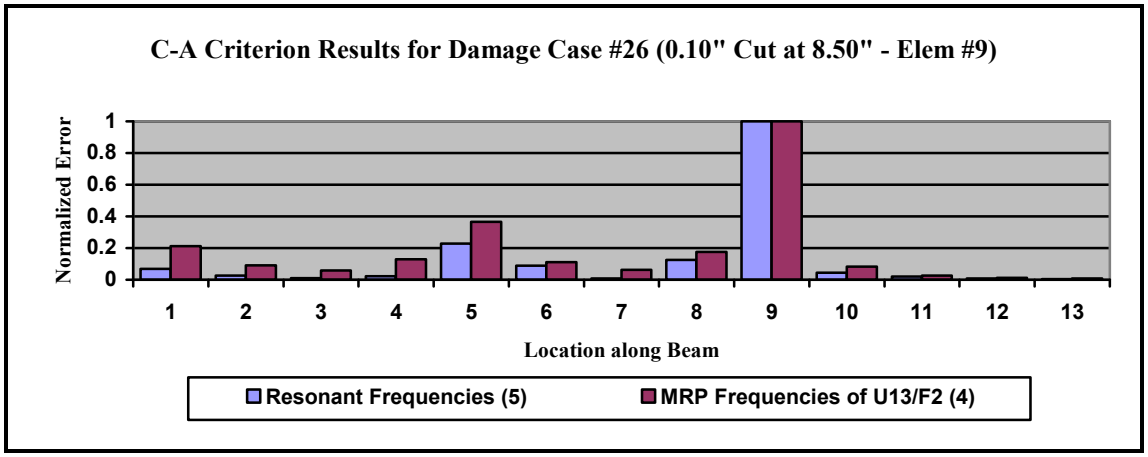

Figure 5.20 Comparison of C-A Results for Damage Case #26

In each figure, the normalized error is plotted for each potential damage location along the beam. Recall that the damage location is indicated where the normalized error is set to a value of 1. In all cases, the use of minimum response point frequency-change was just as effective as resonant frequency change for the determination of the transverse crack location in the analytically represented beam structure. Of course, these cases included only single cracks, and the frequency response data from which the minimum response point information was obtained were free of noise. However, even with the unsophisticated representation of damage in the perturbation of the course model, localization of damage to the prospective element was successful.

It is noted, however, that the normalized error values computed from minimum response frequencies are generally higher for undamaged elements than those computed from resonant frequency changes. This is particularly noticeable for damage cases #7 and #8, shown by Figures 5.7 and 5.8. The localization process was repeated with minimum response points from additional response locations added to the input data set. Disappointingly, for the two subject damage cases, the inclusion of additional response locations did not produce any significant reduction of the normalized error values associated with the undamaged elements.

5.5 Eigenvalue Sensitivity Approach

If the modeled damage can be parameterized, as in the assumption of proportional damage, then the sensitivities of each of these frequencies with respect to the damage parameters can be determined from the corresponding sensitivities of the

mass and stiffness matrices (e.g. equation 3.20). If a proportional damage model is assumed to be representative, then the stiffness change of each element can be represented by a single damage coefficient, for a total of thirteen coefficients for the beam model. As previously stated, a total of twenty-two local response minima points are present among the functions in the FRF set. The interest here is that while the five available resonant frequencies are inadequate for a unique solution of the inverse sensitivity equation (3.10), there are sufficient minimum response frequencies to obtain an overdetermined set of equations, and hence, a unique minimal norm solution for the damage coefficients. Of course, also inherent in the solution is the assumption that the first order approximation built into the formulation of the sensitivity equation is valid.

Minimum response frequency values were extracted from FRF data for the undamaged beam and for the Case #1 damaged beam (0.050-in deep cut at x = 0.25-in). Response locations #10 through #13 were used to provide thirteen frequency values for a determinant solution. Also, a least-squares solution for the damage coefficients was obtained with all frequencies from all locations included. For comparison purposes, the course 13-element beam model was used to create two proportionally damaged beams, with 5% and 15% stiffness reduction applied to element #1. For these two special cases, the *exact* minimum response frequencies of the damaged structures were computed from the eigenvalue equation (Chapter 2), and used as simulated test data.

The computed damage coefficients for the Case #1 crack condition, and the two proportionally damaged conditions, are given in Table 5.2. The goal was to hopefully sort out the errors due to misrepresentation of damage in the sensitivity matrix

calculation, and errors arising from the linear approximation of the sensitivity, so that the benefit of added frequency data could be assessed.

Table 5.2 Calculated Damage Coefficients – Comparison Between Beam Case #1 and Proportionally Damaged Models

	Response Data: 10 – 13 (13 Frequencies)			**Response Data: 1 – 13 (22 Frequencies)**		
		Proportional Damage			**Proportional Damage**	
Element	**Beam Case #1**	**-15% on Element 1**	**-5% on Element 1**	**Beam Case #1**	**-15% on Element 1**	**-5% on Element 1**
1	.10	-.16	-.05	-.15	-.14	-.05
2	-.37	.01	.00	-.01	-.08	-.01
3	-.56	-.07	-.08	-.04	.03	.00
4	.04	.13	.01	-.01	-.04	-.00
5	.13	-.17	-.02	-.02	.01	.00
6	-.26	.17	.02	.01	-.01	-.00
7	-.31	-.18	-.02	-.01	-.00	-.00
8	.80	.17	.02	.01	.01	.00
9	-.62	-.11	-.01	-.00	-.00	-.00
10	.32	.06	.01	.01	.00	.00
11	-.21	-.04	-.00	-.01	-.00	-.00
12	-.14	.04	.00	.00	.01	.00
13	-.20	-.08	-.01	.01	-.01	-.00

Clearly, when only the thirteen frequencies from response points #10 through #13 were included, the assessment of damage for the Case #1 condition was completely false. The addition of the remaining frequency values did significantly improve the assessment so that at least the damage element was adequately identified. The same

effect is also noted for the proportionally damaged cases. It is also noted that the Beam Case #1 damage is fairly well approximated by the 15% proportional-damage case, and the first order approximation errors are certainly apparent in the results for the 15% proportional-damage case, particularly when only thirteen frequencies are used in the solution. Based on these results one would think that perhaps if all minimum response frequencies were included in the solution then a reasonable assessment of damage, at least the location of, could be obtained. However, this was found to not be the case. Similar solutions, with all frequencies included, were obtained for other beam cases with the same minimal crack size, but at other locations along the beam. These results are given in Table 5.3.

The damage predictions for the other more severely damaged beam cases are not included here, but were extremely poor. It is most likely that the frequency changes associated with these damage conditions were more non-linear than the direct application of eigenvalue sensitivity could handle. Admittedly, it was naïve to explore this approach, but the attractiveness of the method was too tempting to resist.

The conclusion derived from the results in Table 5.3 is that an improved model of damage, or parameterization of the damage, is needed to more clearly assess the abilities of minimum response information to serve in a damage assessment process. Not to be misunderstood, the general parameterization of damage as a linear combination of the elemental stiffness contributions is still widely used in the most recent research efforts for damage detection and model updating [19], and certainly represents a computationally practical approach.

Table 5.3 Calculated Damage Coefficients – Comparison Between 0.050-in Crack Beam Damage Cases

	Response Data: 1 – 13 (All 22 Frequencies)					
	Cracks within Element 1			**Cracks within Element 3**		
Element	**Beam Case #1 (0.25")**	**Beam Case #4 (0.50")**	**Beam Case #7 (0.75")**	**Beam Case #10 (2.25")**	**Beam Case #13 (2.50")**	**Beam Case #16 (2.75")**
1	-.15	-.10	-.06	.02	.02	.02
2	-.01	-.12	-.19	-.09	-.05	-.03
3	-.04	.07	.13	-.13	-.13	-.10
4	-.01	-.08	-.11	.01	-.03	-.08
5	-.02	.03	.06	-.01	.01	.04
6	.01	-.01	-.02	.00	-.00	-.01
7	-.01	.01	.01	-.00	.00	-.02
8	.01	.01	.00	.01	-.00	-.01
9	-.00	-.00	.00	-.00	.00	.00
10	.01	-.00	-.00	.00	.00	-.00
11	-.01	-.00	-.00	-.00	-.00	-.00
12	.00	.00	.01	.00	.00	.01
13	.01	.02	.01	.01	.00	.00

5.6 Continuous Beam Theory

The sensitivity-based damage predictions presented in the preceding section provide clear indication of limitations of the proportional-damage model, even for the generation of performance comparisons between two different features. At least, for the primitive methods employed, the proportional-damage model was inadequate for the purpose of this research. Therefore, an alternative approach based on a more

representative model of crack damage was desired, to hopefully provide a more meaningful comparison of performance results.

The use of continuous beam vibration theory, within the context of damage detection, has been studied by many researchers in recent years [3][4][10][20]. The advantage that continuous beam theory provides is that meaningful representation of the highly local nature of crack damage is possible. The disadvantage is that the resulting formulation is not directly applicable to general structure. However, for the purposes of this study, the approach offered a meaningful alternate view for comparison of minimum response information and resonant information in a damage detection scheme.

5.6.1 Model of Transverse Crack in Continuous Beam

Much research has been devoted to the study of the initiation and propagation of crack damage, and more recently, the identification of crack damage [3]. It is beyond the scope of this paper to delve into the related theories. However, the assumptions involved with the formulation presented herein will be mentioned. It will be assumed that the crack is open and is of uniform depth. That is, represented as a transverse slot on one surface of the beam. It has been shown that a slot with sufficiently high depth/width aspect ratio does provide reasonable approximation for a crack [6]. It is also assumed that the presence of the crack imposes a local change in the compliance of the beam such that in the vicinity of the crack the rotational crack compliance is dominant. Thus, the crack can be represented as a rotational spring with a stiffness K_t.

An example sketch of a cracked cantilevered beam and corresponding cracked beam model are illustrated in Figure 5.21. The crack is shown as a slot with depth, *d*, in a beam of rectangular cross-section and thickness, *t*.

Based on fracture mechanics methods, the equivalent stiffness of a transverse crack of uniform depth was proposed [21] as follows,

$$K_t = \frac{\mathrm{E\,I}}{5.346 \cdot t \cdot J(d/t)} \ , \tag{5.4}$$

where *J* is defined as a dimensionless compliance function. Different forms of this compliance function have been proposed for various crack symmetries. The form [21] used for this study is given below,

$$\text{where, } J(d/t) = 1.8624c^2 - 3.95c^3 + 16.37c^4 - 37.226c^5 + 76.81c^6 - 126.9c^7 + 172c^8 - 43.97c^9 + 66.56c^{10} \ , \tag{5.5}$$

for, $c = d/t$.

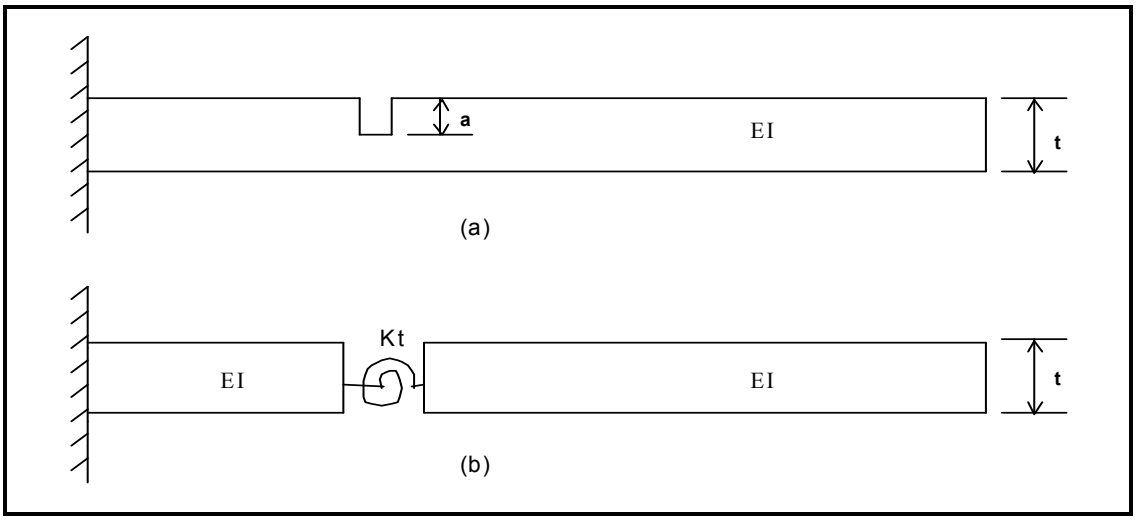

Figure 5.21 Analytical Representation of Crack Damage: (a) Cantilever Beam with Crack (b) Model of Cracked Beam

It was desired to obtain a theoretical formulation for the steady-state response at any chosen location of a cracked beam, with any given crack description (location and depth), and for any given driving point force location. The beam was subdivided into three sections such that the boundaries of the sections were defined by the locations of the crack, the drive force, and the natural boundaries of the beam. This is illustrated in Figure 5.22 for the crack applied at location *aL*, and driving force at location *bL*, for one possible condition ($a < b$). A solution for the general equation for each beam segment was sought, with the boundary conditions and associated compatibility conditions satisfied for all segments. This yielded piecewise solutions for the three beam segments.

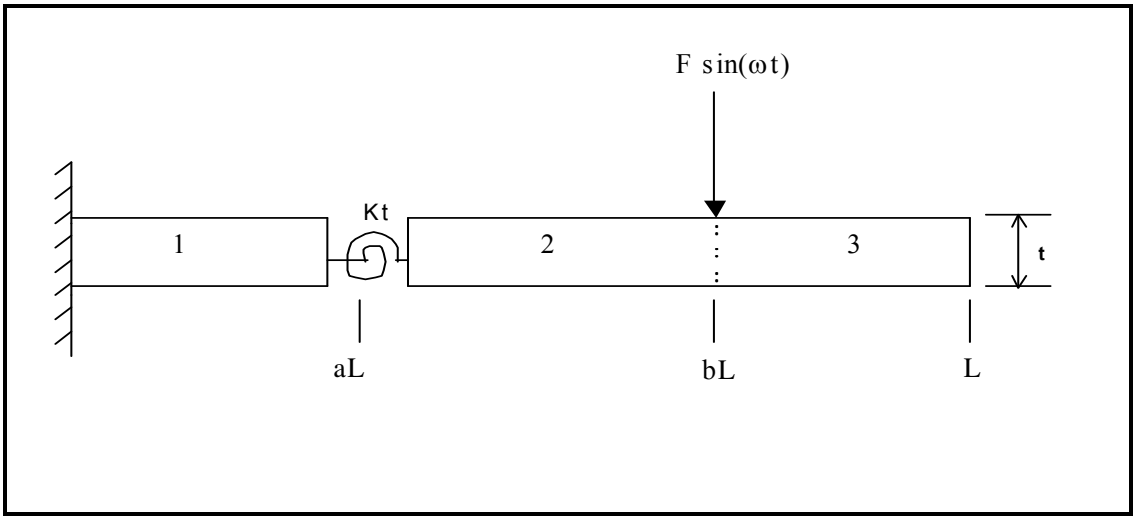

Figure 5.22 Segmented Model of Cracked Cantilever Beam with Single-Point Force

The Euler-Bernoulli equation of motion for the free flexural vibration of a uniform beam is given by,

$$EI\frac{\partial^4 y}{\partial x^4}+\rho A\frac{\partial^2 y}{\partial t^2}=0\,, \tag{5.6}$$

where, E, I, ρ, A are the material/geometric properties, and
y ≡ transverse beam displacement at location x, time t.

For steady-state motion, the solution y(x,t) is assumed to have the form,

$$y(x,t) = Y(x)\, e^{i\omega t}\ . \tag{5.7}$$

For the beam segment, *s*, $Y_s(x)$ is thus defined as,

$$Y_s(x) = A_s \cosh(\lambda x) + B_s \sinh(\lambda x) + C_s \cos(\lambda x) + D_s \sin(\lambda x)\,, \tag{5.8}$$

$$\text{with,}\quad \lambda = \left(\frac{\rho A \omega^2}{EI}\right)^{1/4}\ . \tag{5.9}$$

The boundary and compatibility conditions provide the necessary relationships for determination of the coefficients A_s through D_s, for s = 1…3 beam segments. These result in a total of twelve simultaneous equations that can be arranged into the form $[A]\{C\} = \{B\} \Rightarrow \{C\} = [A]^{-1}\{B\}$, where {C} contains the response coefficients. The derivation of [A] and {B} is not the focus here, but for reference, the matrices [A] and {B}, and the accompanying compatibility/boundary equations are given in Appendix A for three possible crack and driving force orientations. Once the solution for $Y_s(x)$ is known, then it is possible to express the derivative of Y with respect to the excitation frequency, ω, at a selected response location, then find the roots of $dY/d\omega = 0$, to determine the associated minimum response point frequencies.

A check was performed to validate the relationship for K_t and verify that minimum response frequency values determined through use of continuous beam theory were indeed consistent with corresponding results from the detailed finite element model. Recall that frequency response results were generated from the detailed finite element model, to represent test data for various damage conditions for which the damage was modeled by removal of elements to form slots. Minimum response frequency values were extracted from the computed response spectra for each damage case. Likewise, minimum response frequency values were computed through the continuous beam formulation for comparison to those values obtained from the finite element model. Iterative adjustment to the rotational crack stiffness, K_t, was performed until both sets of frequency values were in complete agreement. A crack depth was back calculated from K_t (equations 5.4 and 5.5) for comparison to the *actual* value represented in the finite element model. The results, shown in Table 5.4, indicate very good agreement between the two models, with respect to model of damage and predicted minimum response point frequencies.

Table 5.4 Evaluation of Continuous Cracked-Beam Model

Damage Case	Crack Location (*aL*)	"Actual" Crack Depth (FEM) (*d/t*)	K_t Needed to Match FEM MRP Freqs (x EI)	Crack Depth Needed to Match FEM MRP Freqs (*d/t*)
1	.25	.25	7.3	.286
2	.25	.50	1.35	.500
4	.50	.25	6.4	.303
5	.50	.50	1.21	.512
7	.75	.25	6.4	.303
8	.75	.50	1.21	.512
10	2.25	.25	7.4	.285
11	2.25	.50	1.30	.504
13	2.50	.25	7.2	.288
14	2.50	.50	1.28	.506
16	2.75	.25	7.3	.286
17	2.75	.50	1.30	.504
19	4.50	.25	7.3	.286
20	4.50	.50	1.30	.504
22	6.50	.25	7.3	.286
23	6.50	.50	1.32	.503
25	8.50	.25	7.2	.288
26	8.50	.50	1.31	.503

5.6.2 Optimization Problem Definition and Results

Now with a formulation for local crack damage expressed explicitly in terms of location and depth, it was desired to see if an optimization procedure could be applied to predict damage based on changes in minimum response frequencies. The data

produced from the detailed finite element model was used to represent test data. An objective function was defined as follows,

$$E = (\Delta f - \delta f)^T (\Delta f - \delta f) , \tag{5.10}$$

where, $\Delta f \equiv$ vector of measured frequency-changes, and,

$\delta f \equiv$ vector of analytical (equation model) frequency changes dependent on *d/t* and *a*.

This objective function represents the error between analytical and *measured* frequency-change vectors. Frequency values derived from one or more response locations can be compiled into a single frequency vector. The goal of the optimization is to find *d/t* and *a*, that minimizes this difference error. There are obvious constraints on the optimization parameters – the crack location must be somewhere between x = 0 and x = L, or $0 < a < 1$. This constraint can be further tightened based on the assumption that damage is unlikely to occur at locations near the beam tip. Also, reasonable constraints can be placed on the crack depth parameter *d*. It is necessary to avoid values of *d* near zero, to avoid the singularity of zero crack compliance.

Constrained optimization solutions were attempted for many of the damage cases described in Table 5.1. Significant difficulties with convergence to the correct solution were encountered. It was found that convergence was extremely sensitive to the starting point values of the crack parameters, particularly to the initial guess for the crack location (a_o). The objective function was interrogated at a limited set of parameter values with the intention of locating optimal initial values (corresponding to $E = E_{min}$). However, this resulted in very limited success. The inclusion of frequencies

from multiple response locations did not appear to provide any improvement in solution convergence. For reference, numerical results are given in Table 5.5.

Table 5.5 Results of Damage Detection through Optimization with Continuous Cracked-Beam Formulation

Case	"Actual" Damage		Predicted Damage - U_{13} Response - a_o from E_{min}		Predicted Damage - U_{13} Response - $a_o = 0$		Predicted Damage - U_{13} and U_{11} - $a_o = 0$	
	Location (in)	Depth (d/t)	Location (in)	Depth (d/t)	Location (in)	Depth (d/t)	Location (in)	Depth (d/t)
1	0.25	.25	6.96	.38	0.26	.29	0.26	.29
2	0.25	.50	2.89	.54	0.24	.50	1.31	.9
4	0.50	.25	9.87	.27	0.51	.30	0	.14
5	0.50	.50	3.21	.50	0.49	.51	0.49	.51
7	0.75	.25	9.16	.21	0.77	.31	0.77	.31
8	0.75	.50	6.58	.38	0.75	.51	0.75	.51
10	2.25	.25	11.03	.25	2.23	.28	0	.17
11	2.25	.50	2.23	.50	0	.39	2.22	.50
13	2.50	.25	10.69	.24	2.49	.29	0	.18
14	2.50	.50	2.48	.50	0	.39	2.48	.50
16	2.75	.25	10.37	.24	0	.17	0	.17
17	2.75	.50	2.74	.50	0	.38	0	.38
19	4.50	.25	4.52	.28	0	.14	0	.14
20	4.50	.50	2.00	.46	0	.33	0	.33
22	6.50	.25	6.51	.29	0.38	.22	0.02	.20
23	6.50	.50	0.33	.44	0.33	.44	0.02	.41
25	8.50	.25	4.28	.32	0.19	.18	0	.14
26	8.50	.50	2.64	.47	0.17	.40	0	.33

Although the results in Table 5.5 are generally poor, they are presented herein along with the entire subject of continuous beam theory because there are some interesting observations to be noted. For cases that yielded poor solutions, it was found that selection of an improved initial guess for the crack location (based on knowledge of the damage) did enable the solution process to properly converge. Thus, this damage

detection process can work with minimum response frequencies, but additional constraints are needed. It is interesting to note that in many cases where the crack location was completely misidentified, the crack depth was still reasonably well identified. This is further indication that a modified approach to improve localization of the damage was needed to provide a solution sufficiently robust to allow a more meaningful evaluation.

It was already shown in preceding sections that a supervised damage detection process, based on finite element sensitivity analysis, could provide element-level localization of damage, even with use of a proportional stiffness damage model. This idea prompted the use of a cracked-beam element formulation to provide the basis for a similar optimization procedure, but defined in the framework of finite elements.

5.7 Cracked-Beam Finite Element Approach

The modeling of damage through continuous beam theory equations provided a means to represent highly local crack damage through parameters directly related to physical characteristics of the crack. Also, it was shown previously that the Cawley-Adams criterion, with minimum response point frequency information, was useful for localization of damage to a particular element within the model. With damage localized to a specific element of the model, then the formulation of a cracked-beam element, to include effects of local crack compliance, could be used to provide the basis for a more constrained optimization problem than that presented in the preceding section.

5.7.1 Formulation of a Cracked-Beam Element

The local compliance of a crack can be represented in a two-dimensional beam element as that of a rotational spring, based on the assumption that within the vicinity of the crack the crack compliance is dominant in the flexibility matrix. Thus, a uniform beam of length L can be split into two beams of similar cross-section, with lengths aL and $(1-a)L$, and which are joined through a rotational spring with spring constant K_t. The total element stiffness matrix, generated through superposition of the three respective element components, now contains matrix elements that are dependent on a and K_t, and involves three new degrees-of-freedom associated with the crack. A schematic of the cracked-beam element, with newly formed degrees-of-freedom (U3, θ3, θ4) indicated, is given in Figure 5.23. For reference, the corresponding element stiffness matrix is given in Appendix B.

The presence of the crack will also produce some change in the consistent mass matrix of the beam element. However, this effect has been found to be negligible [7]. Thus, it is only necessary to be concerned with the formulation of the stiffness matrix for a cracked-beam element.

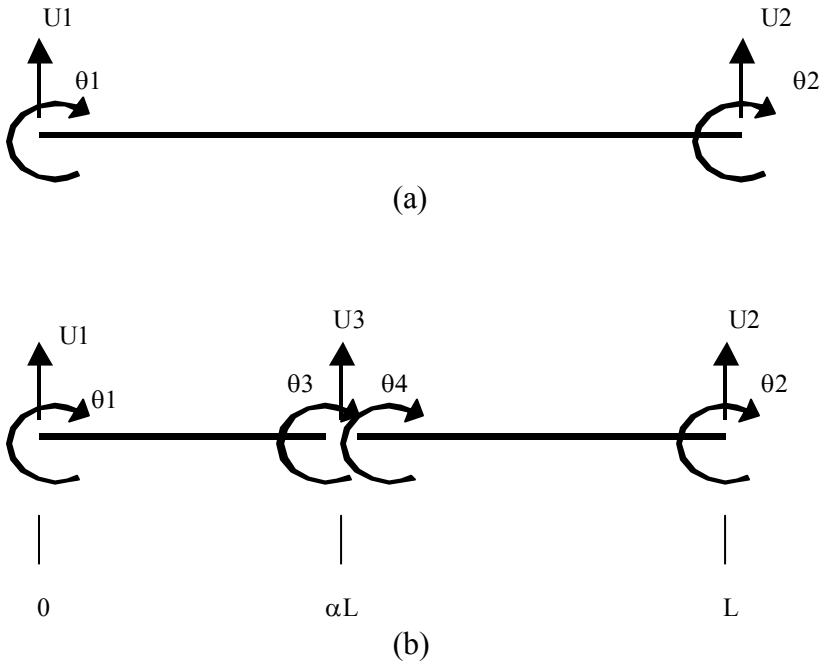

Figure 5.23 Schematic of Beam Element: (a) Undamaged (b) Cracked

5.7.2 Optimization Based on Cracked-Beam Element

Assuming the successful identification of a damaged beam element, the idea of this approach is to replace the stiffness contribution of that element in the global stiffness matrix with the corresponding stiffness contributions for a cracked-beam element. Then, an optimization procedure can be performed to find values for a and K_t that produce response characteristics most correlated to the measured response characteristics of the damaged structure.

The cracked-beam element involves three additional degrees-of-freedom, so direct replacement into the global stiffness cannot be performed without first reducing the coordinate set to that of the original element. Following the assumption that mass

change due to crack damage is insignificant, it was deemed appropriate to use static condensation through the Guyan [14] reduction process for this purpose. The Guyan reduction process is essentially a transformation of a full stiffness matrix to a statically equivalent stiffness matrix represented by a subset of the coordinates. If the full stiffness matrix is partitioned for master and slave coordinates, where the master coordinates are those degrees-of-freedom to be kept, and the slaves are those to be condensed, as indicated below,

$$\left[\mathbf{K}\right] = \begin{bmatrix} \mathbf{K}_{mm} & \mathbf{K}_{ms} \\ \mathbf{K}_{sm} & \mathbf{K}_{ss} \end{bmatrix}, \tag{5.11}$$

then, a transformation matrix, **T**, is defined as,

$$\left[\mathbf{T}\right] = \begin{bmatrix} \mathbf{I} \\ -\mathbf{K}_{ss}^{-1}\mathbf{K}_{sm} \end{bmatrix}. \tag{5.12}$$

The reduced stiffness matrix, $\mathbf{K}_r$, is obtained from the full stiffness matrix by the following transformation: $\mathbf{K}_r = \mathbf{T}^T \mathbf{K}\, \mathbf{T}$. (5.13)

Given an anticipated crack condition (i.e. *a* and *d/t*), the change in the global stiffness matrix is computed, and the corresponding changes in resonant frequencies and minimum response point frequencies can be determined as described in previous chapters. Similarly, an error function is defined to provide a measure of the comparison between these predicted frequency changes and the corresponding measured frequency changes. This is the optimization process used previously, and applied here as well. That is, the same objective function, *E*, defined as $E = (\Delta f - \delta f)^T (\Delta f - \delta f)$, and precisely

the same optimization problem definition described in Section 5.6.3, were used here for this analysis.

5.7.3 Damage Assessment Results

The optimization procedure described in the preceding section was applied to the simulated data generated from a majority of the twenty-seven damage cases that were created from the detailed finite element model. Resonant frequencies and minimum response point frequencies were used in independent assessment processes. A comparison of the results is provided in Table 5.6.

All in all, the results were good, and some interesting observations were noted. Matching of resonant frequency change performed extremely well, and the optimization solution was very fast. All five modes present in the frequency range below 2000 Hz were included in the analyses. The matching of minimum response point frequency information also resulted in very good assessment of all of the transverse crack damage cases, even when only the four available frequencies (< 2000 Hz) from one response location (U_{13}, beam tip) were included. As a reminder, all of the response data was obtained for single-point excitation applied at the node point #2 location.

After acquiring results based on use of only the response from the beam tip, additional detection processes were executed to combine response data from multiple locations. Some of these results are indicated in the final two columns of Table 5.6, for which all available minimum response point frequencies (< 2000 Hz) from five response locations were included. Note that the response at node point #10 (U_{10}) was

not included. The inclusion of frequencies from this measurement location generated significant difficulty for the optimization solution for many of the damage cases. It was found that the first minimum response point, located between the first and second resonant frequencies for this location, exhibited highly non-linear sensitivity to the optimization parameters *a* and *d/t*, particularly the crack depth parameter *d/t*.

Table 5.6 Results of Damage Detection through Optimization with Cracked-Beam Finite Element Formulation

Case	"Actual" Damage		Predicted Damage - Resonant Freq - 5 Modes		Predicted Damage - MRP Freq* - U_{13}/F_2		Predicted Damage - MRP Freq** U_{13}, U_{12}, U_{11}, U_9, U_8	
	Location (in)	Depth (d/t)	Location (in)	Depth (d/t)	Location (in)	Depth (d/t)	Location (in)	Depth (d/t)
1	0.25	.25	0.26	.29	0.30	.30	0.30	.30
2	0.25	.50	0.24	.50	0.21	.49	0.18	.48
4	0.50	.25	0.51	.31	0.50	.30	0.51	.30
5	0.50	.50	0.50	.51	0.53	.52	0.49	.51
7	0.75	.25	0.77	.31	0.77	.30	0.75 [2]	.29 [2]
8	0.75	.50	0.75	.51	0.75	.51	0.70 [2]	.49 [2]
10	2.25	.25	2.22	.29	2.39	.29	2.28	.28
11	2.25	.50	2.22	.51	2.25	.51	2.19 [1]	.50 [1]
13	2.50	.25	2.46	.30	2.50	.30	2.50	.30
14	2.50	.50	2.45	.52	2.29	.51	2.52	.51
16	2.75	.25	2.73	.29	2.75	.29	2.64	.29
17	2.75	.50	2.72	.51	2.71	.51	2.81 [2]	.51 [2]
19	4.50	.25	4.55	.29	4.51	.29	4.49 [1]	.30 [1]
20	4.50	.50	4.56	.51	4.59	.50	4.53 [1]	.51 [1]
22	6.50	.25	6.44	.29	6.49	.29	6.49	.29
23	6.50	.50	6.45	.51	6.72	.50	6.35	.51
25	8.50	.25	8.48	.29	8.51	.30	8.48 [1]	.30 [1]
26	8.50	.50	8.46	.51	8.47	.51	8.40 [1]	.50 [1]

Notes: *Total frequencies available: 4 **Total frequencies available: 14
[1] U_{11} and U_{12} Removed
[2] U_{11} Removed

Additionally, for selected cases, the removal of the U_{11} and U_{12} responses from the analysis was necessary to facilitate a successful solution. The complete exclusion of all of the U_{10}, U_{11}, or U_{12} minimum response points from the analysis was not actually necessary, as only a subset of the frequency points associated with these response locations were responsible for the solution faults. A more refined detection scheme based on minimum response point information would need to provide some means to discern effective minimum response points from all measured responses. Comparisons of mode shapes for an undamaged beam to those of a beam with arbitrary damage (80% crack at 0.75" from root) provide graphical illustration upon which to base one consideration for the selection of optimal response points. See Figures 5.24 and 5.25 for the respective mode shape plots.

Since the response data that was used in the damage assessment analysis was obtained for a driving point located 2 inches from the fixed end, then the mode shapes in Figures 5.24 and 5.25 are phased such that relative deflections at that driving point location are all in the same direction. At the driving point there are no minimum response points between modes, only anti-resonant frequencies. Conversely, at response locations for which adjacent modes are out-of-phase, then a minimum response point is expected to exist between those two resonant frequencies. With this in mind, consider the response location at 10 inches from the root (U_{10}). Note that Mode 2 and Mode 3 are out-of-phase at this location for the undamaged beam, and that Mode 2 exhibits a node point not far away. Then note that for the damaged beam, the node point of Mode 2 has shifted to the other side of the response location.

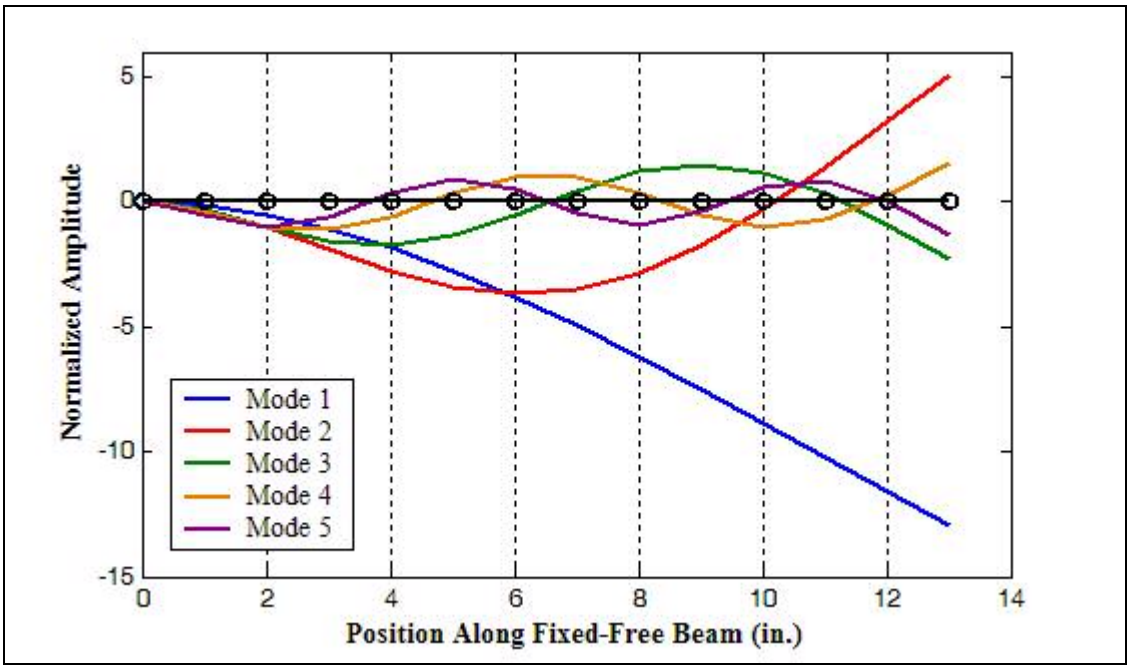

Figure 5.24 Mode Shapes for Undamaged Cantilever Beam

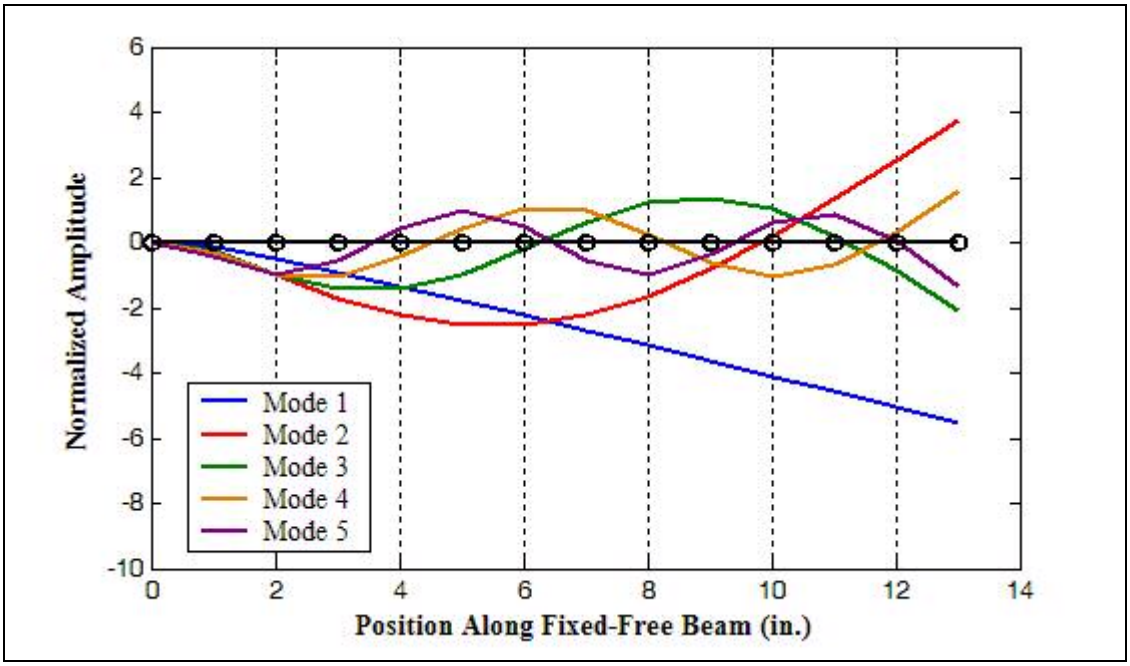

Figure 5.25 Mode Shapes for Damaged (80% Crack at 0.75”) Beam

Thus, for the damaged beam, the minimum response point between the second and third resonant frequencies has vanished. There are also modal node points located in close proximity to the response locations at 11" and 12" from the beam root. So, it is expected that for other damage conditions, or model perturbations, similar difficulties would occur.

Differences will exist between measured and analytical modal responses, due to modeling errors, measurement errors, etc. At response locations in close proximity to modal node points, even small differences can produce highly unstable conditions for a damage assessment process. Likewise, note that the beam-tip location is far from all modal node points. Thus, all minimum response frequencies extracted from the response data collected at this location would be expected to provide positive contribution in the damage prediction. This was the case as indicated in Table 5.6.

There is still potential use for those minimum response points that are deemed to be undesirable, based on the rationale previously discussed, for a damage assessment process. The focus of this work has been directed at damage assessment, with the assumption that some damage is already expected, and the goal is to determine the location and magnitude of the damage. These so-called *undesirable* minimum response points may be useful for the strict purpose of damage detection. That is, to support a decision that damage has occurred.

CHAPTER 6

EXPERIMENTAL APPLICATION TO BEAM STRUCTURE

The results presented in the previous chapter were based on analytically derived test data, free of measurement errors and noise. Tests were performed to evaluate the effectiveness of minimum response point information on assessment of damage in actual structure. For comparison purposes, damage assessment based on changes in measured modal parameters was also conducted. This provided a baseline to support the evaluation of minimum response point information.

For this test series, identical test beams of uniform rectangular cross-section were cut from extruded Aluminum-6063 stock. The beam cross-sectional dimensions were 1 inch wide by 0.188 inches thick. The beams were cut to an overall length of 16 inches, but were configured for a clamped support with an unsupported length of 13 inches. Two ⅜-inch thick steel blocks, 1 inch wide by 3 inches in length, were used to distribute the clamping force generated from two ⅜-inch diameter hardened steel bolts. To maintain uniformity from one beam setup to another, an installation torque of 45 ft-lb was applied to the bolts for all tests.

6.1 Test Procedure

The general test procedure was very simple, and is briefly described as follows. The test beam was mounted in a cantilever condition on a massive support block. An instrumented hammer was used to provide impact excitation at the desired input location. Accelerometer transducers and a Laser Doppler Vibrometer (LDV) were used to provide measurement of response motion. For the first beam tested, only the LDV was used, with the intention of avoiding the mass loading effects produced by accelerometers. However, due to concerns over measurement noise, accelerometers were included for all subsequent beams tested. A brief discussion of measurement noise is presented later in this chapter.

Miniature piezoelectric accelerometers, specifically Model 352C23 sensors manufactured by PCB Piezotronics, were selected for their small size and light mass. Due to availability issues, it was necessary to limit the number of instrumented locations. The accelerometers were placed at five locations, equally spaced at 1-inch intervals from the free end of the beam, and were not moved throughout testing of the beam. These locations matched grid points (Points #9 through #13) of the two-dimensional beam model that was constructed to serve the damage assessment process. A photograph of the overall setup is provided in Figure 6.1.

For each beam tested, an initial set of response measurements was collected to establish the healthy state of the structure. Impact excitation was applied on the centerline of the beam, and at the location 2-inches from the root. The output signals from the hammer force sensor, LDV, and accelerometers were fed into a data

acquisition system, where they were sampled and processed into Frequency Response Functions.

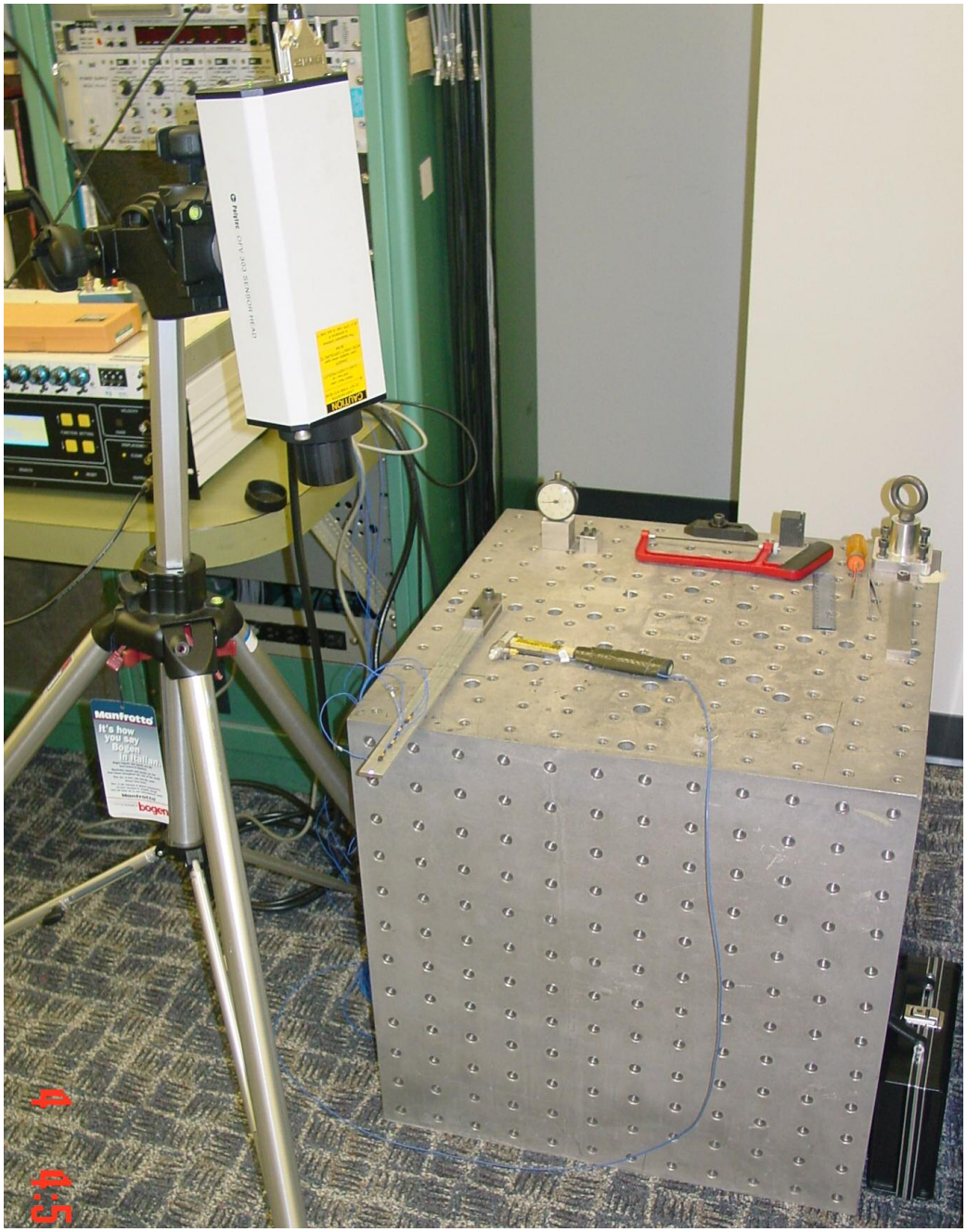

Figure 6.1 Photograph of Test Setup

Since the beam responses were very lightly damped, it was necessary to apply a time-domain exponential window to the response signals prior to transformation into frequency-domain quantities, to minimize leakage effects in the transformed results. A total of ten impact responses were accumulated during the FRF averaging process. The frequency response function values over the frequencies 2 to 2000 Hz, with a frequency resolution of 2 Hz, were retained for use in the damage assessment evaluation.

Following completion of the baseline response measurements, successive damages were introduced at a selected location on the beam. The frequency response measurements were repeated following each successive cut. A narrow-bladed saw was used to cut a transverse slot approximately 0.030-inch wide, as uniformly as possible, across the width of the beam. A depth gage was used to monitor the depth of the slot during the cutting operation. An example of the transverse cut in Beam #4 is shown in Figure 6.2.

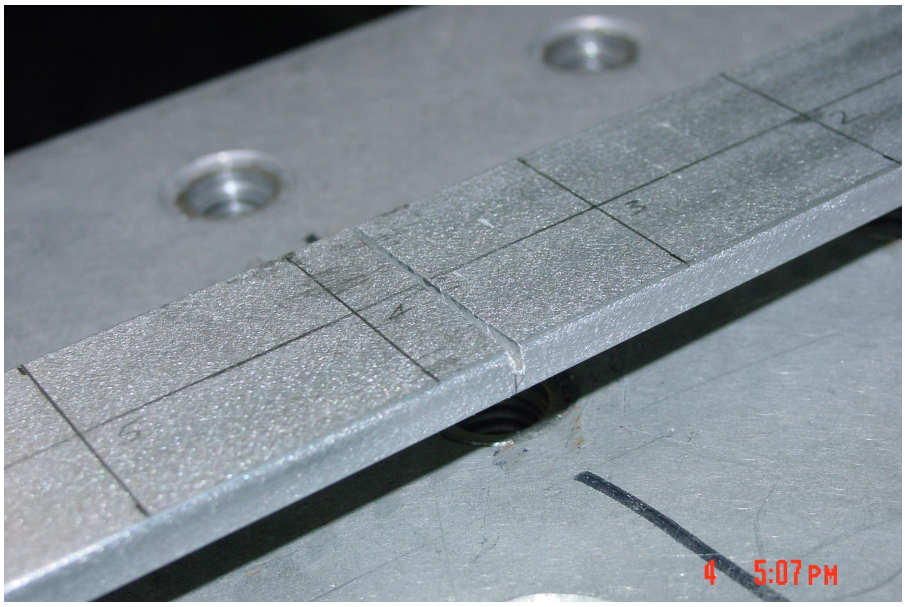

Figure 6.2 Transverse Cut in Beam #4

6.2 Preliminary Analysis and Results from Experimental Data

At this point, measured data was gathered from four beam specimens, with each beam damaged at a unique location. From each measurement set collected, a modal parameter estimation process was conducted to extract the values of all natural frequencies below 2000 Hz. The LMS PolyMAX modal analysis software was used to perform the modal parameter identification. For reference, the corresponding results are provided in Appendix C. These frequency values served as input data for all resonant frequency based damage assessment processes conducted for comparative results. The measured FRF data were imported into MATLAB for input into the minimum response based damage assessment processes. The appropriate integrations were applied to convert the measured Mobility and Accelerance FRF functions into the required Receptance FRF units.

6.2.1 An Evaluation of Measurement Noise

For the first beam under test, only the LDV sensor was used to provide for non-contact measurement of the velocity response motion. Out of concern over the presence of measurement noise, particularly noticeable at the higher frequencies, a series of repeated FRF measurements were collected at the beam tip. A similar set of repeated measurements was also collected after the application of incremental damage to the beam. The purpose here was to evaluate the level of precision in the measurement process. Example FRFs taken before and after the incremental damage are illustrated in Figure 6.3.

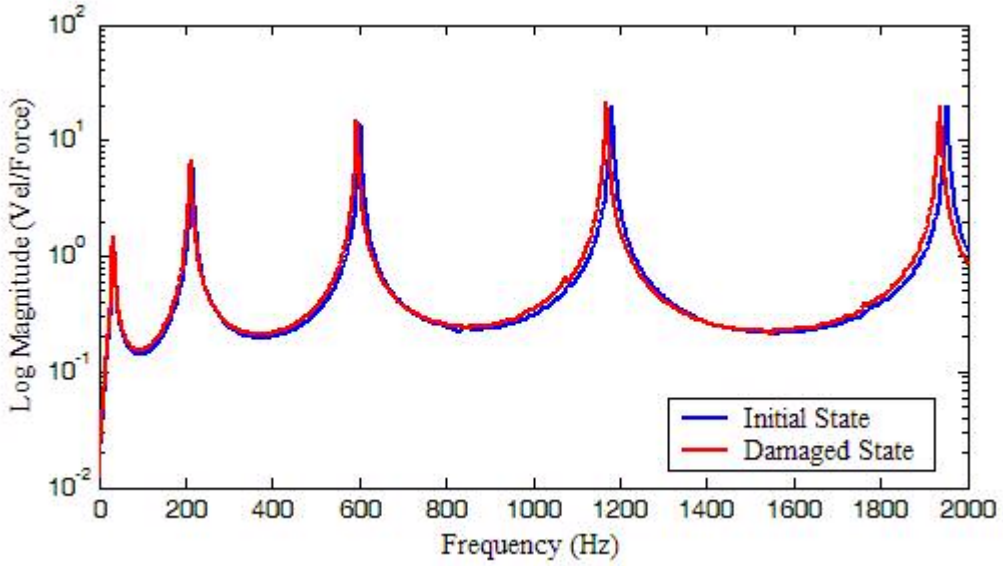

Figure 6.3 Example Mobility FRF Measurements – Before and After Damage

A total of ten measurements were collected for each state of the beam. The minimum response point values were extracted from each measured receptance FRF, from which a statistical evaluation was obtained. The average and standard deviation values determined for all of the beam tip minimum response points are given in Tables 6.1 and 6.2, for the associated frequencies and amplitudes, respectively. Finally, the variances of the frequency and amplitude values, expressed as percentages, were compared to the respective percentage changes that were observed as a result of the incremental damage. This comparison is given in Table 6.3

With the exception of the frequency of the first minimum response point, the variances of the local minima values were quite low. However, the total frequency change realized from the damage was not that significant either. Although percentage-wise, the uncertainties in the amplitude values seem to be generally higher than that

seen with the frequency values, the amplitude values are considerably more sensitive to damage.

Table 6.1 Minimum Response Frequency Statistical Results

Minimum Response Point Frequencies (Hz)			
Damage Increment: Slot at 0.25" extended from 0.050"depth to 0.075" depth			
Before Damage Increment		**After Damage Increment**	
Average	**Std Dev**	**Average**	**Std Dev**
122.30	3.34	120.78	0.76
412.67	0.54	407.68	0.40
894.77	2.06	889.30	1.59
1599.34	1.91	1578.23	3.26

Table 6.2 Minimum Response Amplitude Statistical Results

Minimum Response Point Amplitudes ($x10^{-6}$ in/lb)			
Damage Increment: Slot at 0.25" extended from 0.050"depth to 0.075" depth			
Before Damage Increment		**After Damage Increment**	
Average	**Std Dev**	**Average**	**Std Dev**
1287.4	9.49	1423.0	10.81
496.82	2.40	539.6	3.41
262.84	1.48	278.9	1.69
137.83	0.58	144.53	0.76

Table 6.3 Comparison Between Variance and Change from Damage

Damage Increment: Slot at 0.25" extended from 0.050"depth to 0.075" depth			
Frequency Values		**Amplitude Values**	
Std Dev (%)	**% Change from Damage**	**Std Dev (%)**	**% Change from Damage**
2.73	1.2	0.74	10.5
0.13	1.2	0.48	8.6
0.23	0.6	0.56	6.1
0.11	1.3	0.42	4.9

It is apparent from the results presented in Table 6.3 above, that additional effort should have been devoted in this research toward use of amplitude information. It is not surprising that in the subsequent application of the frequency-based approaches for assessment of damage from the measured test data, difficulties were encountered.

6.2.2 Damage Assessment Evaluation

The damage assessment process described in Section 5.7 was used for this analysis. Based on frequency changes, the Cawley-Adams criterion method was used to attempt localization of the damage to the prospective element of the 13-element MATLAB model. Then an optimization solution was performed to further localize the damage within the element, and estimate the depth of the slot. The damage assessment process performed very well with resonant frequency information, and these results are given in Table 6.4. Unfortunately, the damage assessment process performed very

poorly with extracted minimum response point frequency values. In general, the procedure failed to properly identify the damage condition in most cases.

Table 6.4 Experimental Results Based on Resonant Frequency Change

Case	Actual Damage Location (in)	Actual Damage Depth (in)	Predicted Damage Location (in)	Predicted Damage Depth (in)
Beam1 – Case 1	0.25	.025	0.28	.024
- Case 2	0.25	.050	0.30	.049
- Case 3	0.25	.075	0.30	.071
Beam 2 – Case 1	0.75	.035	0.27	.022
- Case 2	0.75	.050	0.61	.046
- Case 3	0.75	.070	0.72	.072
Beam 3 – Case 1	2.50	.025	2.59	.029
- Case 2	2.50	.035	2.61	.041
- Case 3	2.50	.060	2.53	.066
- Case 4	2.50	.080	2.54	.084
Beam 4 – Case 1	3.75	.023	3.83	.027
- Case 2	3.75	.033	3.84	.039
- Case 3	3.75	.050	3.82	.053
- Case 4	3.75	.070	3.80	.075
- Case 5	3.75	.090	3.78	.087

Note: Error on measured depth ≈ +/- .003-inch

After further scrutiny of the raw FRF data, the extracted minimum response frequencies obtained from the data, and the corresponding analytically predicted frequencies, it became apparent that two primary factors led to failure of the process. The presence of measurement noise, although small, induced excessive error in the identified frequencies. It was also noted that the observed frequency changes did not

correlate well to those predicted by the analytical model, even though the resonant frequency changes were in good agreement. It was not unexpected that identification of a minimum response frequency over a relatively flat spectrum shape would be prone to error, but it was hoped that sufficient correlation to analytical predictions would still be achieved.

It also became apparent that since damage induced amplitude shifts of the minimum response points were much more easily identified, then response amplitude change would represent a more stable parameter for damage assessment. At this point, it was necessary to step back and conduct some analytical development for use of response amplitude information.

6.3 Study of Minimum Response Amplitude

Although the direction of much of this research has tended to focus more on the frequencies associated with local response minima, there were intentions from the start of this work to look at amplitude sensitivity as well. Once the difficulties with extraction of these frequencies from measured data were fully realized, there was a strong desire to shift the focus to amplitude sensitivity. One mathematical view of the response amplitude sensitivity to stiffness change is presented.

6.3.1 Damage Sensitivity of Minimum Response Point Amplitude

The equation of motion for an undamped system under steady-state sinusoidal excitation at a frequency (Ω_m) corresponding to one of the local response minima is given by,

$$(\mathbf{K} - \Omega_{\mathbf{m}}^2 \mathbf{M})\, \mathbf{U}_{\mathbf{m}} = \mathbf{F}, \tag{6.13}$$

where some coordinate within $\mathbf{U}_m$ exhibits the characteristics of a local minimum response point. That is, for $Resp \equiv \mathbf{C}\mathbf{U}_m$, then $\frac{d}{d\Omega} Resp(\Omega_m) = 0$. For some damage condition that induces a stiffness change ($\Delta\mathbf{K}$), accompanied by a negligible change in the mass matrix, there will be a corresponding change in the frequency and amplitude of the minimum response point, and equation (6.13) can be written for this shifted condition as,

$$\left(\mathbf{K} + \Delta\mathbf{K} - (\Omega_m^2 + \Delta\Omega_m^2)\mathbf{M}\right)\left(\mathbf{U}_{\mathbf{m}} + \Delta\mathbf{U}_{\mathbf{m}}\right) = \mathbf{F}. \tag{6.14}$$

Since the quantities $\Delta\Omega_m$ and ΔU_m are intended to represent shifts to new minimum response points, then it is necessary to also impose the requirement on $\Delta\Omega_m$ and ΔU_m that $\frac{d}{d\Omega} Resp(\Omega_m + \Delta\Omega_{\mathbf{m}}) = 0$. If equation (6.14) is expanded, and the 2nd order terms are neglected, then the change in the minimum response point amplitude can be approximated by,

$$\Delta\mathbf{U}_{\mathbf{m}} \approx \Delta\Omega_{\mathbf{m}}^2 (\mathbf{K} - \Omega_{\mathbf{m}}^2 \mathbf{M})^{-1} \mathbf{M}\, \mathbf{U}_{\mathbf{m}} - (\mathbf{K} - \Omega_{\mathbf{m}}^2 \mathbf{M})^{-1} \Delta\mathbf{K}\, \mathbf{U}_{\mathbf{m}}. \tag{6.15}$$

From the general equation, $(\mathbf{K} - \Omega^2 \mathbf{M})\, \mathbf{U} = \mathbf{F}$, the rate of change in the response with respect to the square-frequency can be given as,

$$\frac{d\,\mathbf{U}}{d(\Omega^2)} = (\mathbf{K} - \Omega^2\mathbf{M})^{-1}\,\mathbf{M}\,\mathbf{U} \;\Rightarrow\; \frac{d\,Resp}{d(\Omega^2)} = \mathbf{C}(\mathbf{K} - \Omega^2\mathbf{M})^{-1}\,\mathbf{M}\,\mathbf{U}\,. \tag{6.16}$$

$$\text{At } \Omega = \Omega_m,\ \frac{d\,Resp}{d(\Omega^2)} = 0 \;\Rightarrow\; \mathbf{C}\,(\mathbf{K} - \Omega_m^2\mathbf{M})^{-1}\,\mathbf{M}\,\mathbf{U}_m = 0 \tag{6.17}$$

Combining equations (6.13), (6.15), and (6.17), the approximated change in the response amplitude for a minimum response point can be expressed as,

$$\Delta\,Resp \approx -\mathbf{C}(\mathbf{K} - \Omega_m^2\mathbf{M})^{-1}\,\Delta\mathbf{K}\,(\mathbf{K} - \Omega_m^2\mathbf{M})^{-1}\,\mathbf{F}\,. \tag{6.18}$$

The point of this exercise is to show the sensitivity relationship between minimum response amplitude change and stiffness change. For large models, the matrix inversion indicated in equation (6.18) may not be practical, but that is another issue. The intention here is to show that in theory, theoretical amplitude changes can be directly computed from the finite element model for damage at any location in the structure. Thus the possibility exists that an amplitude-sensitivity method, similar to what has been done based on resonant frequency sensitivity, could be used to identify damage characteristics from changes in measured response. It is first necessary to determine if these amplitude-changes are sufficiently sensitive and unique to provide for an effective process. If so, then efficient numerical methods could be developed.

Many researchers have looked at changes in modal response amplitude for damage detection purposes. One such method, referred to by some as the Transfer Function Parameter Change method [17], was originally developed to utilize changes in the frequencies and amplitudes at resonances. The model of this approach was used to implement a procedure based solely on changes of minimum response point values.

Although the emphasis at this point is for response amplitude, the corresponding frequency information is included in the process to support overall evaluations.

6.3.2 Transfer Function Parameter Change Method

The purpose of this section is to provide an introduction of the method as it is described in the literature. The notation used in the reference material is somewhat different from that used elsewhere in this thesis, but nevertheless is used herein to maintain consistency with the literature. From this introduction, a description of the modifications applied to make use of minimum response information, are better understood.

Recall the equation (2.1) for the *receptance* frequency response function of a linear N-DOF undamped system. This equation represents an approximation, based on the principle of modal superposition with m modes included. A slightly different form of this *transfer function* is given below. The transfer function for the j^{th} output, due to a single-point input, for a healthy system can be expressed as,

$$g_{0j}(\mathrm{s}) = \sum_{l=1}^{k} \frac{b_{0jl}}{s^2 + a_{0l}}, \qquad \text{for } k \text{ modes,} \tag{6.19}$$

where, a_{0l} and b_{0jl} are related to the frequency and amplitudes, respectively, of the l^{th} mode, and for the j^{th} output. Likewise, the corresponding transfer function for the damaged system, with damage of the i^{th} element, can be represented as,

$$g_{ij}(\mathrm{s}) = \sum_{l=1}^{k} \frac{b_{ijl}}{s^2 + a_{il}}. \tag{6.20}$$

The modal based parameters, *a* and *b*, can be assembled into parameter vectors for the undamaged structure, and for each possible damage condition that is to be considered in the analysis. For the healthy structure, the parameter vectors are defined as,

$$\mathbf{p}_{00} = [a_{01} \quad a_{02} \quad \cdots \quad a_{0k}]^{\mathrm{T}}, \text{ and } \mathbf{p}_{0\mathbf{j}} = [b_{0j1} \quad b_{0j2} \quad \cdots \quad b_{0jk}]^{\mathrm{T}}, \tag{6.21}$$

for the j^{th} output. Similarly, for the damaged structure, damaged at the i^{th} element, the corresponding parameter vectors are defined as,

$$\mathbf{p}_{i0} = [a_{i1} \quad a_{i2} \quad \cdots \quad a_{ik}]^{\mathrm{T}}, \text{ and } \mathbf{p}_{i\mathbf{j}} = [b_{ij1} \quad b_{ij2} \quad \cdots \quad b_{ijk}]^{\mathrm{T}}. \tag{6.22}$$

The changes in the parameter vectors due to damage of the i^{th} element can be analytically predicted as,

$$\Delta\mathbf{p}_{ij} = \mathbf{p}_{ij} - \mathbf{p}_{0j}, \text{ for } j = 0, 1, \ldots, m. \tag{6.23}$$

Finally, a weighting factor can be applied to normalize the parameter-change vectors such that for a given output location *j* and mode *k*, the summation of all square values of the associated vector elements, across all of the theoretical damage cases, will equate to unity.

From transfer function measurements collected from the structure under test, a similar parameter-change vector, $\Delta\mathbf{p}_j$, can be determined, and similarly weighted. The measured parameter-change vector can then be compared to those corresponding to the various theoretical damage cases. A coherence function, to provide a means for numerical comparison, is defined as,

$$C_{ij} = \frac{\Delta\mathbf{p_j}^{\mathrm{T}}\,\Delta\mathbf{p_{ij}}}{\left|\Delta\mathbf{p_j}\right|\left|\Delta\mathbf{p_{ij}}\right|}, \qquad \text{for } j = 0, 1, \ldots, m \text{ outputs.} \tag{6.24}$$

A coherence value is associated with the measured frequency-changes, and the measured response amplitude changes at each of *m* outputs. Interpretation of these results now becomes the problem. One approach is to define a minimum coherence vector that identifies the minimum coherence value, for a particular damage perturbation, across all outputs. This can be expressed as,

$$C_i = \min\{C_{i0} \;\; C_{i1} \;\; \ldots \;\; C_{im}\}. \tag{6.25}$$

Also, a magnitude ratio between the parameter vectors can be defined as,

$$R_{ij} = \frac{\left|\Delta \mathbf{p_j}\right|}{\left|\Delta \mathbf{p_{ij}}\right|}. \tag{6.26}$$

Similarly, minimum and maximum magnitude ratio values can be identified across all outputs, for each damage perturbation condition. These are expressed as,

$$R_{i,min} = \min\{R_{i0} \;\; R_{i1} \;\; \ldots \;\; R_{im}\}, \text{ and } R_{i,max} = \max\{R_{i0} \;\; R_{i1} \;\; \ldots \;\; R_{im}\}. \tag{6.27}$$

A number of properties of the quantities C_i , $R_{i,min}$, *and* $R_{i,max}$ are given [17]. Some of these properties are summarized below. Refer to the literature if further explanation is desired. The coherence values will range between 1 and –1, with a value of 1 indicating exact correlation between the two vectors. A negative coherence value indicates that the vector directions differ by more than 90° in the vector space, and thus infers that the associated element is not damaged. With respect to magnitude ratio, if the ratio between the maximum and minimum bounds is much greater that 1, or if both of the minimum and maximum ratio bounds are far away from a value of 1, then it is inferred that the associated element is not damaged.

6.3.3 Adapted Method for Minimum Response

The basis of the transfer function parameter method, as well as others, is that damage will produce changes in the modal parameters of the system, which can be uniquely related to the location of the damage. It has already been shown that, analytically, minimum response point frequencies exhibit damage sensitivity of sufficient uniqueness to allow localization of damage. Also, it has been shown that ratios of the resonant frequency changes are uniquely related to damage location. This alone infers the possibility that amplitude changes at minimum response points could be uniquely related to damage location. Thus, foregoing any rigorous development, the parameter-change method presented in the preceding section was used as a model for a new method of damage assessment based on minimum response information.

Since the resonant frequencies are system characteristics, then the amplitude parameters (residues) extracted from each response location share the same set of frequencies. Minimum response points, on the other hand, are local characteristics. Each response location will exhibit a unique set of frequencies that correspond to points of minimum response amplitude. Also, the number of local minima points will vary considerably from location to location, dependent on the location of the input force.

The modified definition of the parameter-change vectors is presented as follows. All local minima frequencies, from all considered response locations, were compiled into a single frequency vector. For the undamaged system, the parameter vectors for m response locations are defined as,

$$\mathbf{p}_{00} = \begin{Bmatrix} \{\mathbf{f}\}_{01} \\ \vdots \\ \{\mathbf{f}\}_{0m} \end{Bmatrix}, \qquad \mathbf{p}_{0j} = \begin{Bmatrix} \mathrm{A}_{0j1} \\ \vdots \\ \mathrm{A}_{0jn_j} \end{Bmatrix} \quad \text{, for } j=1 \ldots m \text{ locations,} \tag{6.28}$$

where, $\{\mathbf{f}\}_j \equiv$ set of frequencies of n_j local minima of location j,
$\mathrm{A}_{0jl} \equiv$ amplitude of the l^{th} of n_j local minima of location j.

Each parameter vector may have a different length depending on how the minimum response points are distributed among the selected response locations. Likewise, the parameter vectors for the damaged system, with damage of the i^{th} element are defined as,

$$\mathbf{p}_{i0} = \begin{Bmatrix} \{\mathbf{f}\}_{i1} \\ \vdots \\ \{\mathbf{f}\}_{im} \end{Bmatrix}, \qquad \mathbf{p}_{ij} = \begin{Bmatrix} \mathrm{A}_{ij1} \\ \vdots \\ \mathrm{A}_{ijn_j} \end{Bmatrix}. \tag{6.29}$$

With the parameter vectors defined for the baseline and perturbed model conditions, the parameter-change vectors were defined. Rather than use absolute change, as indicated in equation (6.23), it was felt that a percentage change was more appropriate considering that the amplitude values could be spread over a relatively wide dynamic range. The parameter-change vector associated with frequency was similarly defined. Thus, a concise definition of the parameter-change vectors is given as,

$$\Delta\mathbf{p}_{ij} = \frac{\mathbf{p}_{ij} - \mathbf{p}_{0j}}{\mathbf{p}_{0j}}, \text{ (element-by-element division),} \tag{6.30}$$

for, $j = 0, 1, \ldots, m$ outputs.

The coherence and magnitude ratio values are determined from the parameter-change vectors just as was defined in the preceding section.

6.3.4 Application to Simulated Test Data

Before jumping straight to application of the process to the existing measured test data, it was prudent to first test the method on the simulated data produced from the detailed finite element beam model. Of the 27 damage cases available, the parameter-change method was applied to the eighteen single-crack damage cases.

Proportional damage was applied individually to each of the 13 elements in the damage assessment model for determination of the theoretical parameter-change vectors. The measured parameters were extracted directly from the simulated FRF data. The curve fit method discussed in Chapter 4 was used to identify each local response minimum point, and the corresponding frequency and amplitude values were evaluated from the curve fit.

It was desired to include as many response locations as possible. However, it was also desired to select response locations that exhibited at least three local minima. Only the four response locations near the free-end qualified: U_{10} through U_{13}. Also, it was already known from previous analyses that U_{10} was less than optimal. Therefore, only the three end-most response locations were included in the analysis. Coherence values were computed as described in Section 6.3.1, but with the parameter vectors defined as stated in Section 6.3.2 with minimum response point information. In all cases, the minimum coherence function, C_i , provided clear indication of the damaged element. Incidentally, the coherence values associated with the frequency information provided no contribution. These coherence values were generally high for all model perturbations, such that there was very little distinction between damaged and

undamaged elements. The minimum coherence values associated with the amplitude values were widely spread, with clear distinction of the damaged element.

With clear localization of the damage element possible, an optimization solution was added to further localize the damage within the element and estimate crack depth. An objective function was defined from the frequency and amplitude-change vectors. The amplitude-change vectors determined for all available minimum response points were compiled into a single vector, just as the frequency-change vectors were originally formed. Corresponding amplitude and frequency-change vectors were analytically predicted in the optimization solution with iteration values of the crack depth and location. Two error vectors were computed, with one defined as the difference between the theoretical and measured amplitude-change vectors. Similarly, the other error vector was computed as the difference between the theoretical and measured frequency-change vectors. The objective function was defined as the sum of the square magnitudes of these error vectors.

The MATLAB *fmincon* function was used to provide a constrained optimization solution for the crack depth (d/t) and the crack location (a) within the element. The objective function was interrogated at multiple incremental values of d/t and a, to hopefully find starting values nearest to the global minimum of the function. Arbitrarily, upper and lower constraint values of +/- 0.20 from the starting values were set on the optimization parameters. The results of this damage assessment process were very successful for all cases tested. Subsequently, the error function was redefined to include only error between the analytical and *measured* amplitude-changes, and the

solution process was repeated for all of the cases. The results, given in Table 6.5, were virtually identical to the previous results obtained through use of resonant frequency (see Table 5.6). The results listed below provide some analytical verification of the approach. The true test, however, is application of the approach to measured test data.

Table 6.5 Damage Assessment of Analytical Damage Cases Based on Amplitude Changes at Local Response Minima

Case	"Actual" Damage		Predicted Damage MRP Data from: U_{13}, U_{12}, U_{11}	
	Location (in)	Depth (d/t)	Location (in)	Depth (d/t)
1	0.25	.25	0.25	.29
2	0.25	.50	0.25	.50
4	0.50	.25	0.50	.30
5	0.50	.50	0.50	.51
7	0.75	.25	0.70	.29
8	0.75	.50	0.75	.51
10	2.25	.25	2.20	.29
11	2.25	.50	2.23	.51
13	2.50	.25	2.50	.30
14	2.50	.50	2.49	.51
16	2.75	.25	2.70	.29
17	2.75	.50	2.74	.51
19	4.50	.25	4.50	.29
20	4.50	.50	4.52	.51
22	6.50	.25	6.30	.30
23	6.50	.50	6.50	.51
25	8.50	.25	8.50	.29
26	8.50	.50	8.48	.51

6.3.5 Application to Experimental Data

The procedure defined in the preceding section was applied to the experimental data that was acquired from the four aluminum test beams. Since the contributions of frequency-change in the localization and optimization stages were found to be unnecessary in the analysis of the analytical test cases, then only amplitude-change was included in the error function used for this analysis. Also, recall that the initial experimental results attempted through a frequency-based approach were extremely poor. Thus, it was desired to see if amplitude-only data would support an effective assessment process. The numerical results of this updated approach are provided in Table 6.6. While these results show considerable improvement over the initial attempt described in Section 6.2, the process is not very robust. Localization of damage to the correct element was correctly performed for a majority of cases, and the subsequent optimization for assessment of the crack condition for those cases was relatively successful. However, the process was unable to handle two of the lightly damaged beam cases, and user interaction was required on three others.

For the second test case of beam #3, it was necessary to increase the level of model perturbation before sufficient correlation between theoretical and measured changes could exist to allow identification of a damaged element. Additionally, for the second and third test cases of beam #4, it was necessary to remove response minima contributions of points #13 and #12, so that only data from measurement point #11 was included, in order to attain correct identification of the damaged element.

For the questionable test cases of beam #4, the coherence values obtained with the default process settings, did provide indication that the data from response point #11 would best support the damage identification process. However, that judgment was tainted by knowledge of the actual damage. After much consideration, an improved unbiased interpretation of the coherence function values could not be established.

Table 6.6 Damage Assessment of Experimental Cases Based on Amplitude Changes at Local Response Minima

	Actual Damage		**Predicted Damage** Data Used: U_{13}, U_{12}, U_{11}	
Case	**Location (in)**	**Depth (in)**	**Location (in)**	**Depth (in)**
Beam1 – Case 1	0.25	.025	-----	-----
– Case 2	0.25	.050	0.20	.049
Beam 2 – Case 1	0.75	.035	0.70	.045
– Case 2	0.75	.050	0.80	.056
– Case 3	0.75	.070	0.72	.077
Beam 3 – Case 1	2.50	.025	2.50	.033
– Case 2	2.50	.035	2.90*	.045*
– Case 3	2.50	.060	2.63	.070
– Case 4	2.50	.080	2.58	.085
Beam 4 – Case 1	3.75	.023	-----	-----
– Case 2	3.75	.033	3.50**	.056**
– Case 3	3.75	.050	3.80**	.073**
– Case 4	3.75	.070	3.76	.070
– Case 5	3.75	.090	3.74	.086

Notes: *Model Perturbation increased to 50%.
**U_{13} and U_{12} data removed.

Since the beam tip (U_{13}) response has been regarded as the most optimal response location because it is most distant from all modal node points of the lower frequency beam bending modes, then it was a bit alarming that this data had to be removed from the analysis before a reasonably effective assessment could be performed on the second and third damage cases of beam #4. To gain some insight into this problem, a series of theoretical frequency and amplitude changes were produced from the analytical beam model, whereby many incremental steps of proportional damage were applied to each element individually. This provided for the creation of a family of parametric curves of amplitude-change versus frequency-change, with one curve associated with each element. The corresponding measured frequency and amplitude changes of the beam tip minimum response points, from the damage cases of beam #2 and beam #4, were plotted against these curves. The beam #2 data was selected because the damage assessment obtained for it was fairly successful, and thus would be expected to show a good comparison between measured and analytical values. The comparison plots for beam #2 are given in Figure 6.4, and the corresponding plots for beam #4 are given in Figure 6.5. Note that the amplitude-change axes in Figures 6.4 and 6.5 represent the fractional change of the amplitude from that of the undamaged beam.

From Figure 6.5, it is clear that the beam tip response was an effective contributor for the proper localization of the fourth and fifth damage cases of beam #4, as all minimum response points, with the exception of the third, fairly consistently followed the proportional damage curve of Element #4. For the second and third

damage cases, for which the beam tip response had to be removed from the assessment analysis, differences between the measured and analytical changes of the second minimum response point appear to be the primary offenders. Thus, it is expected that a more selective process for removing less than optimal minimum response point information, rather than complete elimination of the response point data, would have enabled an effective damage assessment for these two damage cases. Unfortunately, there was insufficient time to perform this verification for inclusion into this thesis, but it will be done in future work.

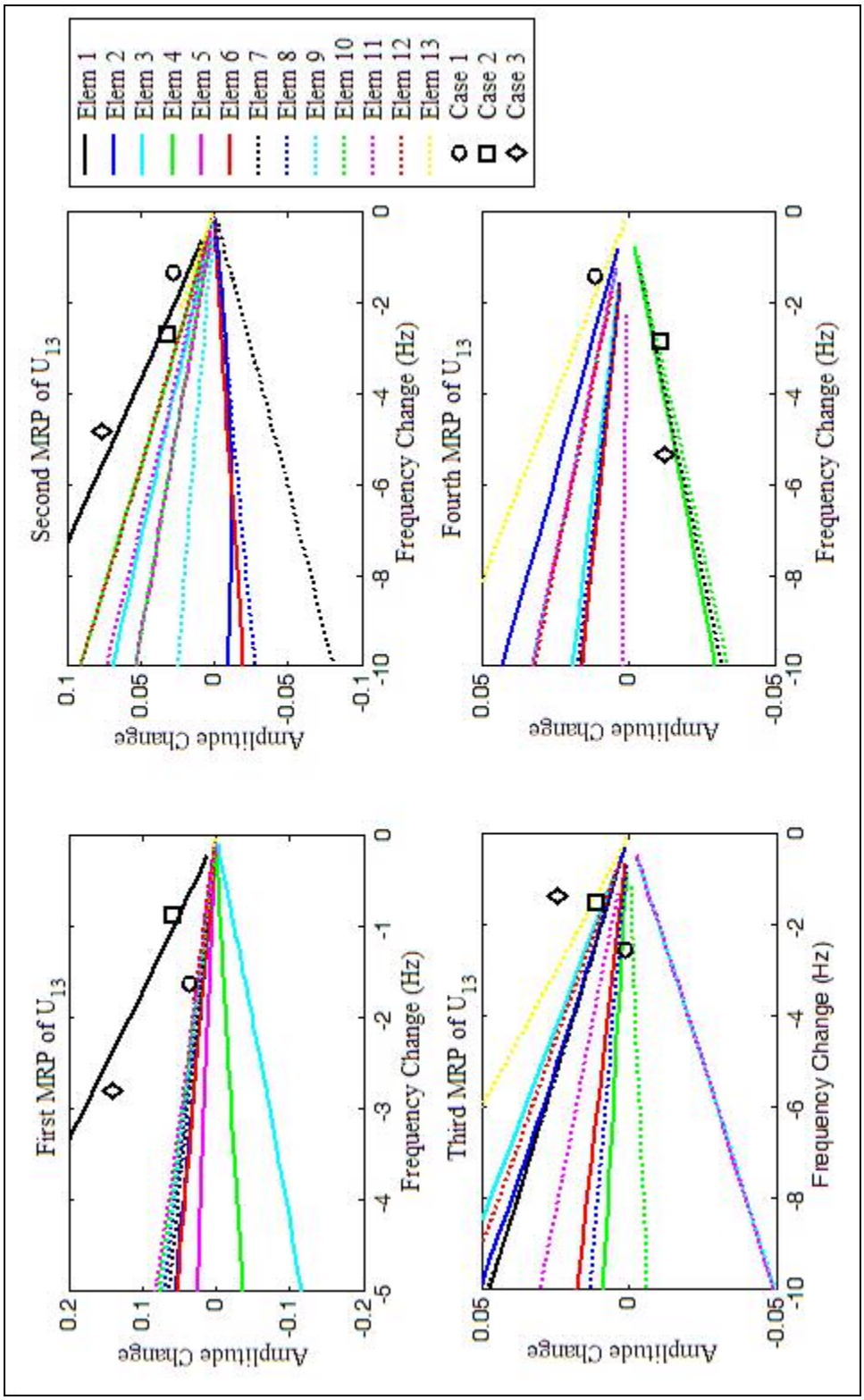

Figure 6.4 Measured Frequency and Amplitude Changes for Beam #2 (Damage within Element 1)

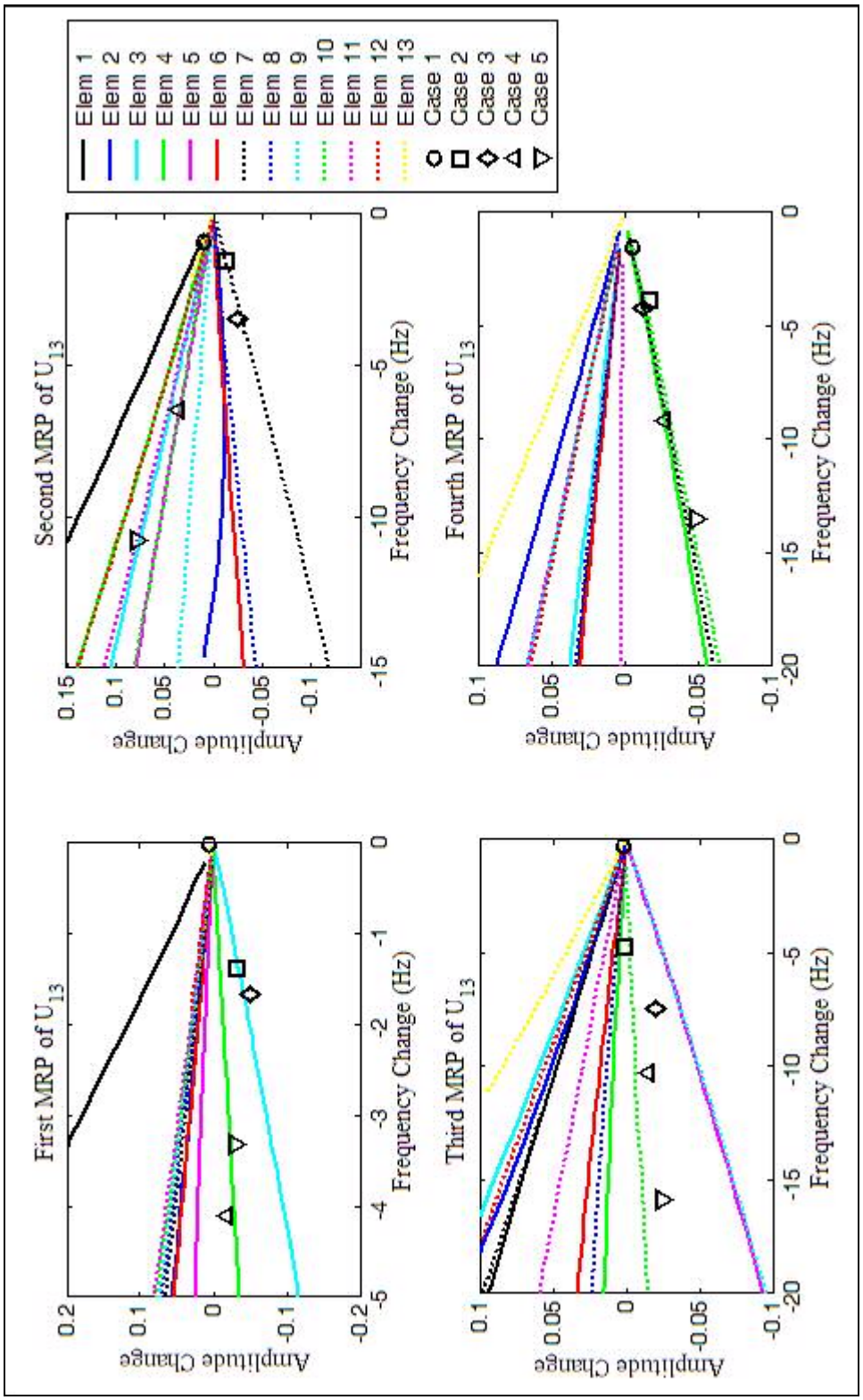

Figure 6.5 Measured Frequency and Amplitude Changes for Beam #4 (Damage within Element 4)

CHAPTER 7

CONCLUSIONS AND FUTURE WORK

The goal of the research was to establish an introduction of local minimum response for potential damage assessment processes. The aim was to determine whether or not minimum response point information could provide measurable detector features, and if so, extract observations that could assist future research.

Since modal parameters have long been considered for damage detection processes, then documented methods associated with these parameters were explored for application of local response minima, so that some comparative evaluation of performance could be gathered. Several of these established methods were adapted to utilize response minima parameters. Analytical development was initiated with a one-dimensional spring-mass system, and then was extended to a beam structure. Finally, some experimental evaluation was performed on simple cantilever beam specimens.

Some conclusions derived from this effort are summarized in the following section. In the final section, there is discussion regarding areas for future work.

7.1 Conclusions

It was demonstrated that minimum response points present in measured response data do exhibit unique sensitivity to damage, and can be used for assessment

of structural health. In analytical test cases, with no measurement noise included, it was found that either frequency or amplitude values provided sufficient information for assessment of damage. However, it was evident in the results that the use of frequency information, alone, required more user intervention than what was necessary when only amplitude information was used. More importantly, though, in the experimental evaluation it was observed that accurate measurement of the frequencies at the minimum response points was very difficult to obtain. For the cantilever beam structure, the minimum response point amplitude values exhibited more sensitivity to crack damage, and relatively speaking, were much more accurately measurable than the corresponding frequency values. It is expected that this would be the case for general structure as well.

There is certainly an issue with robustness of the solution process. In the experimental application, the assessment process that was based on resonant frequency change was very fast, and yielded excellent results without any user intervention. Of course, this is ignoring the fact that some user intervention is required in the modal analysis performed to obtain the modal parameters. On the other hand, the similar process that used minimum response point amplitude-change data, was generally slower, and in some cases resulted in numerical difficulties. It was found in the analytical evaluations that some minimum response points can exhibit sensitivity behavior that is detrimental to a damage assessment process, and must be excluded. The numerical difficulties encountered in the final experimental evaluation were overcome by eliminating some measurements from the analysis.

7.2 Future Work

Based on the results of this research, it is believed that there is sufficient evidence to warrant continued work on this subject. In previous sections of this thesis, some areas for future work were indicated. The most significant of these are listed below as recommendations for future work.

- **Improved minimum response point identification process.**

  An improved method for extracting minimum response point information from measured FRF data is needed. It is not believed that the crude approach used in this work contributed significantly to the large uncertainties in the frequency values extracted from the measured FRF data, because the results from the polynomial curve-fit algorithm were confirmed on visual inspection of the FRF functions. However, it seems that a more mathematically rigorous approach should be employed.

- **Extended Application to Plate Structure.**

  Response locations near the driving point contain few minimum response points, so the beam structure does not permit much flexibility with the selection of input and output locations. A plate structure would allow for study of multiple-input data sets. Additionally, the plate represents a more general structure than the beam, thus the information gained in the study would directly support a general damage assessment application.

- **Determination of Optimal Minimum Response Points.**

  One basis for the rejection of minimum response points was given as: for any response location closely located to the node point of a mode, any minimum response points located at or near the frequency of the mode should be eliminated from the damage assessment process. A focused research effort should be applied to determine other criteria for rejection of *bad* minimum response points, and for identification of *good* points. It is conceivable that perhaps there are very few points that are either good or bad for every possible damage condition. There may be a different set of good and bad points dependent on the particular damage condition. In that case, some adaptive criteria would be needed to interpret the data from the damaged structure and provide decisions for an optimal set of minimum response points.

- **Effect of Damping.**

  For all of this work, damping was ignored. However, out of interest, a brief examination of damping effects was conducted. Frequency response functions were generated for the 6-DOF system with light proportional damping added, then these were compared to the corresponding response functions for the undamped case. It was observed that very little shift of the frequencies of the minimum response points occurred as a result of the added damping. There were, however, noticeable (albeit small) shifts of the amplitudes at the minimum response points as a result of the damping. It is documented in the literature that damage will change the damping characteristics of the structure. Thus, it

would seem prudent that some study should be performed to evaluate the contribution of damping changes in the overall amplitude sensitivity of minimum response. An experimental application of the beam structure was initiated late in the research effort for this thesis, whereby various levels of sinusoidal shaker excitation were applied, and successive damages were induced. The goal was to track the minimum response points, resonant frequencies, and modal damping as a function of the damage condition AND force input level. Unfortunately, there was insufficient time to complete analysis of the measured data for inclusion into this report. Certainly, this should be included in future work.

APPENDIX A

CONTINUOUS BEAM THEORY EQUATIONS

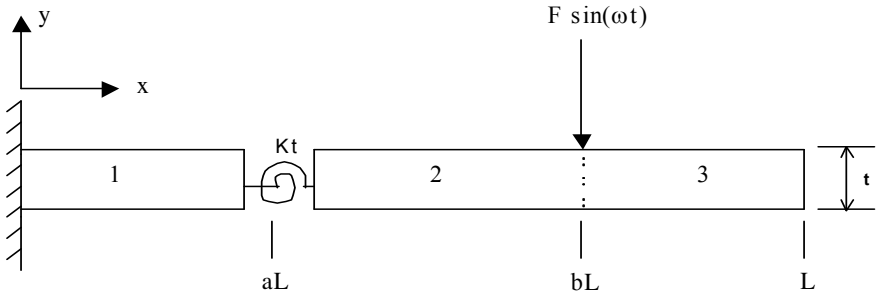

Part 1 (x < aL):

$$y_1 = C_1 \cosh \lambda x + C_2 \sinh \lambda x + C_3 \cos \lambda x + C_4 \sin \lambda x$$

Part 2 (aL < x < bL):

$$y_2 = C_5 \cosh \lambda (x - aL) + C_6 \sinh \lambda (x - aL) + C_7 \cos \lambda (x - aL) + C_8 \sin \lambda (x - aL)$$

Part 3 (x > bL):

$$y_3 = C_9 \cosh \lambda (x - bL) + C_{10} \sinh \lambda (x - bL) + C_{11} \cos \lambda (x - bL) + C_{12} \sin \lambda (x - bL)$$

Boundary Conditions:

1) $y_1(0) = 0$
2) $y_1'(0) = 0$
3) $y_3''(L) = 0$
4) $y_3'''(L) = 0$

Compatibility Conditions:

5) $y_1(aL) = y_2(aL)$
6) $y_1''(aL) = y_2''(aL)$
7) $y_1'''(aL) = y_2'''(aL)$
8) $y_2(bL) = y_3(bL)$
9) $y_2'(bL) = y_3'(bL)$
10) $y_2''(bL) = y_3''(bL)$
11) $y_2'''(bL) = y_3'''(bL) + F/EI$
12) $y_2'(aL) - y_1'(aL) = \dfrac{EI}{K_t} y_1''(aL)$

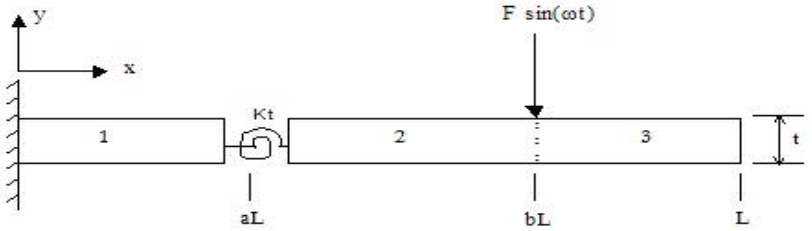

$$\lambda = [\rho A\omega^2/(EI)]^{1/4}$$

$$\begin{bmatrix}
1 & 0 & 1 & 0 & 0 & 0 & 0 & 0 & 0 & 0 & 0 & 0 \\
0 & 1 & 0 & 1 & 0 & 0 & 0 & 0 & 0 & 0 & 0 & 0 \\
0 & 0 & 0 & 0 & 0 & 0 & 0 & 0 & f_1(1-b) & f_2(1-b) & -f_3(1-b) & -f_4(1-b) \\
0 & 0 & 0 & 0 & 0 & 0 & 0 & 0 & f_2(1-b) & f_1(1-b) & f_4(1-b) & -f_3(1-b) \\
f_1(a) & f_2(a) & f_3(a) & f_4(a) & -1 & 0 & -1 & 0 & 0 & 0 & 0 & 0 \\
f_1(a) & f_2(a) & -f_3(a) & -f_4(a) & -1 & 0 & 1 & 0 & 0 & 0 & 0 & 0 \\
f_2(a) & f_1(a) & f_4(a) & -f_3(a) & 0 & -1 & 0 & 1 & 0 & 0 & 0 & 0 \\
0 & 0 & 0 & 0 & f_1(b-a) & f_2(b-a) & f_3(b-a) & f_4(b-a) & -1 & 0 & -1 & 0 \\
0 & 0 & 0 & 0 & f_2(b-a) & f_1(b-a) & -f_4(b-a) & f_3(b-a) & 0 & -1 & 0 & -1 \\
0 & 0 & 0 & 0 & f_1(b-a) & f_2(b-a) & -f_3(b-a) & -f_4(b-a) & -1 & 0 & 1 & 0 \\
0 & 0 & 0 & 0 & f_2(b-a) & f_1(b-a) & f_4(b-a) & -f_3(b-a) & 0 & -1 & 0 & 1 \\
g_1(a) & g_2(a) & g_3(a) & g_4(a) & 0 & 1 & 0 & 1 & 0 & 0 & 0 & 0
\end{bmatrix}
\begin{Bmatrix} c_1 \\ c_2 \\ c_3 \\ c_4 \\ c_5 \\ c_6 \\ c_7 \\ c_8 \\ c_9 \\ c_{10} \\ c_{11} \\ c_{12} \end{Bmatrix}
=
\begin{Bmatrix} 0 \\ 0 \\ 0 \\ 0 \\ 0 \\ 0 \\ 0 \\ 0 \\ 0 \\ 0 \\ F/EI\lambda^3 \\ 0 \end{Bmatrix}$$

$$f_1(x) = \cosh(\lambda Lx), \qquad f_2(x) = \sinh(\lambda Lx), \qquad f_3(x) = \cos(\lambda Lx), \qquad f_4(x) = \sin(\lambda Lx)$$

$$g_1(x) = -f_2(x) - \frac{EI\lambda}{K_t} f_1(x), \quad g_2(x) = -f_1(x) - \frac{EI\lambda}{K_t} f_2(x), \quad g_3(x) = f_4(x) + \frac{EI\lambda}{K_t} f_3(x), \quad g_4(x) = -f_3(x) + \frac{EI\lambda}{K_t} f_4(x)$$

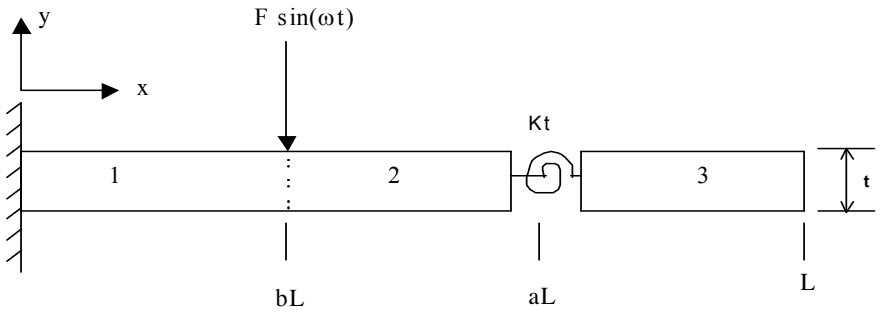

Part 1 ($x < bL$):

$$y_1 = C_1 \cosh \lambda x + C_2 \sinh \lambda x + C_3 \cos \lambda x + C_4 \sin \lambda x$$

Part 2 ($bL < x < aL$):

$$y_2 = C_5 \cosh \lambda (x - bL) + C_6 \sinh \lambda (x - bL) + C_7 \cos \lambda (x - bL) + C_8 \sin \lambda (x - bL)$$

Part 3 ($x > aL$):

$$y_3 = C_9 \cosh \lambda (x - aL) + C_{10} \sinh \lambda (x - aL) + C_{11} \cos \lambda (x - aL) + C_{12} \sin \lambda (x - aL)$$

Boundary Conditions:

1) $y_1(0) = 0$
2) $y_1'(0) = 0$
3) $y_3''(L) = 0$
4) $y_3'''(L) = 0$

Compatibility Conditions:

5) $y_2(aL) = y_3(aL)$
6) $y_2''(aL) = y_3''(aL)$
7) $y_2'''(aL) = y_3'''(aL)$
8) $y_1(bL) = y_2(bL)$
9) $y_1'(bL) = y_2'(bL)$
10) $y_1''(bL) = y_2''(bL)$
11) $y_1'''(bL) = y_2'''(bL) + F/EI$
12) $y_3'(aL) - y_2'(aL) = \dfrac{EI}{K_t} y_2''(aL)$

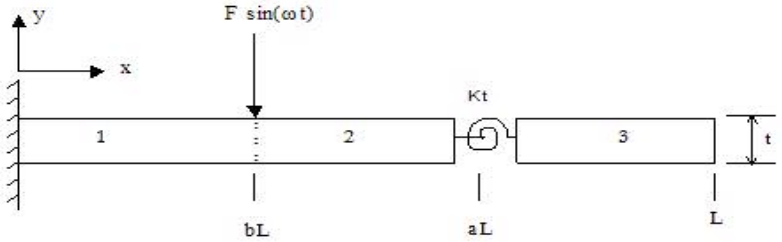

$$\lambda = [\rho A\omega^2/(EI)]^{1/4}$$

$$\begin{bmatrix}
1 & 0 & 1 & 0 & 0 & 0 & 0 & 0 & 0 & 0 & 0 & 0 \\
0 & 1 & 0 & 1 & 0 & 0 & 0 & 0 & 0 & 0 & 0 & 0 \\
0 & 0 & 0 & 0 & 0 & 0 & 0 & 0 & f_1(1-a) & f_2(1-a) & -f_3(1-a) & -f_4(1-a) \\
0 & 0 & 0 & 0 & 0 & 0 & 0 & 0 & f_2(1-a) & f_1(1-a) & f_4(1-a) & -f_3(1-a) \\
0 & 0 & 0 & 0 & f_1(a-b) & f_2(a-b) & f_3(a-b) & f_4(a-b) & 0 & 0 & 0 & 0 \\
0 & 0 & 0 & 0 & f_1(a-b) & f_2(a-b) & -f_3(a-b) & -f_4(a-b) & 0 & 0 & 0 & 0 \\
0 & 0 & 0 & 0 & f_2(a-b) & f_1(a-b) & f_4(a-b) & -f_3(a-b) & 0 & 0 & 0 & 0 \\
f_1(b) & f_2(b) & f_3(b) & f_4(b) & -1 & 0 & -1 & 0 & 0 & 0 & 0 & 0 \\
f_2(b) & f_1(b) & -f_4(b) & f_3(b) & 0 & -1 & 0 & -1 & 0 & 0 & 0 & 0 \\
f_1(b) & f_2(b) & -f_3(b) & -f_4(b) & -1 & 0 & 1 & 0 & 0 & 0 & 0 & 0 \\
f_2(b) & f_1(b) & f_4(b) & -f_3(b) & 0 & -1 & 0 & 1 & 0 & 0 & 0 & 0 \\
0 & 0 & 0 & 0 & g_1(a-b) & g_2(a-b) & g_3(a-b) & g_4(a-b) & 0 & 1 & 0 & 1
\end{bmatrix}
\begin{Bmatrix} c_1 \\ c_2 \\ c_3 \\ c_4 \\ c_5 \\ c_6 \\ c_7 \\ c_8 \\ c_9 \\ c_{10} \\ c_{11} \\ c_{12} \end{Bmatrix}
=
\begin{Bmatrix} 0 \\ 0 \\ 0 \\ 0 \\ 0 \\ 0 \\ 0 \\ 0 \\ 0 \\ 0 \\ F/EL\lambda^3 \\ 0 \end{Bmatrix}$$

$$f_1(x) = \cosh(\lambda Lx), \qquad f_2(x) = \sinh(\lambda Lx), \qquad f_3(x) = \cos(\lambda Lx), \qquad f_4(x) = \sin(\lambda Lx)$$

$$g_1(x) = -f_2(x) - \frac{EL\lambda}{K_t} f_1(x), \quad g_2(x) = -f_1(x) - \frac{EL\lambda}{K_t} f_2(x), \quad g_3(x) = f_4(x) + \frac{EL\lambda}{K_t} f_3(x), \quad g_4(x) = -f_3(x) + \frac{EL\lambda}{K_t} f_4(x)$$

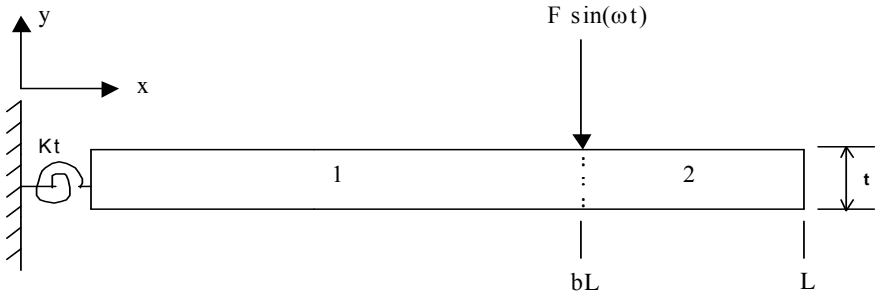

Part 1 (x < bL):

$$y_1 = C_1 \cosh \lambda x + C_2 \sinh \lambda x + C_3 \cos \lambda x + C_4 \sin \lambda x$$

Part 2 (x > bL):

$$y_2 = C_5 \cosh \lambda (x - bL) + C_6 \sinh \lambda (x - bL) + C_7 \cos \lambda (x - bL) + C_8 \sin \lambda (x - bL)$$

Boundary Conditions:

1) $y_1(0) = 0$

2) $y_1'(0) = \frac{EI}{K_t} y_1''(0)$

3) $y_2''(L) = 0$

4) $y_2'''(L) = 0$

Compatibility Conditions:

5) $y_1(bL) = y_2(bL)$

6) $y_1'(bL) = y_2'(bL)$

7) $y_1''(bL) = y_2''(bL)$

8) $y_1'''(bL) = y_2'''(bL) + F/EI$

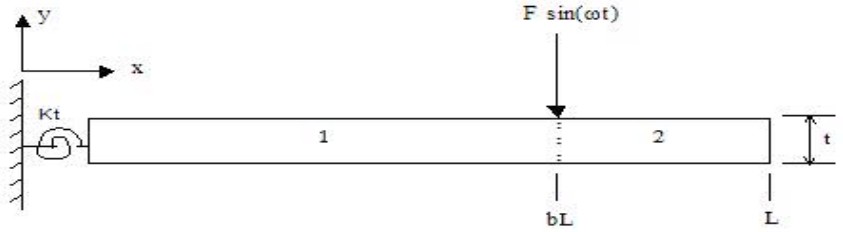

$$\lambda = [\rho A \omega^2/(EI)]^{1/4}$$

$$\begin{bmatrix}
1 & 0 & 1 & 0 & 0 & 0 & 0 & 0 \\
-\frac{EI\lambda}{K_t} & 1 & \frac{EI\lambda}{K_t} & 1 & 0 & 0 & 0 & 0 \\
0 & 0 & 0 & 0 & f_1(1-b) & f_2(1-b) & -f_3(1-b) & -f_4(1-b) \\
0 & 0 & 0 & 0 & f_2(1-b) & f_1(1-b) & f_4(1-b) & -f_3(1-b) \\
f_1(b) & f_2(b) & f_3(b) & f_4(b) & -1 & 0 & -1 & 0 \\
f_2(b) & f_1(b) & -f_4(b) & f_3(b) & 0 & -1 & 0 & -1 \\
f_1(b) & f_2(b) & -f_3(b) & -f_4(b) & -1 & 0 & 1 & 0 \\
f_2(b) & f_1(b) & f_4(b) & -f_3(b) & 0 & -1 & 0 & 1
\end{bmatrix}
\begin{Bmatrix} c_1 \\ c_2 \\ c_3 \\ c_4 \\ c_5 \\ c_6 \\ c_7 \\ c_8 \end{Bmatrix}
=
\begin{Bmatrix} 0 \\ 0 \\ 0 \\ 0 \\ 0 \\ 0 \\ 0 \\ F/EI\lambda^3 \end{Bmatrix}$$

$f_1(x) = \cosh(\lambda Lx)$, $f_2(x) = \sinh(\lambda Lx)$, $f_3(x) = \cos(\lambda Lx)$, $f_4(x) = \sin(\lambda Lx)$

APPENDIX B

CRACKED-BEAM ELEMENT FORMULATION

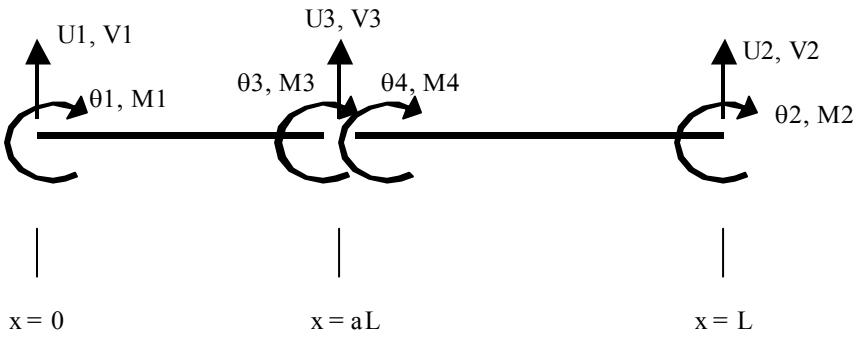

Stiffness Matrix Formulation:

$$\mathbf{K}\,\{\mathbf{U}\} = \{\mathbf{F}\}$$

$$\mathbf{K} = \begin{bmatrix}
\frac{12}{(aL)^3} & \frac{6}{(aL)^2} & -\frac{12}{(aL)^3} & \frac{6}{(aL)^2} & 0 & 0 & 0 \\
\frac{6}{(aL)^2} & \frac{4}{(aL)} & -\frac{6}{(aL)^2} & \frac{2}{(aL)} & 0 & 0 & 0 \\
-\frac{12}{(aL)^3} & -\frac{6}{(aL)^2} & \frac{12}{(aL)^3}+\frac{12}{(1-a)^3L^3} & -\frac{6}{(aL)^2} & \frac{6}{(1-a)^2L^2} & -\frac{12}{(1-a)^3L^3} & \frac{6}{(1-a)^2L^2} \\
\frac{6}{(aL)^2} & \frac{2}{(aL)} & -\frac{6}{(aL)^2} & \frac{4}{(aL)}+K_T & -K_T & 0 & 0 \\
0 & 0 & \frac{6}{(1-a)^2L^2} & -K_T & \frac{4}{(1-a)L}+K_T & -\frac{6}{(1-a)^2L^2} & \frac{2}{(1-a)L} \\
0 & 0 & -\frac{12}{(1-a)^3L^3} & 0 & -\frac{6}{(1-a)^2L^2} & \frac{12}{(1-a)^3L^3} & -\frac{6}{(1-a)^2L^2} \\
0 & 0 & \frac{6}{(1-a)^2L^2} & 0 & \frac{2}{(1-a)L} & -\frac{6}{(1-a)^2L^2} & \frac{4}{(1-a)L}
\end{bmatrix}$$

where, $\{\mathbf{U}\} = [\, U_1 \quad \theta_1 \quad U_2 \quad \theta_2 \quad \theta_3 \quad U_3 \quad \theta_4 \,]^T$,

$\{\mathbf{F}\} = [\, V_1 \quad M_1 \quad V_2 \quad M_2 \quad M_3 \quad V_3 \quad M_4 \,]^T$.

APPENDIX C

EXPERIMENTAL BEAM RESONANT FREQUENCY DATA

BEAM #1
Test Date: 4-15-2005

	Resonant Frequencies (Hz)		
Mode	**Undamaged**	**Case 1**	**Case 2**
1	34.73	34.58	34.21
2	217.46	216.71	214.86
3	608.13	606.51	602.21
4	1190.79	1187.91	1181.09
5	1965.63	1961.82	1952.81

Repeatability Test Data (Based on Beam Tip Response Only)
Test Date: 4-16-2005

	Statistics on Frequency from 10 Data Samples			
	Case 2		**Case 3**	
Mode	**Average**	**Std Dev**	**Average**	**Std Dev**
1	34.24	.010	33.50	.010
2	214.86	.008	211.27	.004
3	602.25	.022	594.22	.013
4	1181.08	.046	1168.69	.027
5	1952.89	.075	1936.89	.027

Case 1: 0.025-in Cut at x = 0.25 in.
Case 2: 0.050-in Cut at x = 0.25 in.
Case 3: 0.075-in Cut at x = 0.25 in.

BEAM #2
Test Date: 4-19-2005

	Resonant Frequencies (Hz) (with Five Accelerometers Installed)				
Mode	**Undamaged**	**Case 1**	**Case 2**	**Case 3**	**Case 4**
1	33.80	33.53	33.26	32.41	32.09
2	215.26	214.21	213.02	210.35	210.38
3	601.47	599.86	597.94	594.10	592.15
4	1178.87	1177.25	1175.66	1172.67	1162.66
5	1947.02	1943.64	1943.44	1942.61	1927.43

Case 1: 0.035-in Cut at x = 0.75 in.
Case 2: 0.050-in Cut at x = 0.75 in.
Case 3: 0.070-in Cut at x = 0.75 in.
Case 4: 0.070-in Cut at x = 0.75 in. and 0.050-in Cut at x = 2.50 in.

BEAM #3
Test Date: 4-22-2005

	Resonant Frequencies (Hz) (with Five Accelerometers Installed)				
Mode	**Undamaged**	**Case 1**	**Case 2**	**Case 3**	**Case 4**
1	33.76	33.68	33.56	33.16	32.57
2	214.99	214.97	214.95	214.88	214.83
3	600.72	600.27	599.75	598.11	595.58
4	1177.76	1175.04	1172.32	1163.49	1149.77
5	1942.10	1938.36	1934.86	1921.05	1902.78

Case 1: 0.025-in Cut at x = 2.50 in.
Case 2: 0.035-in Cut at x = 2.50 in.
Case 3: 0.060-in Cut at x = 2.50 in.
Case 4: 0.080-in Cut at x = 2.50 in.

BEAM #4
Test Date: 4-25-2005

	Resonant Frequencies (Hz) (with Five Accelerometers Installed)					
Mode	**Undamaged**	**Case 1**	**Case 2**	**Case 3**	**Case 4**	**Case 5**
1	33.85	33.81	33.71	33.57	33.25	32.73
2	215.37	215.28	215.18	215.01	214.54	213.99
3	601.76	600.47	599.15	596.70	589.93	581.50
4	1179.14	1177.88	1176.53	1174.15	1167.82	1160.39
5	1945.74	1945.35	1944.84	1944.31	1943.30	1942.41

Case 1: 0.023-in Cut at x = 3.75 in.
Case 2: 0.033-in Cut at x = 3.75 in.
Case 3: 0.050-in Cut at x = 3.75 in.
Case 4: 0.070-in Cut at x = 3.75 in.
Case 5: 0.090-in Cut at x = 3.75 in.

REFERENCES

1. Abe, M., "Structural Damage Detection by Natural Frequencies", AIAA-1996-1440, *Proceedings of the AIAA/ASME/ASCE/AHS/ASC 37th Structures, Structural Dynamics and Materials Conference*, AIAA, April 1996, pp. 1064-1069.

2. Baktiari-Nejad, F., Esfandiari, A., Rahai, A., "Structural Damage Detection and Assessment Using Measured Natural Frequencies", *Proceedings of the 23rd International Modal Analysis Conference*, 2005.

3. Bamnios, Y., Douka, E., Trochidis, A., "Crack Identification in Beam Structures Using Mechanical Impedance", *Journal of Sound and Vibration*, **256**(2), 2002, pp. 287-297.

4. Boltezar, M., Strancar, B., Kuhelj, A., "Identification of Transverse Crack Location in Flexural Vibrations of Free-Free Beams", *Journal of Sound and Vibration*, **211**(5), 1998, pp. 729-734.

5. Cawley, P., Adams, R.D., "The Location of Defects in Structures from Measurements of Natural Frequencies", *Journal of Strain Analysis*, Vol. 14, No. 2, 1979, pp. 49-57.

6. Cawley, P., Ray, R., "A Comparison of the Natural Frequency Changes Produced by Cracks and Slots", *Journal of Vibration, Acoustics, Stress and Reliability in Design, Transactions of the ASME*, **110**, 1988, pp. 366-370.

7. Chondros, T., Dimarogonas, A., "Dynamic Sensitivity of Structures to Cracks", *Journal of Vibration, Acoustics, Stress and Reliability in Design, Transactions of the ASME*, **111**, 1989, pp. 251-256.

8. Cook, R.D., *Finite Element Modeling for Stress Analysis*, John Wiley & Sons, New York, 1995.

9. Craig, R.R., Jr., *Structural Dynamics An Introduction to Computer Methods*, John Wiley & Sons, New York, 1981.

10. Dilena, M., Morassi, A., "The Use of Antiresonances for Crack Detection in Beams", *Journal of Sound and Vibration*, **276**, 2004, pp. 195-214.

11. Farrar, C.R., "The Statistical Pattern Recognition Paradigm for Structural Health Monitoring", *Basics of Structural Health Monitoring* presented at the 23rd International Modal Analysis Conference, 2005.

12. Fox, R.L., Kapoor, M.P., "Rates of Change of Eigenvalues and Eigenvectors", *AIAA Journal*, Vol. 6, No. 12, 1968, pp 2426-2429.

13. Genovese, M, Brito, J., Doz, G., "Evaluation of Structural Integrity through Dynamic Characteristics", *Transactions*, Paper No. 1578, Aug 2001.

14. Guyan, R.J., "Reduction of Stiffness and Mass Matrices", *AIAA Journal*, Vol. 3, No. 2, 1965, p. 380.

15. He, J., Fu, Z., *Modal Analysis*, Butterworth-Heinemann, Oxford, 2001.

16. Jones, K., "Finite Element Model Updating Using Antiresonant Frequencies", *Journal of Sound and Vibration*, **252**(4), pp. 717-727.

17. Lew, J., "Using Transfer Function Parameter Changes for Damage Detection of Structures", *AIAA Journal*, Vol. 22, No. 11, Nov 1995, pp. 2189-2193.

18. Maia, N., Silva, J, etal, *Theoretical and Experimental Modal Analysis*, Research Studies Press, Herefordshire, England, 1997.

19. Mares, C., Mottershead, J.E., "Inverse Propagation and Identification of Random Parameters in Model Updating", *Proceedings of the 23rd International Modal Analysis Conference*, 2005.

20. Narkis, Y., "Identification of Crack Location in Vibrating Simply Supported Beams", *Journal of Sound and Vibration*, **172**(4), 1994, pp. 549-558.

21. Paipetis, S.A., Dimarogonas, A.D., *Analytical Methods in Rotor Dynamics*, Elsevier Applied Research, London, 1986.

22. Palacz, M., "Vibration Parameters for Damage Detection in Structures", *Journal of Sound and Vibration*, **249**(5), 2002, pp. 999-1010.

23. Ratcliffe, C.P., "A Frequency and Curvature Based Experimental Method for Locating Damage in Structures", *Journal of Vibration and Acoustics*, Vol. 122, July 2000, pp. 324-329.

24. Seher, C., Smith, C., "Managing the Aging Aircraft Problem", *AVT Symposium on Aging Mechanisms and Control* and the *Specialists Meeting on Life Management Techniques for Aging Vehicles*, Oct 2001.

25. Steenackers, G., Guillaume, P., "Structural Health Monitoring of the Z-24 Bridge in Presence of Environmental Changes Using Modal Analysis", *Proceedings of the 23rd International Modal Analysis Conference*, 2005.

26. Ugural, A.C., Fenster, S.K., *Advanced Strength and Applied Elasticity*, 4th ed., Prentice Hall Professional Technical Reference, New Jersey, 2003.

27. Wang, B.P., "Minimum Responses of Undamped Structures", Course Handout, ME5322 Advanced Structural Dynamics, University of Texas at Arlington, Fall, 2004.

28. Williams, E.J., Messina, A., Payne, B.S., "A Frequency-Change Correlation Approach to Damage Detection", *Proceedings of the 15th International Modal Analysis Conference*, 1997, pp 652-655.

29. Worden, K., Manson, G., Sohn, H., Farrar, C., "Extreme Value Statistics from Differential Evolution for Damage Detection", *Proceedings of the 23rd International Modal Analysis Conference*, 2005.

BIOGRAPHICAL INFORMATION

Jeffrey Kirk obtained his Bachelors degree in Mechanical Engineering from New Mexico State University in December of 1983. Immediately after graduation, he began his career with Vought Aircraft, which after many name changes, is now Lockheed Martin Missiles and Fire Control – Dallas. The first four years were spent in the Loads and Dynamics group, where he was primarily involved with finite element analysis and rigid body simulation. Subsequently, he transferred into what is now the Environmental Test Laboratory (ETL). His primary responsibilities include coordination and conduct of vibration, transient shock, and acoustic tests. His special contributions to the ETL capabilities include modal testing and signal analysis.